Reaction Mechanism of HutZ-type Heme Degradation Enzymes with Unique Structure

（特異な構造を有する **HutZ** 型ヘム分解酵素の反応機構）

Nobuhiko Dojun

道順 暢彦

Graduate School of Chemical Sciences and Engineering,

Hokkaido University

北海道大学大学院　総合化学院

2019

ACKNOWLEDGEMENTS

This work “Reaction Mechanism of HutZ-type Heme Degradation Enzymes with Unique Structure” supervised by Prof. Koichiro Ishimori (Department of Chemistry, Faculty of Science, Hokkaido University) has been conducted from March 2013 to March 2019.

First, I would like to express my great gratitude to Prof. Koichiro Ishimori. His wide knowledge, invaluable suggestions, and warm encouragements support and motivate me at any time. I gratefully appreciate Dr. Takeshi Uchida for giving me a lot of enormous advices and technical helps. I am also indebted to Dr. Hiroshi Takeuchi and Dr. Tomohide Saio for their helpful discussion and warmhearted encouragement. Secretary Maki Tanaka for accepting the troublesome office procedure. I also thank the previous and current members of Ishimori Laboratory for helps and assistances, especially Dr. Yukari Sekine, Mr. Soichiro Muneta, Ms. Miho Sasaki, Mr. Noriyuki Kobayashi, Mr. Takumi Funamizu, Mr Issei Omura, Mr. Kazuki Ota, Mr. Kazuyoshi Muranishi, and Ms. Yuina Nakamura for contributing to this work.

It should be emphasized that the researches in this thesis have required this thesis have required the cooperation with a number of investigator. I express my special gratitude to Dr. Toshitaka Matsui (Tohoku University) for their instruction of the reaction intermediates. Grateful acknowledgment is indebted to Prof. Yoshikazu Tanaka (Tohoku University) for measurement of isolate calorimetry of HutZ and iron chelator.

I have received a generous support from Japan Society for the Promotion of Science (JSPS) Research Fellowship DC2 since April 2018. This work was financially supported by a Grant-in-Aid for Scientific Research

Lastly, I would like to express my cordial appreciation to my dear family. Mr. Tuguo Dojun, Ms. Sizuka Dojun, and Ms. Kaede Dojun, They have mentally supported me a lot, and there is no doubt that I have spent unforgettable times and had invaluable experiences in Hokkaido University for nine years owing to their warm encouragements and helps. Moreover, I would like to express my gratitude to Ms. Ayaka Nakashima for supporting me. I'm certain of spending unforgettable times and having invaluable experiences in Hokkaido University for nine years owing to their assistances.

March, 2019

Sapporo

Nobuhiko Dojun

LIST OF PUBLICATIONS

PART II

1. Takeshi Uchida, Yukari Sekine, Nobuhiko Dojun, Ariel Lewis-Ballester, Izumi Ishigami, Toshitaka Matsui, Syun-Ru Yeh and Koichiro Ishimori, "Reaction intermediates in the heme degradation reaction by HutZ, from *Vibrio cholerae*", *Dalton Trans.*, 2017, **46**, 8104-8109

2. Takeshi Uchida, Nobuhiko Dojun, Yukari Sekine, and Koichiro Ishimori, "Heme Proximal Hydrogen Bonding between His170 and Asp132 Plays an Essential Role in the Heme Degradation Reaction of HutZ from *Vibrio cholerae*" *Biochemistry*, 2017, **56**, 2723-2734

PART III

Nobuhiko Dojun, Yukari Sekine, Koichiro Ishimori and Takeshi Uchida "Iron chelators inhibit the heme-degradation reaction by HutZ from *Vibrio cholerae*", *Dalton Trans.*, 2017, **46**, 5147-5150

PART IV

Nobuhiko Dojun, Koichiro Ishimori and Takeshi Uchida "A single mutation converts Alr5027 from cyanobacteria *Nostoc* sp. PCC 7120 to a heme-binding protein with heme-degrading ability", to be submitted

LIST OF PRESENTATIONS

Oral Presentations

1. Nobuhiko Dojun, Yukari Sekine, Koichiro Ishimori, and Takeshi Uchida
   "Self-regulation mechanism in HutZ from Vibrio cholerae: The heme degradation activity of HutZ is regulated by iron released from its own heme degradation."
   The 96th CSJ Annual Meeting (Kyoto, Japan) March 24-27, 2016

2. Nobuhiko Dojun, Koichiro Ishimori and Takeshi Uchida
   "Elucidation of evolutionary acquisition of the heme-degradation function of HutZ, from vibrio cholerae"
   The 97th CSJ Annual Meeting (Tokyo, Japan) March 16-19, 2017

Poster Presentations

1. Nobuhiko Dojun, Yukari Sekine, Koichiro Ishimori, and Takeshi Uchida
   "Effects of Hydrogen Bonds on Heme Degradation by HutZ from *Vibrio cholerae*."
   The 6th Symposium on Biorelevant Chemistry CSJ (Nagoya, Japan) September 27-29, 2013

2. Nobuhiko Dojun, Yukari Sekine, Koichiro Ishimori, and Takeshi Uchida
   "Regulation of Heme Binding to Active Site on Heme Degradation Enzyme of HutZ from Vibrio cholerae."
   Annual Metting of Japan Biochemical Society /Hokkaido Branch (Sapporo, Japan) July 18, 2014

3. Nobuhiko Dojun, Yukari Sekine, Koichiro Ishimori, and Takeshi Uchida
   "Regulation of Heme Cleavage Site in Heme Degradation Reaction by HutZ from *Vibrio cholerae*."
   The 7th Symposium on Biorelevant Chemistry CSJ (Okayama, Japan) September 11-13, 2014

4. Nobuhiko Dojun, Yukari Sekine, Koichiro Ishimori, and Takeshi Uchida
   "Fe^{2+} Chelators Repress Heme Degradation Reaction of HutZ from *Vibrio Cholerae*"
   The 25th Symposium on Role of Metals in Biological Reactions, Biology and Medicine (Nagasaki, Japan) May 30-31, 2015

5. Nobuhiko Dojun, Yukari Sekine, Koichiro Ishimori, and Takeshi Uchida
"Iron chelating agents repress the heme degradation activity of HutZ from *Vibrio cholerae*."
The 8th Symposium on Biorelevant Chemistry CSJ (Kumamoto, Japan) September 11-13, 2015

6. Nobuhiko Dojun, Yukari Sekine, Koichiro Ishimori, and Takeshi Uchida
"Inhibition Mechanism for the Heme Degradation Activity of HutZ by Iron Chelators"
The 26th Symposium on Role of Metals in Biological Reactions, Biology and Medicine (Sapporo, Japan) June 17-18, 2016

7. Nobuhiko Dojun, Yukari Sekine, Koichiro Ishimori, and Takeshi Uchida
"Inhibition of Heme Degrading Activity by Chelator in HutZ from Vibrio cholera and Its Molecular Mechanism"
The 9th Symposium on Biorelevant Chemistry CSJ (Kanazawa, Japan) September 7-9, 2016

8. Nobuhiko Dojun, Yukari Sekine, Koichiro Ishimori, and Takeshi Uchida
"Iron chelators inhibit the heme-degradation reaction by HutZ from *Vibrio cholerae*"
8th Asian Biological Inorganic Chemistry Conference (ASBIC-VIII) (Oakland, New Zealand) December 4-9, 2016

9. Nobuhiko Dojun, Koichiro Ishimori, and Takeshi Uchida
"The mechanism for acquisition of the heme-degrading activity of HutZ form *Vibrio cholerae* by molecular evolution approach"
The 10th Symposium on Biorelevant Chemistry CSJ (Tokyo, Japan) September 7-9, 2017

TABLE OF CONTENTS

PART I: General Introduction

Almost all bacteria require iron to survive. Pathogen bacteria acquire iron from hosts upon entry into the mammalian host. The regulation of bacterial iron metabolic system is led to inhibit the effective bacterial growth. Recently, the Gran-negative pathogens present the most acute threat of developing untreatable multidrug-resistant infections, posing a particular threat owing to their dual-membrane envelope that prevents these antibiotics from accessing their targets. Thus, development of new drugs acting on the iron metabolic system is promising for therapy and prevention for infection

1.1 Iron Uptake by Bacteria

Iron is an essential element for bacteria because it acts as a cofactor to play key roles in metabolic processes such as oxygen transport, electron transfer, and energy transduction. While iron is generally required for metabolic processes in organisms ferric iron (Fe^{3+}) is extremely insoluble and the concentration of free ferric iron is very low (10^{-18} M) at neutral pH[1]. The concentration of iron available for bacterial pathogen is even significantly lower (10^{-24} M)[2] because ferric iron is sequestered by host iron-carrier proteins such as lactoferrin and transferrin and by heme. Because iron is essential for growth and pathogenesis of bacteria even under such low-iron conditions, invading microorganisms have developed intricate iron uptake pathways from one or more of the diverse mammalian iron sources to overcome the iron restriction.

One way by which invading microbes acquire iron is production and secretion of small molecular weight compounds called siderophores, which strongly and specifically chelate ferric iron, solubilize it from mineral or organic complexes. In Gram-negative bacteria, iron-siderophore complexes are recognized by specific outer membrane such as periplasmic protein-dependent ABC permeases, through which iron-siderophore are delivered into cells. In addition to siderophore secretion, iron-binding proteins directly bind[3,4] and reduce the insoluble ferric iron to usable soluble form (Fe^{2+})[5], secreted extracellular proteinases degrade host iron-binding proteins[6,7] or lethal compounds (exotoxins) that may eliminate competitors for usable iron resources are produced[8,9]. However, because of the strongly-limited availability of free iron

in vertebrate hosts, acquisition of iron by siderophores, especially for pathogenic bacteria, is insufficient. Therefore, pathogens have evolved another system in which heme (iron-protoporphyrin IX)-containing proteins in hosts are utilized as an iron source[10].

Although heme is necessary as an iron source for some bacteria, free heme is toxic as iron. it causes oxidative damage to cells by catalyzing formation of reactive oxygen species through the Fenton-type reactions[11]. To avoid this deleterious effect, free heme present in plasma is rapidly sequestered by the host heme-binding proteins such as hemopexin and human serum albumin. Under pathologic conditions, hemopexin, human serum albumin, hemoglobin and hemoglobin-binding haptoglobin are, therefore, potential heme-iron sources to invading bacteria[12]. Because the affinity of these proteins for heme is extremely high affinity, bacteria have developed sophisticated mechanism to sequester the heme from these sources and transport it into the cytoplasm, where the porphyrin ring of heme is oxidized by heme-degrading enzyme and broken to release iron[13,14].

1.2 Heme Utilization System in *Vibio cholreae*

Vibrio cholerae, a Gram-negative bacterium, is the causative agent of cholera, which is still a significant public health threat in areas where clean water is not widely available. To acquire iron from heme, *V. chorela* has their own heme utilization (Hut) system[15]. Based on the genome sequence of *V. cholerae* and bioinformatics-based predictions, proteins involved in the transport of heme into the cell have been proposed (Fig. 1)[16]. Two distinct outer membrane receptors, HutA and HutR, specifically transport heme across the outer membrane[17]. In periplasm, the heme-binding protein, HutB, binds to heme[18], and transfer it to the inner-membrane HutC-HutD protein complex[15]. HutC/HutD in turn transfers heme into cytoplasm across the inner membrane. In cytoplasm, HutX functions as a heme transport protein to HutZ[19], which degrades heme[20].

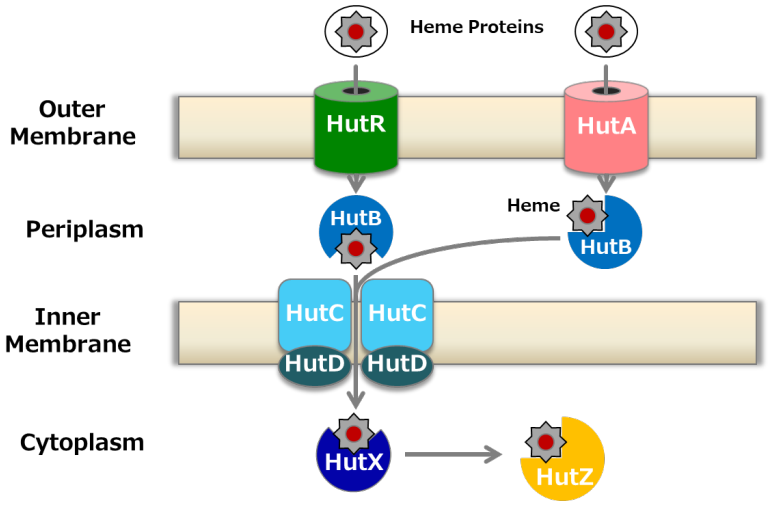

Fig 1 Model for heme utilization in *V. cholerae*. Heme crosses the outer membrane through one of two outer membrane receptors, HutA[21] and HutR[22]. Heme is then transport across the inner membrane most likely by the HutBCD transport system[23]. HutZ degrades heme after when HutX transports heme to HutZ *in vitro*.

1.3 HugZ-type Heme Degrading Enzyme

In many bacteria, heme oxygenase is required for the use of heme as a source of iron. HutZ, from *V. cholerae*[15,20], is a heme-degrading protein in spite of no homology to the human HOs from some bacteria[24–27]. Homologous proteins to HutZ are recently discovered from *Campylobacter jejuni* (ChuZ)[28], and *Helicobacter pylori* (HugZ)[29,30]. HutZ is homologous to HugZ (31% sequence identity), but not to the human HOs. Although the crystal structure of the heme-HutZ complex are not resolved, the structure of heme-bound ChuZ and HugZ are reported. They form a homodimer with split β-barrels[28,30], which are distinct from human HOs (Fig. 2A). Heme is located at the intermonomer interface and is bound by two monomers. The structure of HugZ shows that Arg166 (corresponding to Arg92 in HutZ), which is located at the distal site of heme, acts as a hydrogen bond donor for the iron-bound O_2 (Fig. 2B)[20]. The axial heme ligand is His245 (corresponding to His170 in HutZ), which is located within the hydrogen-bonding distance to Asp207 (corresponding to Asp132 in HugZ) (Fig. 2B). The heme-degrading product of HugZ is similar to human HOs, biliverdin IXδ, although the crystal structure and heme binding site structure of HugZ is distinct from those of the HOs[29].

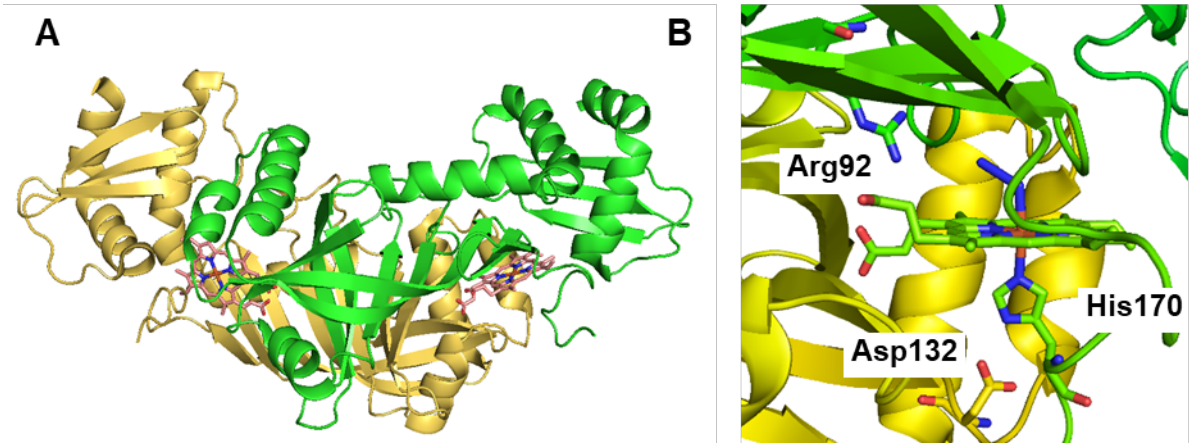

Fig. 2 (A) Crystal structures of HugZ dimmer ant (B) its heme binding site. Resides are numbered according to the amino acid sequence of HutZ from *V,cholerae*.(PDB code: 3GAS)

1.4 Heme-Degradation Mechanism by HOs

The heme degradation reaction bases on the protein's own structures. In heme, iron is tightly bound to the porphyrin ring, and cannot be removed by a simple reaction. Thus, the heme-degrading enzymes catalyze the stereospecific cleavage of heme to release iron with biliverdin and carbon monoxide (CO) by three successive self-oxygenation reaction[31]. In mammalian HO, the mechanisms of the heme degradation reactions are revealed as described below[32,33]. After the enzyme binds ferric heme (Fig. 3a), one electron is donated by the reducing substrate, converting the heme-iron to the ferrous form (Fig. 3b). Then, O_2 binds to the reduced 5-coordinate heme and forms a *meta*-stable oxy complex (Fig. 3c). A one-electron reduction of the oxy heme generates a ferric-hydroperoxo complex (Fig. 3d), which self-hydroxylates to produce α-*meso*-carbon of the porphyrin ring (Fig. 3e)[34]. A spontaneous auto-oxidation of the reactive α-*meso*-hydroxyheme produced verdoheme (Figs. 3e and 3f). The mechanism of the second step remains elusive, but HO unlikely plays a critical role in it, because that hydroxyheme immediately react with O_2 to afford verdoheme (Fig. 3f) even in the absence of HO[35]. The second oxygenation (Figs. 3f and 3g) by verdoheme cleaves its porphyrin macrocycle to release biliverdin (Fig. 3g) and free ferrous iron. Thus, heme-degradation reaction is sensitive based on the structure, and molecular mechanisms. In most heme enzymes

(i.e. peroxidases) , when the heme oxidation reaction the O-O bond of hydroperoxy heme (Fig. 3d) is homolytically cleaved to generate a ferryl (Fe^{4+}=O) intermediate called compound I or compound II[36]. In the HO's oxidation, the OH group of hydroperoxy heme attacks to the *meso*-carbon of porphyrin. The protein structure has evolved to avoid the production of compound I or compound II[37]. The HOs structure shows that the highly conserved two glycine resides bend the O-O bond of hydroperoxy heme to attack to the *meso*-carbon of porphyrin[38,39]. Although the structure of HugZ-type enzyme was different from that of HO-1, however, the HugZ-type enzymes degrade heme to biliverdin. The heme degradation mechanism and acquisition of heme degradation ability based on the protein structure of HugZ-type enzymes remains to be unknown

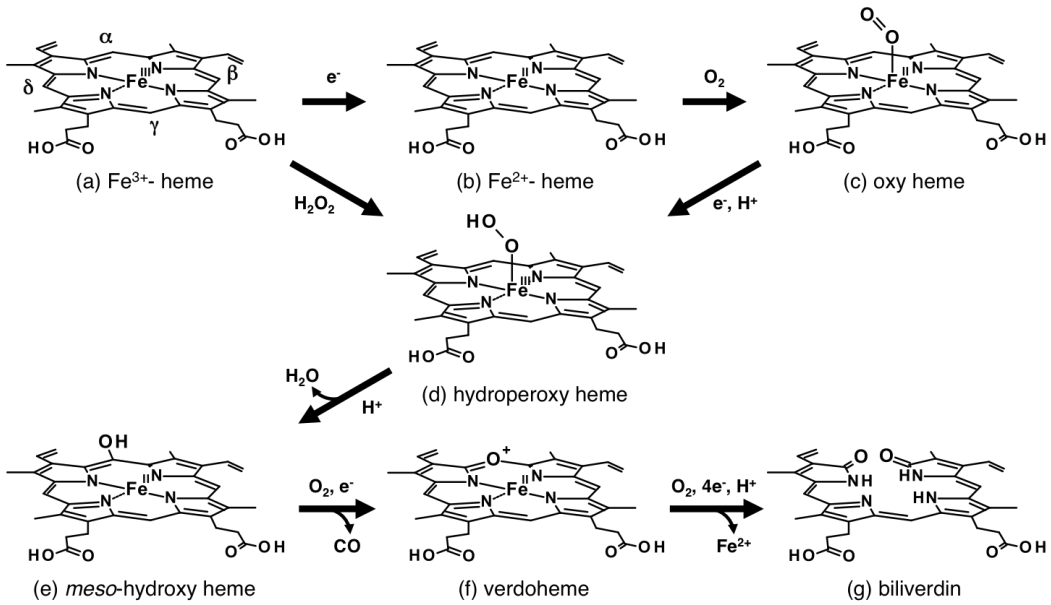

Fig. 3 Schematic of heme oxygenase catalytic intermediates Degradation of heme by HO yields ferrous iron, biliverdin and CO

1.5 Heme-Degradation Enzyme HutZ from *V. cholerae*

The heme degradation intermediates of HutZ were partly identified by spectroscopic techniques. The absorption and resonace Raman spectra of the ferric heme (Fig. 3a) and ferrous heme (Fig 3b) complexes are similar to those of the heme-myoglobin complex, suggesting that

the heme iron of HutZ is bound to a histidine. The oxy heme of HutZ (Fig. 3c) was unstable for short lifetime because of the rapid autoxidation to ferric-heme. However, the oxy heme of HutZ could be observed by the resonance Raman measurement combined with rapid-mixing technique[40]. In addition, the heme degrading products of biliverdin IXβ and biliverdin IXδ were detected by LC-MS and HPLC analysis[20]. These products of HutZ are the same as those of HO-1, except for the cleavage site of the *meso*-carbon of porphyrin. The key intermediates, *meso*-hydroxyheme (Fig. 3e) and verdoheme (Fig. 3f), were not yet observed, because the *meso*-hydroxyheme is immediately non-enzymatically converted to verdoheme in the aerobic conditions, and the absorption band of verdoheme in HutZ is different from that of HO-1. Thus, the heme-degradation intermediates of HutZ except for meso-hydroxyheme and verdoheme are the same as those of HO-1, I predict that the heme degradation mechanism of HutZ is the same as that of HO-1, and determine the production of key intermediates to elucidate the reaction mechanism of HutZ-type enzymes. Next, I focus on the structural unique of HutZ, the proximal hydrogen bond between Asp132 and His170 (Fig. 2B), which seems to be disadvantage for heme-degradation reaction to promote the formation of ferryl species (Fe^{4+}=O). This hydrogen bond is necessary for the forming ferryl species in the peroxidases. Although the wild-type HutZ can degrade heme to biliverdin, the role of this hydrogen bound is unknown in heme degradation by HutZ.

1.6. Study on Heme-Degradation Mechanism of HutZ-type Enzymes

In part II of chapter I, to determine the heme-degradation mechanism by HutZ, I observed *meso*-hydroxyheme and characterizing verdoheme of HutZ by UV-vis spectra. The *meso*-hydroxyheme was produced by mixing the ferric heme-HutZ complex with one equivalent of H_2O_2 under the anaerobic conditions. Although the valence of verdoheme-iron of HutZ (Fe^{3+}) is different from other HO-1 (Fe^{2+}), the heme degradation intermediates of HutZ are the same as those of the canonical HOs.

The distinct active site structure of HutZ from HO-1 suggests that the hydrogen bond between

Asp132 and His170 is unique in the heme degradation enzymes. In part II of chapter II, to investigate the role of proximal hydrogen bonding of HutZ, I prepared Asp132Leu, Asn, Glu, and His170Ala mutants, in which the hydrogen bond between Asp132 and His170 was cleaved. When the proximal hydrogen bond was intact, I predicted that HutZ could not reduce heme to ferrous heme because of strong electron donation from the proximal histidine. However, mutations at both sites led to a significant loss of heme degrading activity and heme affinity, except for the substitution of glutamate acid for Asp132, likely because the heme would be not held in an appropriate position to attack the *meso* carbon of the porphyrin ring for heme degradation. Only a slight modulation of the distance of hydrogen bond between His170 and Asp132 is a key to activate the degradation reaction of the heme-HutZ complex.

The investigation of heme degradation mechanism by HutZ, which is the same as that of HO-1, suggests that the different molecular evolution of HutZ-type enzymes occurs from that of HO-1 to acquire heme-degrading function. In part III, to investigate that the heme-degrading ability of HutZ-type enzymes is evolutionally conserved, I expressed Alr5027 from cyanobacteria, which is homologous to HutZ, in *Escherichia coli* and examined its heme-binding and heme-degradation properties. Alr5027 did not bind to heme because the putative heme ligand is not conserved. To acquire the heme degradation ability for Alr5027, introduction of histidine at position 164 rendered the mutant with high affinity for heme ($K_{d,heme}$ of 240 nM) with a stoichiometry of 1:1. Although heme was not degraded by the K164H mutant when ascorbic acid was used as an electron source, reaction with H_2O_2 produced verdoheme, indicating the heme-degrading ability for the Alr5027 mutant. These findings suggest that the members of HutZ family have acquired their heme-degradation function through molecular evolution from a common ancestor of HutZ and Alr5027.

In part IV, to gain enzymatic information for HutZ, I tested the heme-degradation ability of HutZ by detecting the amount of ferrous iron. When I added iron chelators to a reaction solution containing heme-HutZ and ascorbic acid, the reaction proceeded very slowly in the presence of

iron chelators, indicating that iron chelators inhibit the heme-degradation reaction by HutZ. Based on kinetic analysis of the heme-degradation reaction of HutZ, kinetic analysis of each heme-degradation step suggested that iron chelator would inhibit the conversion of oxy heme (Fig. 3c) to hydorxyheme (Fig 3d). Tetracycline, which is the most effective current treatment of the antibiotics for *V. cholera*e, is an inhibitor of protein synthesis as well as iron chelator. Thus, I speculated that the tetracycline affects the heme degradation activity of HutZ. The heme degradation reaction of HutZ was repressed in the presence of tetracycline, whereas the heme was degraded in the presence of chloramphenicol, a representative antibiotic, suggesting that iron-chelating agents are good candidate antibiotics for use against *V. cholerae*.

References

(1) Braun, V.; Killmann, H. *Trends Biochem. Sci.* **1999**, *24* (3), 104.

(2) Granger, J.; Price, N. M. *Limnol. Oceanogr.* **1999**, *44* (3 I), 541.

(3) Cornelissen, C. N.; Sparling, P. F. *Mol. Microbiol.* **1994**, *14* (5), 843.

(4) Mietzner, T.; Morse, S. *Annu. Rev. Nutr.* **1994**, *14* (c), 471.

(5) Coulanges, V.; Andre, P.; Ziegler, O.; Buchheit, L.; Vidon, D. J. M. *Infect. Immun.* **1997**, *65* (7), 2778.

(6) Wolz, C.; Hohloch, K.; Ocaktan, A.; Poole, K.; Evans, R. W.; Rochel, N.; Albrechtgary, A. M.; Abdallah, M. A.; Doring, G. *Infect Immun* **1994**, *62* (9), 4021.

(7) Wilderman, P. J.; Vasil, A. I.; Johnson, Z.; Wilson, M. J.; Cunliffe, H. E.; Lamont, I. L.; Vasil, M. L. *Infect. Immun.* **2001**, *69* (9), 5385.

(8) Bjorn, M. J.; Iglewski, B. H.; Ives, S. K.; Sadoff, J. C.; Vasil, M. L. *Infect. Immun.* **1978**, *19* (3), 785.

(9) Calderwood, S. B.; Mekalanos, J. J. *J. Bacteriol.* **1987**, *169* (10), 4759.

(10) Huang, W.; Wilks, A. *Annu. Rev. Biochem.* **2017**, *86* (1), 799.

(11) Touati, D. *Arch. Biochem. Biophys.* **2000**, *373* (1), 1.

(12) Ascenzi, P.; Bocedi, A.; Visca, P.; Altruda, F.; Tolosano, E.; Beringhelli, T.; Fasano, M. *IUBMB Life* **2005**, *57* (11), 749.

(13) Ratliff, M.; Zhu, W.; Deshmukh, R.; Wilks, A.; Stojiljkovic, I. *J. Bacteriol.* **2001**, *183* (21), 6394.

(14) Barker, K. D.; Barkovits, K.; Wilks, A. *J. Biol. Chem.* **2012**, *287* (22), 18342.

(15) Wyckoff, E. E.; Schmitt, M.; Wilks, A.; Payne, S. M. *J. Bacteriol.* **2004**, *186* (13), 4142.

(16) Wyckoff, E. E.; Mey, A. R.; Payne, S. M. *Biometals* **2007**, *20* (3–4), 405.

(17) Henderson, D. P.; Payne, S. M. *J. Bacteriol.* **1994**, *176* (11), 3269.

(18) Uchida, T.; Funamizu, T.; Ogura, M.; Ishimori, K. *Bull. Chem. Soc. Jpn.* **2017**, *90* (8), 924.

(19) Sekine, Y.; Tanzawa, T.; Tanaka, Y.; Ishimori, K.; Uchida, T. *Biochemistry* **2016**, *55* (6), 884.

(20) Uchida, T.; Sekine, Y.; Matsui, T.; Ikeda-Saito, M.; Ishimori, K. *Chem. Commun.* **2012**, *48* (53), 6741.

(21) Henderson, D. P.; Payne, S. M. *Infect. Immun.* **1994**, *62* (11), 5120.

(22) Mey, a R.; Payne, S. M. *Mol. Microbiol.* **2001**, *42* (3), 835.

(23) Occhino, D. A.; Wyckoff, E. E.; Henderson, D. P.; Wrona, T. J.; Payne, S. M. *Mol Microbiol* **1998**, *29*, 1493.

(24) Hirotsu, S.; Chu, G. C.; Unno, M.; Lee, D.-S.; Yoshida, T.; Park, S.-Y.; Shiro, Y.; Ikeda-Saito, M. *J. Biol. Chem.* **2004**, *279* (12), 11937.

(25) Schuller, D. J.; Zhu, W.; Stojiljkovic, I.; Wilks, A.; Poulos, T. L. *Biochemistry* **2001**, *40* (38), 11552.

(26) Friedman, J.; Lad, L.; Li, H.; Wilks, A.; Poulos, T. L. *Biochemistry* **2004**, *43* (18), 5239.

(27) Skaar, E. P.; Gaspar, A. H.; Schneewind, O. *J. Biol. Chem.* **2004**, *279* (1), 436.

(28) Zhang, R.; Zhang, J.; Guo, G.; Mao, X.; Tong, W.; Zhang, Y.; Wang, D. C.; Hu, Y.; Zou, Q. *Biochem. Biophys. Res. Commun.* **2011**, *415* (1), 82.

(29) Guo, Y.; Guo, G.; Mao, X.; Zhang, W.; Xiao, J.; Tong, W.; Liu, T.; Xiao, B.; Liu, X.; Feng, Y.; Zou, Q. *BMC Microbiol.* **2008**, *8* (1), 226.

(30) Hu, Y.; Jiang, F.; Guo, Y.; Shen, X.; Zhang, Y.; Zhang, R.; Guo, G.; Mao, X.; Zou, Q.; Wang, D. C. *J. Biol. Chem.* **2011**, *286* (2), 1537.

(31) Unno, M.; Matsui, T.; Ikeda-Saito, M. *Nat. Prod. Rep.* **2007**, *24* (3), 553.

(32) Kikuchi, G.; Yoshida, T.; Noguchi, M. *Biochem. Biophys. Res. Commun.* **2005**, *338* (1), 558.

(33) Matsui, T.; Unno, M.; Ikeda-Saito, M. *Acc. Chem. Res.* **2010**, *43* (2), 240.

(34) Davydov, R. M.; Yoshida, T.; Ikeda-Saito, M.; Hoffman, B. M. *J. Am. Chem. Soc.* **1999**, *121* (45), 10656.

(35) Morishima, I.; Fujii, H.; Shiro, Y.; Sano, S. *Inorg. Chem.* **1995**, *34* (6), 1528.

(36) Poulos, T. L. *Chem. Rev.* **2014**, *114* (7), 3919.

(37) Chen, H.; Moreau, Y.; Derat, E.; Shaik, S. *J. Am. Chem. Soc.* **2008**, *130* (6), 1953.

(38) Liu, Y.; Lightning, L. K.; Huang, H.; Moënne-Loccoz, P.; Schuller, D. J.; Poulos, T. L.; Loehr, T. M.; Ortiz de Montellano, P. R. *J. Biol. Chem.* **2000**, *275* (44), 34501.

(39) Lad, L.; Koshkin, A.; Ortiz De Montellano, P. R.; Poulos, T. L. *J. Biol. Inorg. Chem.* **2005**, *10* (2), 138.

(40) Uchida, T.; Sekine, Y.; Dojun, N.; Lewis-Ballester, A.; Ishigami, I.; Matsui, T.; Yeh, S. R.; Ishimori, K. *Dalt. Trans.* **2017**, *46* (25), 8104.

PART II: Heme-Degradation Mechanism of HutZ

Chapter I: Identified the Key Intermediates of Heme-Degradation Reaction by HutZ

Abstract

HutZ converts heme to biliverdin, suggesting that it follows the same reaction mechanism as that of mammalian heme oxygenase. However, the key intermediates, *meso*-hydroxyheme and verdoheme, have not been identified. In this chapter, I applied UV-vis absorption spectroscopy to study the reaction of heme-HutZ complex with H_2O_2 or ascorbic acid. First, I identified the production of *meso*-hydroxyheme. The *meso*-hydroxyheme of HutZ was produced with 1 equivalent H_2O_2 in anaerobic condition, because the conversion of meso-hydroxyheme to verdoheme was non-enzymatic reaction in aerobic conditions Next, I tried to characterize vedoheme complex. The 644 nm species was produced by reacting the ferric heme-HutZ complex with H_2O_2 under aerobic conditions. Compared with the verdoheme species in other HO-1, the 644 nm species is about 20 nm shorter than that of other HO-1. When ascorbic acid added to this reaction solution, this species shifted 644 nm to 671 nm, indicating that production of verdoheme of HutZ by H_2O_2 was the ferric-verdoheme, because the axial ligand His170 is imidazolate by hydrogen bonding with Asp132. Our data supports the view that HutZ degrades heme in a manner similar to mammalian heme oxygenase, despite their low sequence and structural homology.

2.1.1. Introduction

As previously shown in Part I, HutZ from *Vibrio cholerae* is capable of degrading the heme, and producing verdoheme and biliverdin[1], as observed in the reaction catalyzed by mammalian heme oxygenase (HO)[2–4], suggesting that HutZ follows the same reaction mechanism as that of HO (Fig 1)[5]. In that mechanism, the initial step is the reduction of ferric heme to ferrous heme. Then, O_2 binds to the ferrous heme to generate oxyferrous heme (Fe^{2+}-O_2). Further reduction and protonation of the oxyferrous heme leads to ferric hydroperoxy heme (Fe^{3+}-OOH), which then reacts with the heme macrocycle to give *meso*-hydroxyheme. Subsequently, in the presence of O_2, the hydroxylated *meso*-carbon is eliminated as carbon monoxide (CO) with a concomitant formation of the verdoheme. The verdoheme is then oxygenated to generate biliverdin.

Fig. 1 Proposed heme degradation mechanism of HutZ.

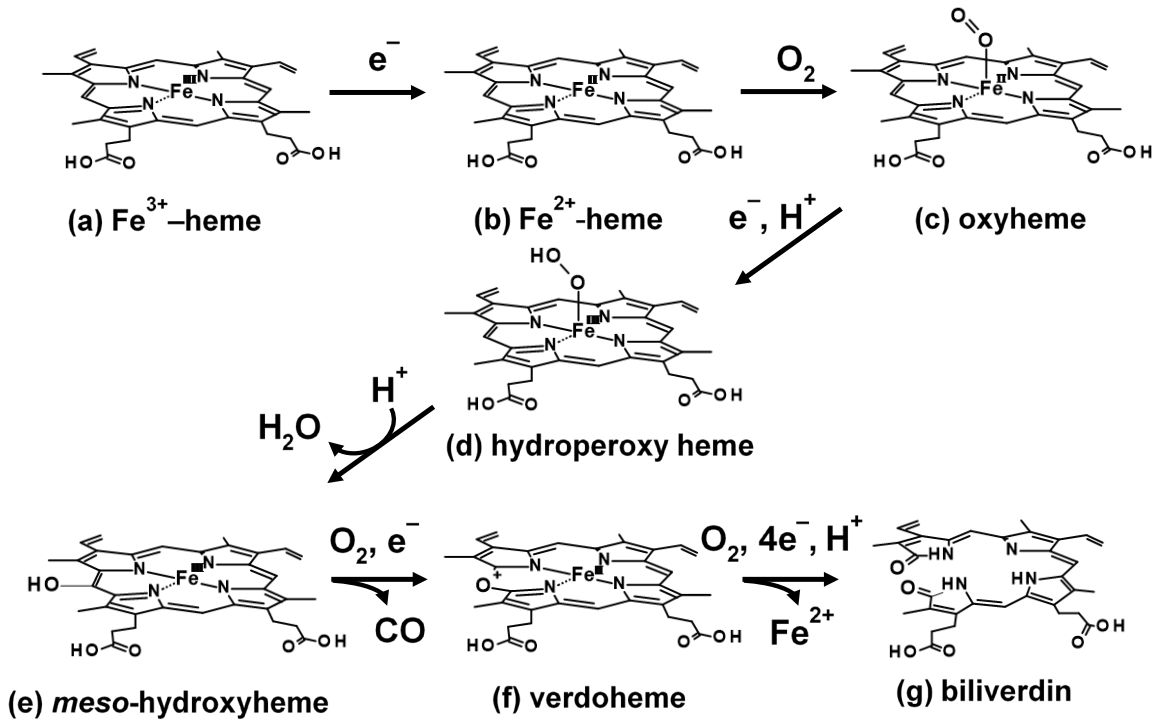

The unusual self-oxygenation reactions of HO are achieved by its unique structure, namely a water cluster in its heme distal pocket (Fig. 2A). The water cluster of HO play critical roles in both *meso*-hydroxylation of heme and ring opening of verdoheme[6,7], whereas no such water

molecules were found in the structure of a homologous protein, HugZ, from *Helicobacter pylori* (Fig. 2B)[8]. The water cluster is also absent in IsdG-type heme degrading enzymes, which produce distinct heme catabolites[9–11]. Recently, an IsdG-type enzyme from *Mycobacterium tuberculosis* is shown to degrade heme by sequential mono- and dioxygenation reactions in contrast to the canonical three monoxygenation mechanisms of HO[12]. The mechanistic diversity prompted us to examine whether HutZ catalyzes the HO-type heme degradation in spite of their structural dissimilarity. In this chapter, I have characterized key reaction intermediates of HutZ, including *meso*-hydroxyheme and verdoheme using UV-visible absorption, thereby determining its heme-degradation mechanism.

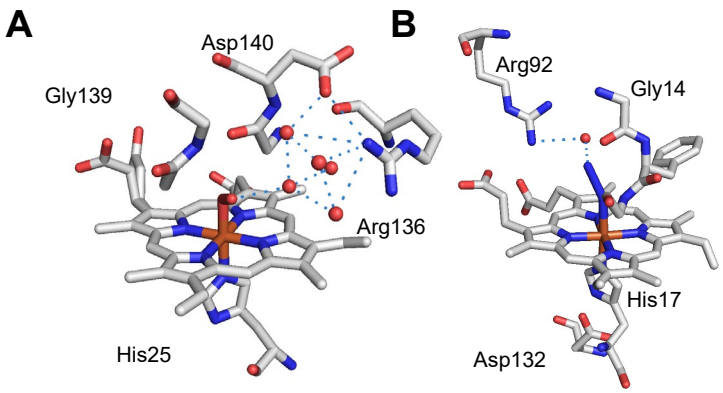

Fig. 2 Crystal structures of (A) rat HO-1 (PDB ID 4G7L) and (B) a HutZ homologous protein HugZ from *Helicobacter pylori* (3GAS). The residue numbering in (B) is based on *V. cholerae* HutZ. In HO-1, Asp140 forms a hydrogen bonding network with a water cluster, which is essential for the heme degradation activity of the enzyme. Arg92 in HugZ forms a hydrogen bond with iron-bound azide through a water molecule.

2.1.2 Materials and Methods

Materials

The chemicals used in this study were purchased from Wako Pure Chemical Industries (Osaka, Japan), Nacalai Tesque (Kyoto, Japan), or Sigma-Aldrich (St. Louis, MO, USA), and used without further purification. $^{18}O_2$ was purchased from Icon Isotopes (Summit, NJ, USA). Nitrogen and $^{16}O_2$ gas were purchased from Tech Air (White Plains, NY, USA)

Expression and Purification

HutZ was expressed in *Escherichia coli* and purified as described previously.[1] Briefly, the *hutZ* gene was subcloned into pET-28b (Merck Millipore, Darmstadt, Germany) via *Nde*I and *EcoR*I sites, and the thrombin recognition site (Leu-Val-Pro-Arg-Gly-Ser) in the pET-28b construct was mutated to the HRV 3C protease recognition site (Leu-Glu-Val-Leu-Phe-Gln-Gly-Pro)[13]. *E. coli* strains transduced with HutZ expression plasmids were grown at 37 °C in LB broth supplemented with 50 μg/mL kanamycin. Expression of His-tagged fusion protein in *E. coli* BL21(DE3) was induced by adding isopropyl-β-D-thiogalactopyranoside to a final concentration of 0.4 mM, after which cells were further incubated at 28 °C overnight. His_6-tagged HutZ was purified by affinity chromatography using a HisTrap HP column (GE Healthcare, Uppsala, Sweden). After cleavage of the His_6-tag, the reaction mixture was applied to the HisTrap column. The column flow-through was collected and then applied to a gel-filtration column (HiLoad 16/60 Superdex 200 pg, GE Healthcare) equilibrated with 50 mM Tris-HCl and 150 mM NaCl (pH 8.0). The protein concentration was determined on the basis of absorbance at 411 nm using extinction coefficient (ε_{412}) of 166 $mM^{-1}cm^{-1}$.[14]

Absorption Spectra Measurements

The reaction of HutZ with H_2O_2 was monitored by UV-visible absorption spectrophotometer (V-660, Jasco, Tokyo, Japan). Briefly, 1.9 mL of hemin-HutZ solution (final concentration, 10

μM) in 50 mM Tris-HCl and 150 mM NaCl (pH 8.0) was placed in a cuvette, and the reaction was started by adding H_2O_2 in the same buffer at 25 °C. Spectra were recorded at 1-min intervals. Time-resolved UV-Vis absorption spectra were measured using stopped-flow apparatus (Applied Photophysics, Surrey, U.K.). The enzyme was rapidly mixed with O_2-containing buffer. The reaction kinetics were monitored using a photodiode array detector, and these data were analyzed with the ProK software from Applied Photophysics.

2.1.3 Results and discussion

Observation of *meso*-hydroxyheme-HutZ

I tried generating the *meso*-hydroxyheme by mixing the ferric heme-HutZ complex with one equivalent of H_2O_2 under an anaerobic condition[15]. An anaerobic condition was essential as O_2 converts *meso*-hydroxyheme to verdoheme in a non-enzymatic fashion (see Fig. 1)[16,17]. The H_2O_2 reaction was monitored by UV-vis absorption spectroscopy. As shown in Fig. 4, following the initiation of the reaction the Soret band at 405 nm decreased with time, which reached a plateau at ~5 min. The spectral change was associated with the appearance of a weak band at ~619 nm, similar to that of the *meso*-hydroxyheme of HO. It has been reported that the α-, β-, and δ-*meso*-hydroxyheme of HO have absorption maxima at 405 nm, with a relatively featureless absorption band in the visible region, while the γ-*meso*-hydroxyheme of HO has an absorption maximum at 413 nm[18]. Hence our current data support the view that the heme of HutZ is cleaved at β- or δ-*meso* carbon[1]. Upon the exposure to O_2, the 405/619 nm species immediately converted to a new species with an intense absorption at 644 nm (Fig. 3, red), which I tentatively assign to the ferric verdoheme-HutZ complex.

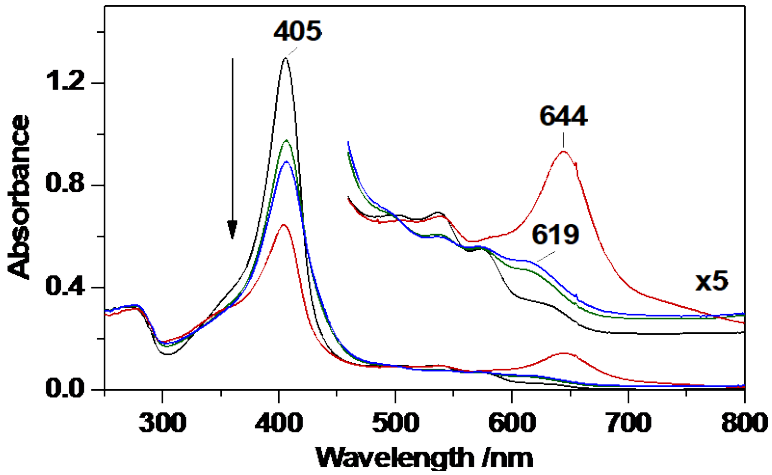

Fig. 3 Reaction of ferric heme-HutZ (10 μM) with 1 equivalent of H_2O_2 at pH 6.0. Black, before the reaction; green and blue, 20 sec and 5 min after the reaction, respectively; red, 15 min after addition of air to the blue species. Reaction was conducted under an anaerobic condition.

Characterization of verdoheme-HutZ

To further confirm the assignment of the 644 nm species, redox dependence of the spectrum was investigated. First, the 644-nm species was produced by reacting the ferric heme-HutZ complex with H_2O_2 under an aerobic condition (Fig. 4, green). Then, remaining H_2O_2 was removed by catalase, followed by anaerobic addition of ascorbic acid. The maximum of the band shifted from 644 to 671 nm (Fig. 4, red), consistent with the formation of the ferrous β-(667-668 nm) or δ-verdoheme (663-664 nm)[18,19]. Further addition of CO to the ferrous verdoheme caused a blue shift of the band to 625 nm (Fig. 4, blue), in good agreement with the production of CO-bound β-verdoheme (623-624 nm) or δ-verdoheme (624-626 nm)[18,19]. These results confirm that the 644-nm species is a ferric verdoheme as typically observed for other HOs, not a ferrous verdoheme.

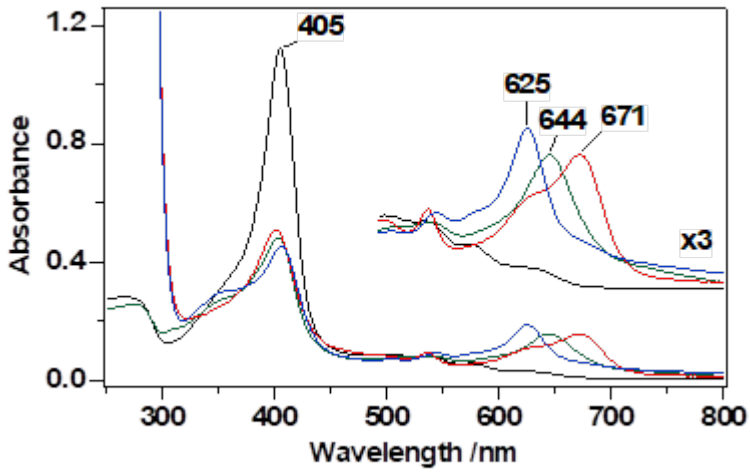

Fig. 4 Absorption spectra of verdoheme-HutZ complex. Black, ferric heme-HutZ; green, Fe^{3+}-verdoheme generated by reaction of ferric heme with 1 equivalent of H_2O; red, Fe^{2+}-verdoheme generated by reaction of Fe^{3+}-verdoheme with 1 mM ascorbic acid; blue, CO-bound Fe^{2+}-verdoheme generated by reaction of Fe^{2+}-verdoheme with CO. Reaction was conducted under an anaerobic condition.

Lastly, I investigated the peroxidation activity of heme-HutZ using *o*-methoxyphenol (guaiacol) as a substrate (Fig. 5). The 470 nm absorption, which is derived from the oxidized guaiacol oligomer, showed a pronounced lag phase (<200 s) before a linear production phase

was observed. During the first stage with negligible peroxidation, absorbance at 644-nm increases due to formation of ferric verdoheme from heme-HutZ. This observation strongly suggests highly efficient self-oxygenation of heme-HutZ to yield *meso*-hydroxyheme without generating ferryl heme. In fact, the anaerobic reaction with one mole equivalent of H_2O_2 (Fig. 4) yields approximately 70 % verdoheme after exposure to air as judged from the absorbance increase at 644-nm. At the latter stage of the peroxidation assay (>200 s), the 470-nm absorbance shows linear increase with small decrease in the 644-nm absorption, suggesting efficient peroxidation by ferric verdoheme. It has been reported that the verdoheme complex of HO-1 is active towards H_2O_2 only in its ferrous state[20], because a water molecule (or OH^-), which is bound to ferric heme as the sixth ligand, inhibits the reaction with H_2O_2. To react with heme, H_2O_2 must replace the water molecule. Therefore, the low reactivity of ferric verdoheme-HO is plausibly ascribed to tight water ligation on the ferric iron, which inhibits the H_2O_2 binding. Accordingly, the unexpected peroxidation activity of ferric verdoheme-HutZ is possibly a result of a weaker water coordination.

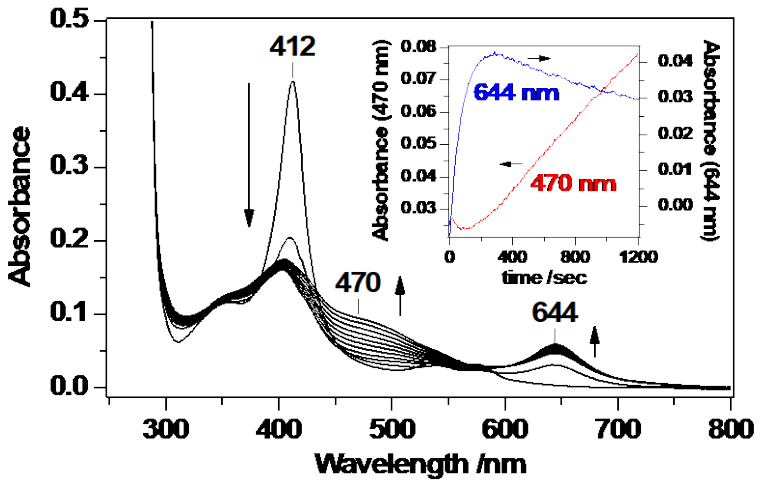

Fig. 5 Reaction of ferric heme-HutZ with H_2O_2 in the presence of 1 mM guaiacol. The inset shows the time courses of the absorbance at 470 and 644 nm. The spectra were measured at 2-min intervals for 30 min after addition of 0.1 mM H_2O_2.

2.1.4. Conclusions

I characterized two intermediates populated during the heme degradation reaction of HutZ from *V. cholerae*: *meso*-hydroxyheme, and verdoheme. HutZ is found to specifically convert the ferric heme into *meso*-hydroxyheme, at least in the reaction with H_2O_2 (Fig. 3), supporting that its active site is highly optimized as a heme-degrading enzyme. The observation that the reaction intermediates of HutZ are similar to those observed in the HO-1 reaction indicates that the heme degradation pathway of HutZ is the same as that of mammalian or canonical HOs, although HutZ has a unique hydrogen bonding between Asp132 and His170, which is disadvantage to degrade heme.

.

Reference

(1) Uchida, T.; Sekine, Y.; Matsui, T.; Ikeda-Saito, M.; Ishimori, K. *Chem. Commun.* **2012**, *48* (53), 6741.

(2) Ortiz de Montellano, P. R. *Acc. Chem. Res.* **1998**, *31* (9), 543.

(3) Matsui, T.; Unno, M.; Ikeda-Saito, M. *Acc. Chem. Res.* **2010**, *43* (2), 240.

(4) Kikuchi, G.; Yoshida, T.; Noguchi, M. *Biochem. Biophys. Res. Commun.* **2005**, *338* (1), 558.

(5) Dojun, N.; Sekine, Y.; Ishimori, K.; Uchida, T. *Dalt. Trans.* **2017**, *46* (16), 5147.

(6) Matsui, T.; Furukawa, M.; Unno, M.; Tomita, T.; Ikeda-Saito, M. *J. Biol. Chem.* **2005**, *280* (4), 2981.

(7) Fujii, H.; Zhang, X.; Tomita, T.; Ikeda-Saito, M.; Yoshida, T. *J. Am. Chem. Soc.* **2001**, *123* (27), 6475.

(8) Hu, Y.; Jiang, F.; Guo, Y.; Shen, X.; Zhang, Y.; Zhang, R.; Guo, G.; Mao, X.; Zou, Q.; Wang, D. C. *J. Biol. Chem.* **2011**, *286* (2), 1537.

(9) Reniere, M. L.; Ukpabi, G. N.; Harry, S. R.; Stec, D. F.; Krull, R.; Wright, D. W.; Bachmann, B. O.; Murphy, M. E.; Skaar, E. P. *Mol. Microbiol.* **2010**, *75* (6), 1529.

(10) Matsui, T.; Nambu, S.; Ono, Y.; Goulding, C. W.; Tsumoto, K.; Ikeda-Saito, M. *Biochemistry* **2013**, *52* (18), 3025.

(11) Unno, M.; Ardèvol, A.; Rovira, C.; Ikeda-Saito, M. *J. Biol. Chem.* **2013**, *288* (48), 34443.

(12) Matsui, T.; Nambu, S.; Goulding, C. W.; Takahashi, S.; Fujii, H.; Ikeda-Saito, M. *Proc. Natl. Acad. Sci.* **2016**, *113* (14), 3779.

(13) Uchida, T.; Sasaki, M.; Tanaka, Y.; Ishimori, K. *Biochemistry* **2015**, *54* (43), 6610.

(14) Wyckoff, E. E.; Schmitt, M.; Wilks, A.; Payne, S. M. *J. Bacteriol.* **2004**, *186* (13), 4142.

(15) Liu, Y.; Moënne-Loccoz, P.; Loehr, T. M.; Ortiz De Montellano, P. R. *J. Biol. Chem.* **1997**, *272* (11), 6909.

(16) Wilks, A.; Ortiz de Montellano, P. R. *J. Biol. Chem.* **1993**, *268* (30), 22357.

(17) Chu, G. C.; Katakura, K.; Zhang, X.; Yoshida, T.; Ikeda-Saito, M. *J. Biol. Chem.* **1999**, *274* (30), 21319.

(18) Zhang, X.; Fujii, H.; Mansfield Matera, K.; Migita, C. T.; Sun, D.; Sato, M.; Ikeda-Saito, M.; Yoshida, T. *Biochemistry* **2003**, *42* (24), 7418.

(19) Sakamoto, H.; Omata, Y.; Adachi, Y.; Palmer, G.; Noguchi, M. *J. Inorg. Biochem.* **2000**, *82* (1–4), 113.

(20) Matsui, T.; Nakajima, A.; Fujii, H.; Matera, K. M.; Migita, C. T.; Yoshida, T.; Ikeda-Saito, M. *J. Biol. Chem.* **2005**, *280* (44), 36833.

Chapter II: Heme Proximal Hydrogen Bonding between His170 and Asp132 Plays an Essential Role in the Heme-Degradation Reaction by HutZ

ABSTRACT

HutZ degrades heme via the same steps as HO-1, although the structure of HutZ is different from that of HO-1. Hydrogen bonding between His170 and Asp132 in HutZ appears to be disfavored in heme-degrading enzymes, because it can contribute to the imidazolate character of the axial histidine, as observed in most heme-containing peroxidases. Thus, I investigated the role of this potential hydrogen bond in the heme degradation reaction by mutating Asp132 to Leu, Asn or Glu, and His170 to Ala. Heme degradation activity was almost completely lost in D132L and D132N mutants, whereas verdoheme formation through reaction with H_2O_2 was comparable in the D132E mutant and wild-type enzyme. However, even at pH 6.0, when the heme is in a high-spin state, the D132E mutant was inactive toward ascorbic acid owing to a significant reduction in its affinity (K_d) for heme (4.1 μM) compared with that at pH 8.0 (0.027 μM). The heme degradation activity of the H170A mutant was also substantially reduced, although this mutant bound heme with a K_d of 0.067 μM, despite the absence of an axial ligand. Thus, this study showed that proximal hydrogen bonding between Asp132 and His170 plays a role in retaining the heme in an appropriate position for oxygen-dependent heme degradation.

2.2.1. Introduction

In Part II of chapter I, I investigated two key intermediates of HutZ, *meso*-hydoxyheme and verdoheme, indicating HutZ is the same intermediates as HO-1, although the structure of HutZ is different from that of HO-1. The structural unique point in HutZ indicates that Asp132 in HutZ is located within hydrogen-bonding distance of the heme axial ligand His170 (Fig. 1). A hydrogen bond between His170 and Asp132 could contribute to the imidazolate character of the axial His, as observed in oxygen-activating heme enzymes (i.e., peroxidases)[1–3]. This unique structure reflects a pH-dependence of the heme degradation activity of HutZ, indicating that HutZ is inactive at pH 8.0, whereas it is active at pH 6.0[4]. Our group found that the activity is correlated with the ratio of high-spin heme (Fe^{3+}–H_2O) to low-spin heme (Fe^{3+}–OH^-) (unpublished observations). Because of the imidazolate character of heme-HutZ, the rate of heme reduction by ascorbic acid is quite low at pH 8.0 (unpublished observations). Thus, the heme degradation reaction is inhibited at the step of heme reduction when ascorbic acid is used as an electron source.

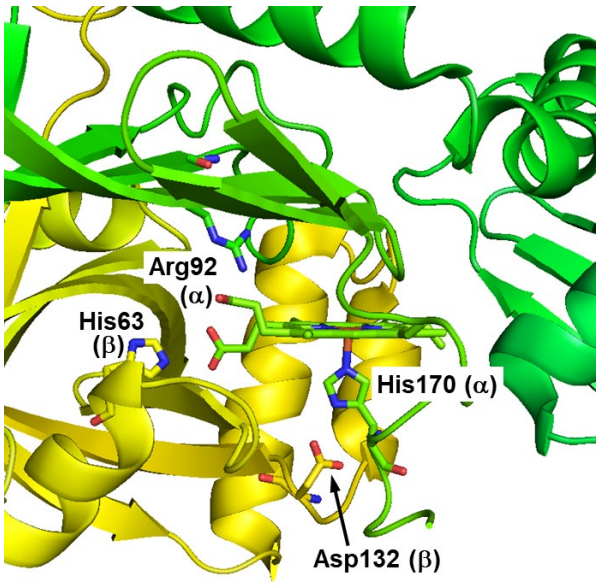

Fig. 1. **Crystal structure of HugZ from *H. pylori* (PDB ID code 3GAS).** Residues are numbered according to the amino acid sequence of HutZ from *V. cholerae*. α and β indicate the subunits.

In mammalian HO-1, the proximal His is hydrogen bonded with Glu29[5,6]. However, this hydrogen bond is not as strong as those observed in peroxidases, because the redox potential is -65 mV[7]. which is far from that of most peroxidases with imidazolate as an axial ligand[8]. Additionally, the Fe-His stretching mode, $\nu_{\text{Fe-His}}$, was observed at 218 cm^{-1},[9] which is almost identical to that observed for myoglobin (220 cm^{-1})[10,11] and hemoglobin (215 and 221 cm^{-1})[12], which contain a typical neutral His as an axial ligand, and is far from that of most peroxidases [13,14]. The weaker hydrogen bond between the proximal His and Glu29 in HO-1 seems to be favorable for the heme degradation reaction, because it prevents the O-O bond of the hydroperoxy species from being cleaved. Considering that the high-valent iron-oxo species has no heme degradation activity,[15] O-O bond cleavage prior to hydroxylation of a *meso*-carbon of the porphyrin ring would not be preferable for heme degradation. Therefore, the role of this weak hydrogen bonding imposed by Glu29 in HO-1 is considered to define the orientation of the proximal His[16].

Despite the prediction of the presence of a hydrogen bond between His170 and Asp132, the $\nu_{\text{Fe-His}}$ of ferrous heme-HutZ is identical to that of heme-HO[4,17], indicating a moderate hydrogen bond. In contrast, on the basis of a correlation plot of $\nu_{\text{Fe-CO}}$ versus $\nu_{\text{C-O}}$, the hydrogen bond between His170 and Asp132 in ferrous CO-bound heme-HutZ is predicted to be stronger than that in other heme-degrading enzymes[4]. This discrepancy seems to be attributed to the presence of the distal heme ligand in heme-HutZ. Formation of the distal hydrogen bond between Arg92 and heme ligand (O_2, CO, or OH^-) would be coupled with formation of the proximal hydrogen bond. The fast autoxidation rate of oxyferrous heme-HutZ supports this conclusion[4].

The strong electron donation from the imidazolate group of the axial His is known to promote heterolytic cleavage of the O-O bond to form a ferryl species (called a 'push' effect)[18]. Because the ferryl species is not susceptible to heme degradation[15], heme-degrading enzymes have evolved to avoid this pathway. Therefore, the presence of a strong hydrogen bond between the proximal His and nearby Asp in HutZ is not expected to be favored in a heme-degrading

enzyme.

In this chapter, I employed two approaches to assess the role of hydrogen bonding between Asp132 and His170. In the first, I replaced Asp132 with Leu, Asn, or Glu; in the second, I substituted Ala for His170. Mutations at both sites led to a significant loss in heme-degrading activity, except the substitution of Glu for Asp132. When the proximal hydrogen bond was intact, heme-HutZ was inactive, because heme could not be reduced to ferrous heme owing to strong electron donation from the proximal His. However, disruption of the hydrogen bond did not lead to a gain of enzymatic activity, likely because the heme was not held in an appropriate position; thus, the proximal hydrogen bond is necessary for heme binding to HutZ. Collectively, only a slight modulation of the strength of the hydrogen bond between His170 and Asp132 is key to activation of the degradation reaction of heme-HutZ.

2.1.2 Materials and Methods

Materials.

The chemicals used in this study were purchased from Wako Pure Chemical Industries (Osaka, Japan), Nacalai Tesque (Kyoto, Japan) or Sigma-Aldrich (St. Louis, MO, USA), and were used without further purification.

Expression and Purification of HutZ.

Mutant HutZ proteins were expressed in *Escherichia coli* and purified as described previously[4]. The *hutZ* gene was subcloned into pET-28b (Merck Millipore, Darmstadt, Germany) via *Nde*I and *EcoR*I sites, and the thrombin recognition site (Leu-Val-Pro-Arg-Gly-Ser) in the pET-28b construct was mutated to the HRV 3C protease recognition site (Leu-Glu-Val-Leu-Phe-Gln-Gly-Pro).[19] Mutagenesis was conducted utilizing a PrimeSTAR mutagenesis basal kit from Takara Bio (Otsu, Japan). DNA oligonucleotides were purchased from Eurofins Genomics Inc. (Tokyo, Japan). The mutated genes were sequenced (Eurofins Genomics Inc., Tokyo, Japan) to ensure that only the desired mutations were introduced.

Measurement of Heme Binding to HutZ.

Heme binding was tracked by difference spectroscopy in the Soret region of the UV-visible spectrum. Successive aliquots of 0.5 mM hemin in 0.1 M NaOH were added to both the sample cuvette, which contained 10 μM apo-HutZ, and the reference cuvette. Spectra were recorded 3 min after the addition of each heme aliquot. The absorbance difference at 411–413 nm was plotted as a function of heme concentration, and the dissociation constant ($K_{d,heme}$) was calculated using the quadratic binding equation,

$$\Delta A = \Delta A_{max} \frac{[P]+[H]+K_{d,heme} - \sqrt{([P]+[H]+K_{d,heme})^2 - 4[P][H]}}{2[P]}, \quad (1)$$

where [P] and [H] represent the total protein and hemin concentrations, respectively. The pH of the protein solution was not changed by the addition of the alkaline hemin solution.

Spectroscopy.

Optical spectra of purified proteins were recorded with a UV-visible spectrophotometer (V-660; Jasco, Tokyo, Japan) at room temperature. Resonance Raman spectra were obtained with a single monochromator (SPEX500M; Jobin Yvon, Edison, NJ, USA) equipped with a liquid nitrogen-cooled CCD detector (Spec-10:400B/LN; Roper Scientific, Princeton, NJ, USA). Excitation wavelengths employed were 413.1 nm, delivered by a krypton ion laser (BeamLok 2060; Spectra Physics, Mountain View, CA, USA), and 441.6 nm, delivered by a helium-cadmium laser (IK5651R; Kimmon Koha, Tokyo, Japan). The laser power at the sample point was adjusted to ~5 mW for the ferric and ferrous forms; a lower power (0.1 mW) was used for the CO-bound form to prevent photodissociation. Raman shifts were calibrated with indene, CCl_4, acetone, and an aqueous solution of ferrocyanide. The accuracy of peak positions of well-defined Raman bands was ±1 cm^{-1}. Samples for resonance Raman experiments were prepared at a concentration of approximately 10 μM in 50 mM Tris-HCl/150 mM NaCl (pH 8.0).

Heme Degradation Activity.

The heme degradation reaction of HutZ was monitored by spectrophotometry. Briefly, 1.9 mL of hemin-reconstituted protein solution (final concentration, 10 μM) in 50 mM Tris-HC/150 mM NaCl (pH 8.0) was placed in a cuvette, and the reaction was started by adding 100 μl of 4 mM H_2O_2 or 20 mM ascorbic acid in the same buffer at 25 °C. Spectra were recorded at 1-min

intervals for 10 min for H_2O_2, and at 2-min intervals for 30 min for ascorbic acid. In the case of reactions with ascorbic acid (final concentration, 1 mM), 1 mg/mL of bovine liver catalase was added to suppress H_2O_2. After the reaction, ferrozine (Dojindo, Kumamoto, Japan) was added to a final concentration of 1 mM. The amount of released iron was calculated by measuring absorbance at 562 nm using an extinction coefficient (ε_{562}) of 29 $mM^{-1}cm^{-1}$.

Cyanide Binding Rate Constants.

Cyanide (CN) binding was measured using a stopped-flow apparatus (Unisoku, Osaka, Japan) by following the decrease in absorbance at 412 nm. In a typical CN binding experiment, one syringe contained 3 μM HutZ (50 mM Na-Pi/150 mM NaCl, pH 8.0), and second syringe contained at least a 100-fold excess of CN. Three determinations were performed for each ligand concentration. The mean of the pseudo-first-order rate constants, k_{obs}, was used to calculate second-order rate constants, obtained from the slope of a plot of k_{obs} versus ligand concentration ($k_{obs} = k_{on}[CN] + k_{off}$).

2.2.3. Results

Purification and Heme Reconstitution of Asp132 Mutants.

Three Asp132 mutant proteins (D132L, D132N, and D132E) were purified using the same procedure used for wild-type (WT) HutZ[4]. Elution profiles of gel-filtration columns showed that all three mutants, like the WT, exist as a dimer (data not shown). Titration of the mutants with heme was monitored using difference absorption spectra, which provided dissociation constant ($K_{d,heme}$) values of 0.47 ± 0.07, 0.15 ± 0.02, and 0.027 ± 0.004 μM for D132L, D132N, and D132E mutants, respectively (Fig. 2, insets; Table 1). A comparison of these values with that for WT HutZ (0.052 ± 0.004 μM)[4] showed that replacement of Asp132 with Leu or Asn resulted in approximately a 5–10-fold decrease in heme affinity, where replacement with Glu had little effect.

Absorption Spectra of Heme-Asp132 Mutants.

Absorption spectra of heme-Asp132 mutants are shown in Fig. 2. The Soret maximum of the ferric heme of the heme-D132L mutant was 410 nm, which is slightly blue-shifted from the 412 nm peak for heme-WT HutZ, indicating a slight decrease in the content of low-spin heme (Fig. 2A). Upon reduction, the Soret band shifted to 429 nm, with a Q-band of 555 nm, and addition of carbon monoxide (CO) to the reduced heme shifted the Soret band to 418 nm, with Q-bands of 538 and 570 nm. The absorption spectra of heme-D132N and heme-D132E were almost the same as those for heme-WT HutZ (Fig. 2B, C).

Table 1. Heme dissociation constant (K_d) and kinetic constants of H_2O_2 and CN (k_{Soret} and k_{CN}) for heme-WT and Asp132 mutants of HutZ

	$K_{d,heme}$		k_{Soret}	k_{CN}	Ref.
	pH 8.0	pH 6.0			
	μM		min^{-1}	$mM^{-1}s^{-1}$	
WT	0.052 ± 0.004	0.13 ± 0.06	0.52 ± 0.06	0.88 ± 0.01	4
D132L	0.47 ± 0.07	ND[a]	0.24 ± 0.01	1.26 ± 0.02	this study
D132N	0.15 ± 0.02	1.9 ± 0.3	0.35 ± 0.02	0.77 ± 0.01	this study
D132E	0.027 ± 0.004	4.1 ± 6.5	0.42 ± 0.02	0.99 ± 0.01	this study

[a]ND, not determined owing to extremely weak affinity.

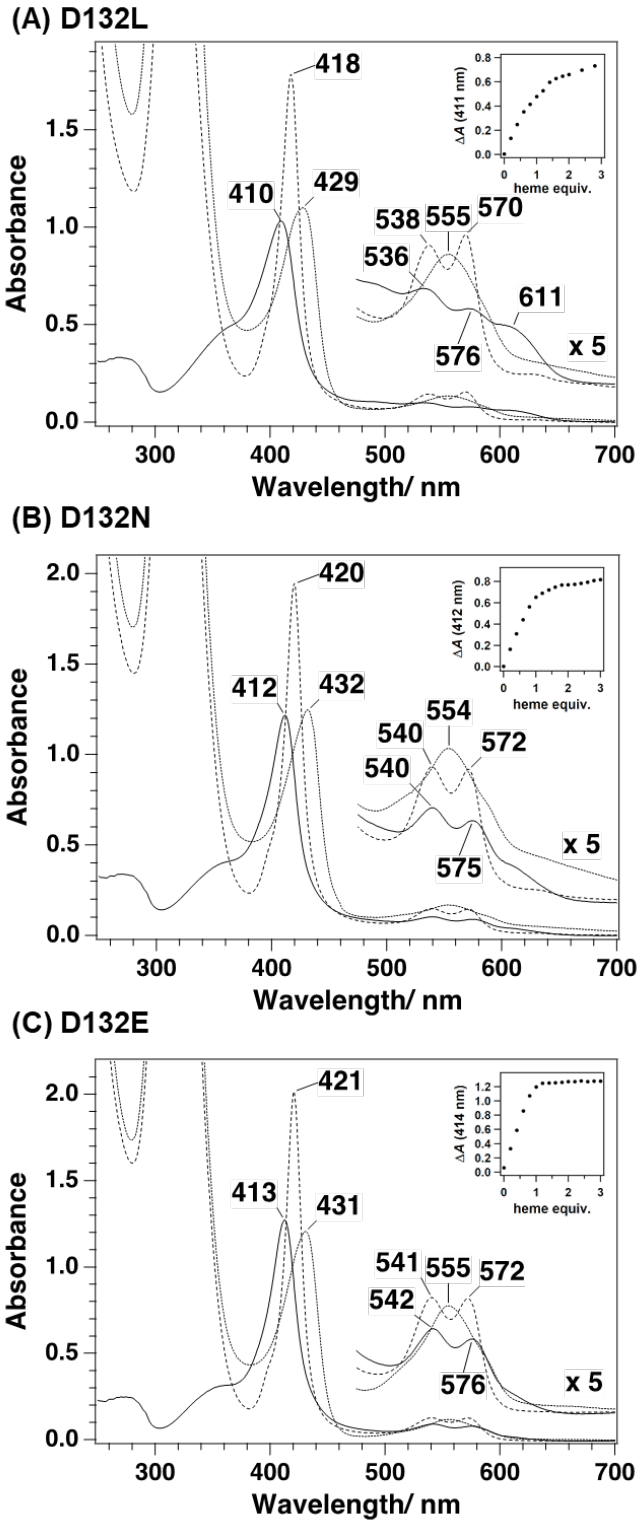

Fig. 2. **Absorption spectra of the heme-HutZ complex.** The protein concentration was 5 μM (on a per heme basis) in 50 mM Tris-HCl/150 mM NaCl, pH 8.0. Spectra shown are in the ferric (solid line), ferrous (dotted line), and CO-bound (dashed line) forms. Inset: Heme-binding curve generated from difference absorbance spectra by plotting ΔA versus the molar ratios of heme to the protein. (A) Heme-D132L; (B) heme-D132N; and (C) heme-D132E.

Reaction of Heme-Asp132 Mutants with H_2O_2.

The heme degradation reaction of heme-Asp132 mutants was first examined using H_2O_2 as an electron source. In the reaction of heme-D132L mutant with H_2O_2, the Soret band gradually diminished (Fig. 3A). The time course of the decrease in the Soret band for the heme-D132L mutant yielded a rate constant (k_{Soret}) of 0.24 min^{-1}, which is ~2-fold smaller than that of heme-WT (0.52 min^{-1}) (Table 1). In contrast to the reaction of heme-WT HutZ with H_2O_2, in which the 644-nm band derived from verdoheme increased with time[4], the absorption at approximately 650 nm was increased only slightly in the heme-D132L mutant, indicating that verdoheme did not accumulate in this mutant. Addition of pyridine to the reaction solution provided no absorption at around 660 nm supported this conclusion (data not shown). Replacement of Asp132 with Asn caused absorbance of the Soret band to disappear slightly faster than that of the heme-D132L mutant in the reaction with H_2O_2 (Fig. 3B); k_{Soret} for the heme-D132N mutant was 0.35 min^{-1} (Table 1). The 654-nm band was smaller than that of the heme-WT enzyme[4], but was slightly larger than that observed in the heme-D132L mutant (Fig. 3A).

As described above, mutation of Asp132 to Leu or Asn led to a dramatic decrease in verdoheme formation (Fig. 3A and 3B), indicating that the hydrogen bond between Asp132 and His170 is important for the heme degradation reaction of HutZ. Hence, I next mutated Asp132 to Glu, which has a carboxylic acid group like the WT enzyme. In the reaction of the heme-D132E mutant with H_2O_2, the absorbance at 412 nm decreased with a concomitant increase in absorbance at ~652 nm (Fig. 3C). This behavior is quite similar to that observed for heme-WT HutZ[4], but different from that of heme-D132L and heme-D132N mutants (Fig. 3A and 3B). Accordingly, Glu at position 132 can play the same role as Asp in the heme degradation reaction of HutZ when H_2O_2 is used as an electron donor.

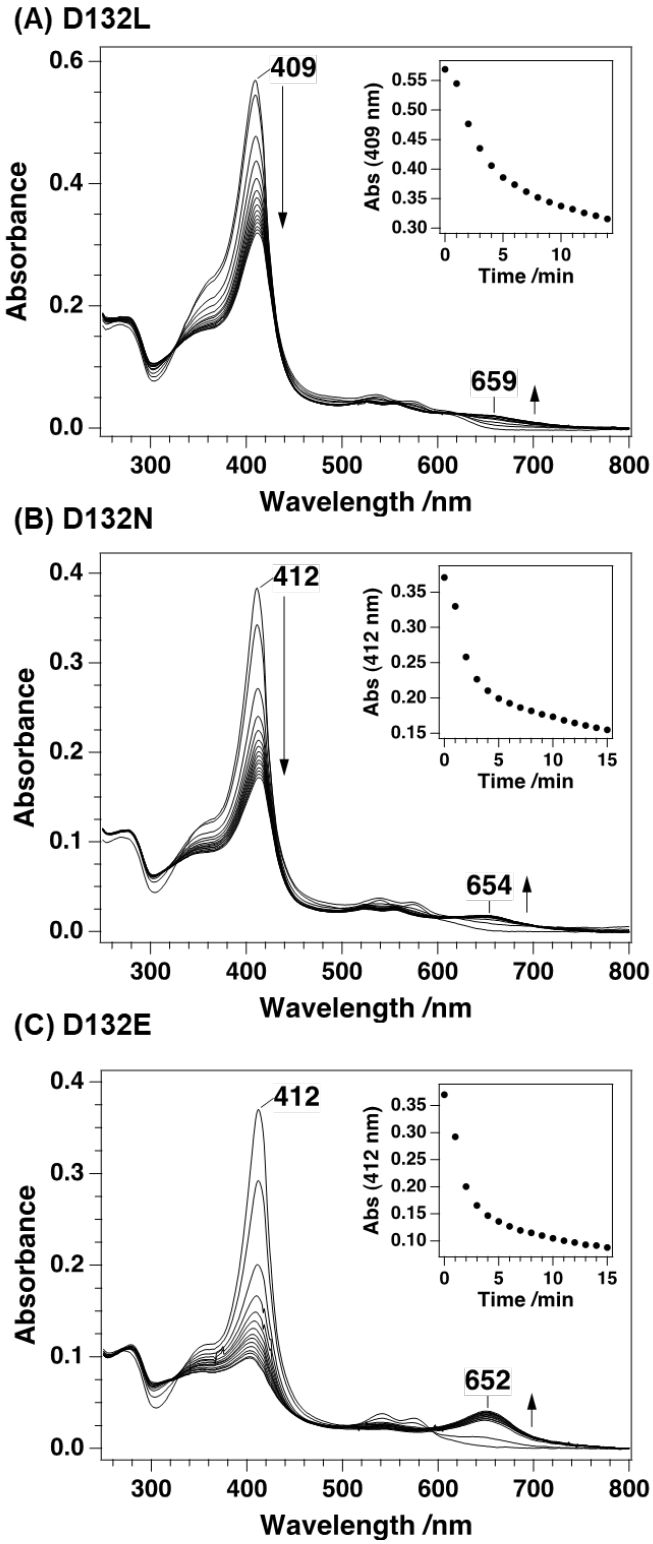

Fig. 3. **Heme degradation reaction of the heme-HutZ complex with H_2O_2 (0.2 mM) at pH 8.0**. Spectra were measured before addition of H_2O_2, and at 1-min intervals for 15 min after addition of H_2O_2. Inset: Time course of absorbance at the Soret maximum. (A) Heme-D132L; (B) heme-D132N; and (C) heme-D132E.

Ligand Binding Rates of Heme-Asp132 Mutants.

If mutation of Asp132 induces a conformational change that inhibits the binding of H_2O_2 to the heme, the heme degradation reaction should be slower. To determine whether these mutants induce a conformational change, I measured their ligand-binding rates. CN ion was used as a probe for evaluating the accessibility of ligands to the active site, and the rate of CN binding ($k_{on,CN}$) was determined using a stopped-flow apparatus. A typical time trace for the reaction of the heme-D132L mutant with CN ion, monitored at 407 nm, is shown in Fig. 4A. Under conditions of excess of CN, the pseudo-first-order rate constants (k_{obs}) obtained from single-exponential fits increased linearly with increasing concentrations of CN (Fig. 4B). The second-order rate constant ($k_{on,CN}$) for the heme-D132L mutant obtained from the slope was 1.26 $mM^{-1}s^{-1}$, which is somewhat faster than that of heme-WT HutZ (0.88 $mM^{-1}s^{-1}$) (Table 1). Therefore, decreased ligand accessibility to the heme does not account for the small amount of verdoheme formation in the D132L and D132N mutants.

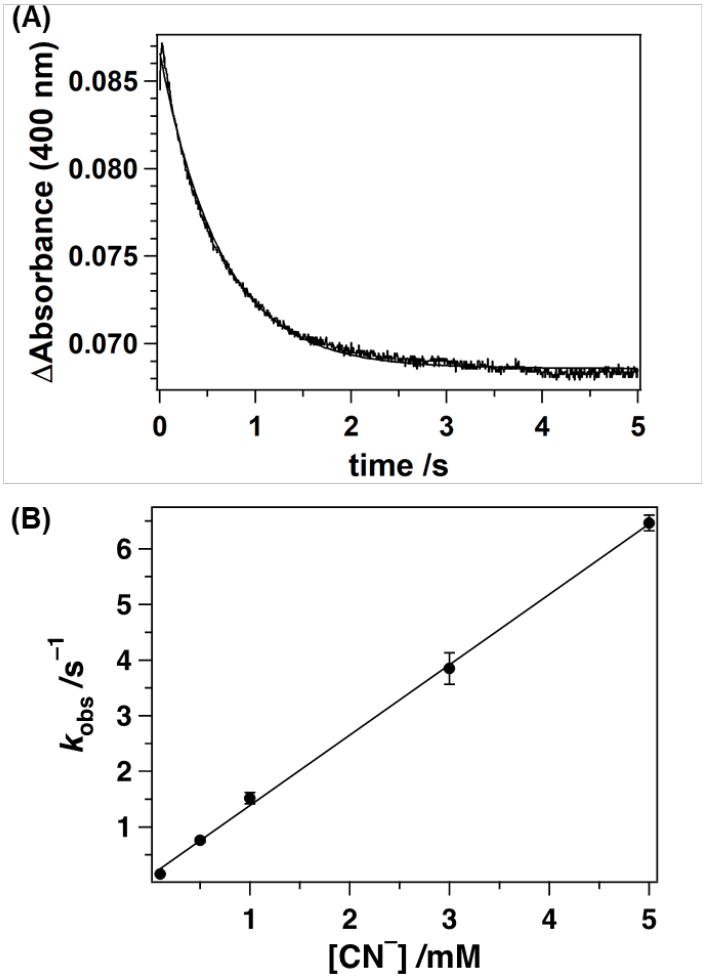

Fig. 4. **CN binding to the heme-D132L mutant.** (A) Typical time trace of absorbance changes at 400 nm upon mixing 5 μM protein with 1 mM CN in 50 mM Tris-HCl/150 mM NaCl (pH 8.0), and (B) plots of calculated k_{obs} versus CN concentration.

Reaction of Heme-Asp132 Mutants with Ascorbic Acid.

The heme degradation reaction of heme-Asp132 mutants was also examined using ascorbic acid as an electron donor. All reactions were conducted in the presence of catalase to scavenge H_2O_2. Spectral changes following addition of ascorbic acid at pH 8.0 are shown in Fig. 5. In reactions of all three Asp132 mutants, the Soret band diminished very little, and no clear band was observed in the 500–800 nm region derived from the products of heme degradation[20]. These spectral changes suggest that no heme degradation occurred for the heme-Asp132 mutants under these reaction conditions, similar to previously reported results for heme-WT HutZ.[4]

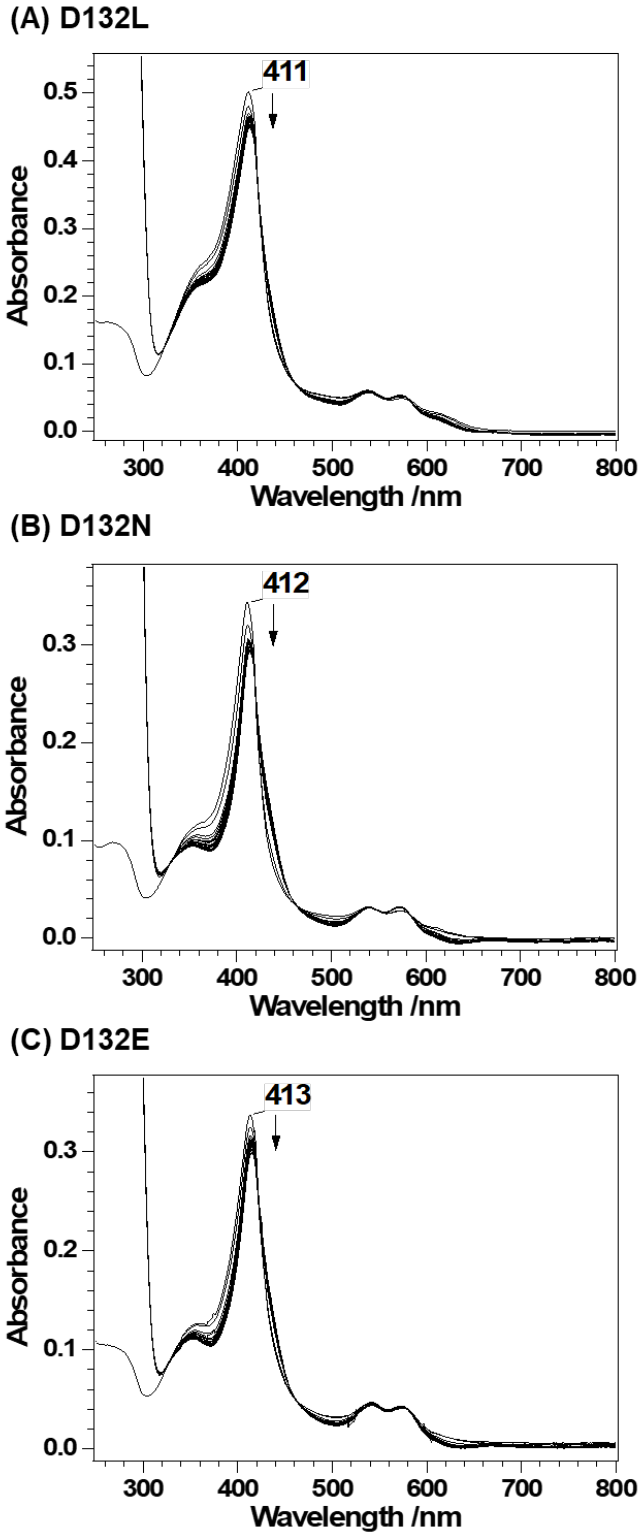

Fig. 5. **Heme degradation reaction of the heme-HutZ complex with ascorbic acid (1.0 mM) at pH 8.0**. Spectra were measured before addition of ascorbic acid, and at 2-min intervals for 30 min after addition of ascorbic acid. (A) Heme-D132L; (B) heme-D132N; and (C) heme-D132E

As reported previously[4], the heme degradation reaction of heme-WT HutZ with ascorbic acid is significantly accelerated at pH 6.0. This activation is related to a change in the heme spin-state: when the heme is in a low-spin state, the enzyme is inactive, whereas it is active when the heme is in a high-spin state. Upon lowering the pH to 6.0, the Soret band of all three Asp132 mutants shifted to 403 nm (Fig. 6A), indicating that some low-spin heme was converted to high-spin heme. Additionally, the absorbance at ~370 nm was significantly enhanced, suggesting that heme was partially released from the protein. In the reaction of the heme-D132E mutant, which showed a similar amount of verdoheme in the reaction with H_2O_2, the Soret band at 401 nm was significantly diminished with ascorbic acid at pH 6.0 (Fig. 6B). To quantify the amount of Fe^{2+} released by the reaction, I added ferrozine to the solution after the reaction. No increase in absorbance at 562 nm, which is derived from the Fe^{2+}-ferrozine complex, was observed. The yields of Fe^{2+} for the all three Asp132 mutant were less than 10%, which is significantly smaller than that of WT (~80%). These results indicate that the Soret band decreased upon reaction of the D132E mutant with ascorbic acid at pH 6.0, but almost no Fe^{2+} was released from the heme during the reaction. A new band appeared at 430 nm in the reaction with ascorbic acid, indicating accumulation of ferrous heme. Therefore, the heme in the Asp132 mutants was reduced and partly broken, but iron remains in the macrocycle, which suggests that heme is degraded in a different manner from that by which WT HutZ degrades heme, owing to the unstable heme ligation.

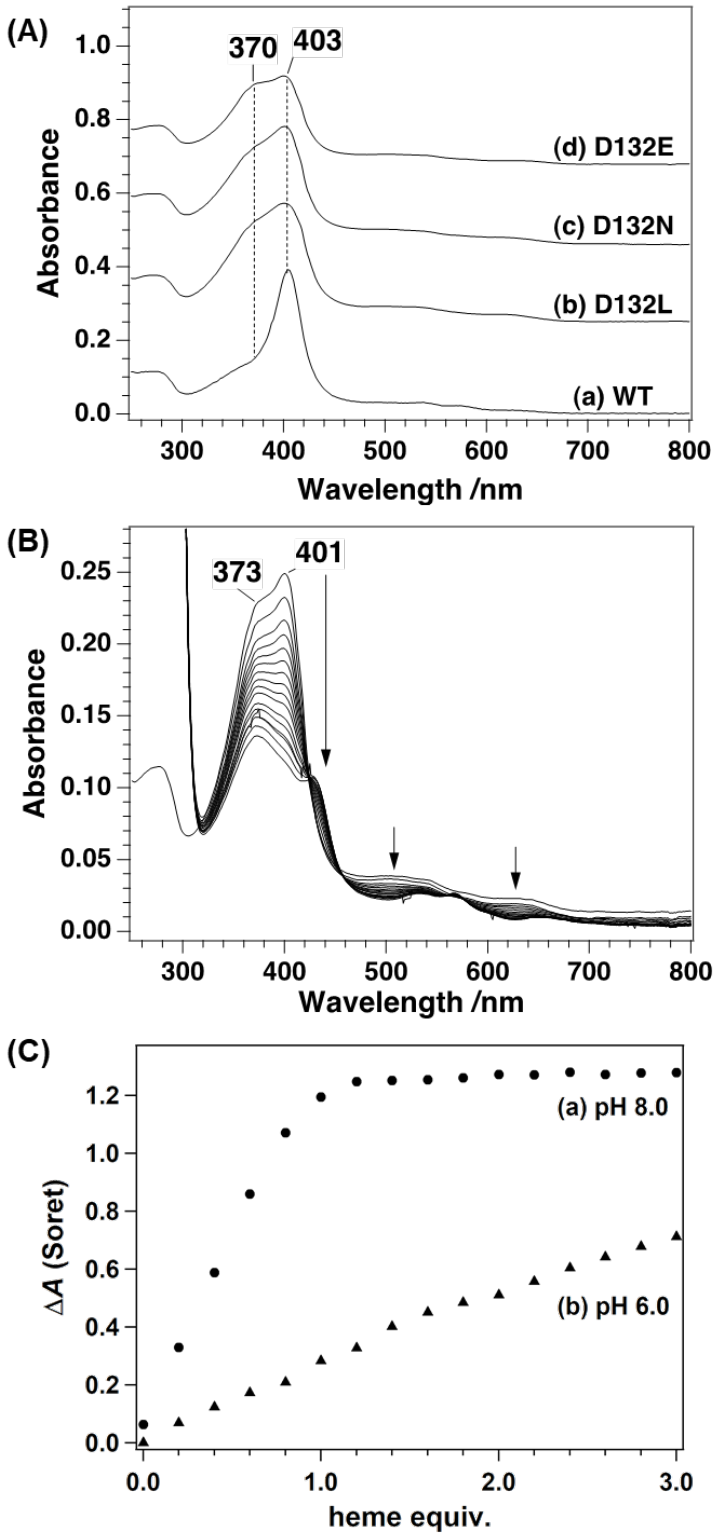

Fig. 6. (A) Absorption spectra of heme-Asp132 mutants and heme-WT HutZ at pH 6.0. (B) Heme degradation reaction of the heme-D132E mutant with ascorbic acid (1.0 mM) at pH 6.0. Spectra were measured before addition of ascorbic acid, and at 2-min intervals for 30 min after addition of ascorbic acid. (C) Heme-binding curve generated from difference absorbance spectra by plotting ΔA versus the molar ratios of heme to D132E mutant at pH 8.0 (a) and pH 6.0 (b)

Resonance Raman Spectra of Heme-Asp132 Mutants.

The active site structures of Asp132 mutants were investigated by resonance Raman spectroscopy. Fig. 7 shows the resonance Raman spectra of these heme-Asp132 mutants. For the heme-D132L mutant (Fig. 7A), the intensity of the band at 1490 cm^{-1}, which is derived from the five-coordinate high-spin heme, increased significantly at the expense of the band at 1503 cm^{-1} compared with that of heme-WT HutZ. The increase in the 1490 cm^{-1} band in the heme-D132L mutant suggests that replacement of Asp132 with Leu induces partial elimination of the sixth ligand, probably a hydroxide ion, from the heme. The spin-state marker bands ν_3 for the ferric heme-D132N and heme-D132E mutants were mainly composed of a band at 1503 cm^{-1} (Fig. 7A), which is derived from the six-coordinate low-spin heme, as observed in heme-WT HutZ. These findings indicate that the spin-state of heme remains intact in the D132N and D132E mutants.

Fig. 7B shows the resonance Raman spectra for the ferrous form excited at 441.6 nm. It is well known that resonance Raman spectra for proteins with ferrous five-coordinate species contain the Fe-His stretching mode, $\nu_{Fe\text{-}His}$, at 200–250 cm^{-1}.[11,21] The $\nu_{Fe\text{-}His}$ mode for heme-D132L mutants was observed at 210 cm^{-1}, which is dramatically downshifted from the 227 cm^{-1} value observed in the heme-WT enzyme[4]. This downshift implies disruption of hydrogen bonding between the proximal His and the amino acid residue at position 132. In contrast, the frequency of $\nu_{Fe\text{-}His}$ for the heme-D132N mutant was 219 cm^{-1}, a value much close to that of heme-WT HutZ. This frequency of $\nu_{Fe\text{-}His}$ suggests that the amide group of Asn132 forms a relatively weak hydrogen bond with His170. The frequency of $\nu_{Fe\text{-}His}$ for the heme-D132E mutant was 227 cm^{-1}, a value identical to that of heme-WT HutZ, although the intensity of the band was decreased.

Resonance Raman spectra of CO-bound heme-Asp132 mutants in the low-frequency region are shown in Fig. 7C. For all these mutant enzymes, two isotope-sensitive bands were observed

at 503 and 519 cm^{-1}, both of which were assignable to the Fe-CO stretching mode ($\nu_{Fe\text{-}CO}$) based on the $^{13}C^{18}O$ isotope shift. The frequency of 503 cm^{-1} was almost the same as that observed for heme-WT HutZ with six-coordinate CO-heme[4], whereas that of 519 cm^{-1} would be derived from five-coordinate CO-heme[22]. In contrast, the C-O stretching mode, $\nu_{C\text{-}O}$, was observed at 1963, 1936 and 1933 cm^{-1} for heme-D132L, heme-D132N and heme-D132E mutants, respectively (Fig. 8). Correlation plots of $\nu_{Fe\text{-}CO}$ versus $\nu_{C\text{-}O}$ for the three Asp132 mutants are shown in Fig. 7D. These spectra imply that replacement of Asp with Glu keeps the structure of the heme environmental intact.

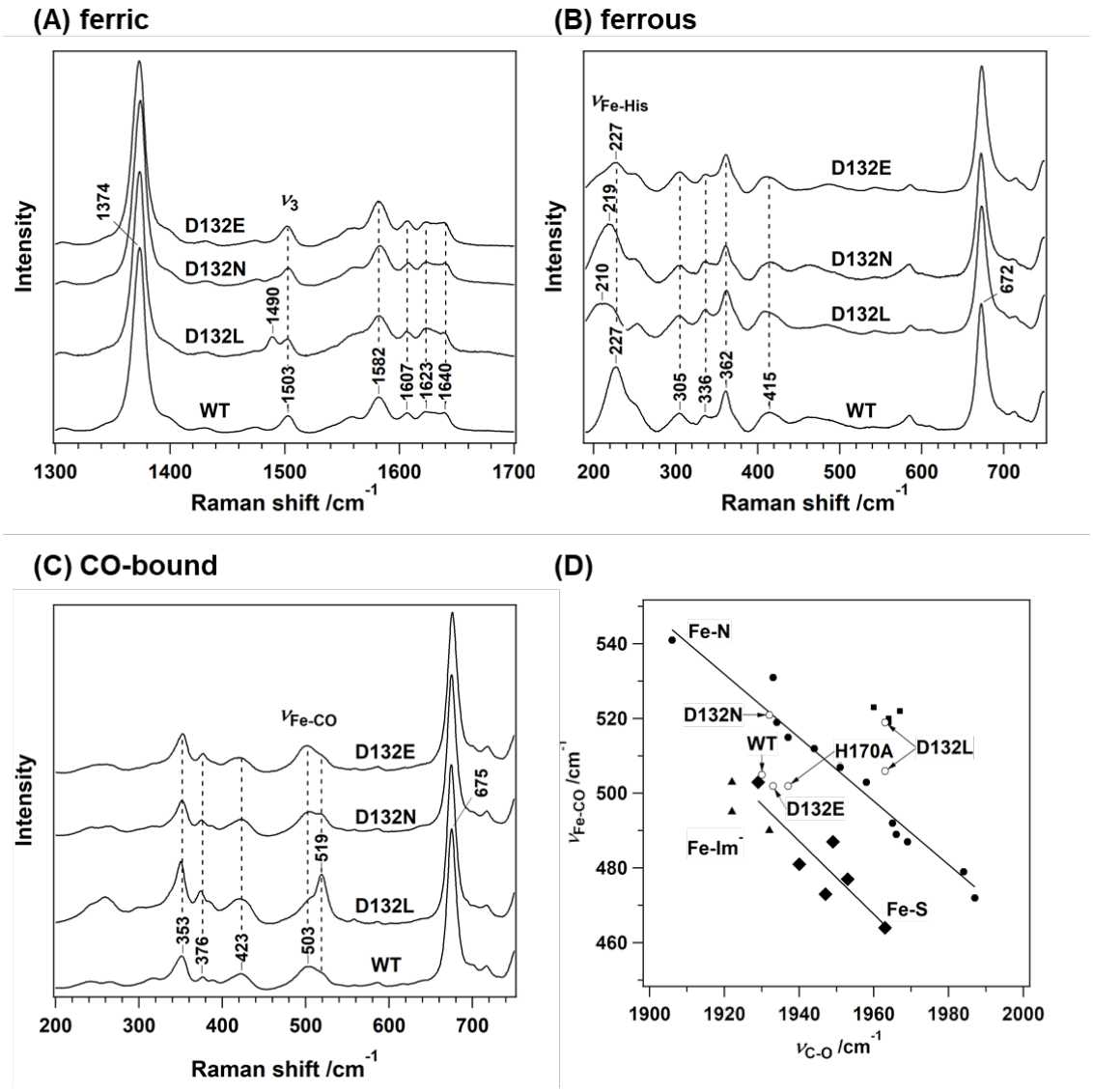

Fig. 7. **Resonance Raman spectra of the heme-HutZ complex.** The protein concentration was 10 μM in 50 mM Tris-HCl/150 mM NaCl, pH 8.0. The excitation wavelength for ferric and CO-bound forms was 413.1 nm, and that for the ferrous form was 441.6 nm. (A) Ferric form in the high-frequency region; (B) ferrous form in the low-frequency region; (C) CO-bound form in the low-frequency region; and (D) correlation plot of frequency of $\nu_{Fe\text{-}CO}$ versus $\nu_{C\text{-}O}$. The two solid lines correspond to correlations for proximal imidazoles (solid black circles), proximal imidazolate (solid green triangles), and thiolate-ligated hemoproteins (solid diamonds). Data points for oxidase superfamily members are depicted as solid squares. The data point for heme-HutZ is presented as an open circle in red. The data shown in the $\nu_{Fe\text{-}CO}$ versus $\nu_{C\text{-}O}$ inverse correlation plot are taken from references [23–25].

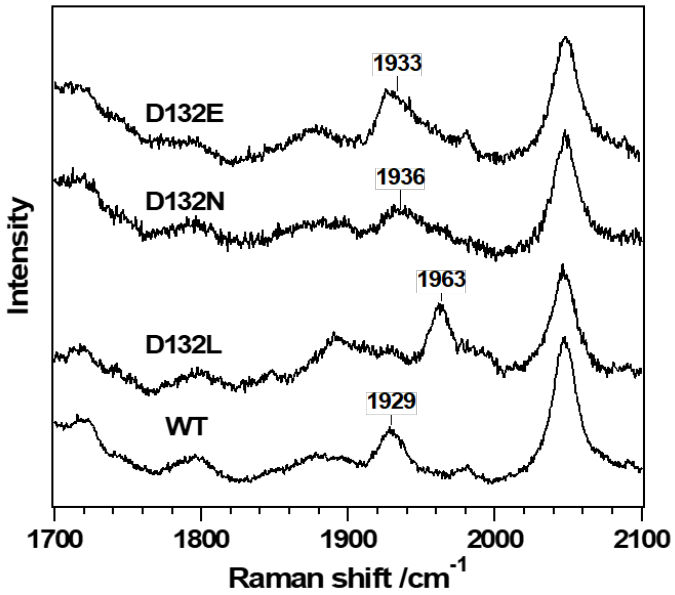

Fig. 8. Resonance Raman spectra of the heme-Asp132 mutants and heme-WT HutZ in the CO-bound form.

Purification of the H170A Mutant.

The H170A mutant was also purified using the same procedure as used for the WT enzyme[4]. The elution profile of the H170A mutant in gel-filtration chromatography was almost identical to that of WT HutZ (data not shown), indicating that the mutant, like WT HutZ, also forms a dimer. The mutant protein was purified in an apoprotein form. Titration of the mutant with heme was monitored by difference absorption spectra as was done for the Asp132 mutant. The titration curve clearly indicated that the H170A mutant is capable of binding heme. The calculated $K_{d,heme}$ value for the H170A mutant was 0.067 ± 0.011 μM (Fig. 9, inset), which is comparable to that of WT HutZ[4], despite removal of the proximal His. To further determine whether heme was retained in the protein or was released from the protein into the buffer, I conducted a gel-filtration experiment. The absorption spectrum of the heme-H170A complex was not altered after passing over the gel-filtration column, indicating that heme in the H170A mutant was retained in the protein, even in the absence of a heme axial ligand.

Fig. 9 shows the absorption spectrum of purified H170A reconstituted with an equivalent amount of hemin. The spectrum has a Soret maximum at 410 nm and absorption bands in the visible region at 541 and 577 nm, which are almost the same as those of the heme-D132L mutant protein (Fig. 2A). Although the peak of the Soret band was slightly blue-shifted compared with that of the heme-WT HutZ complex[4], the spectral features show that the ferric heme-H170A mutant is mainly constituted of six-coordinate low-spin heme, as observed in heme-WT HutZ[4], despite replacement of the heme axial ligand with Ala. Upon reduction, the Soret band was red-shifted to 433 nm, with a Q-band at 558 nm, suggesting that ferrous heme is in a five-coordinate high-spin state. Upon addition of CO to the ferrous heme, the Soret band shifted to 420 nm and two peaks appeared at 541 and 572 nm.

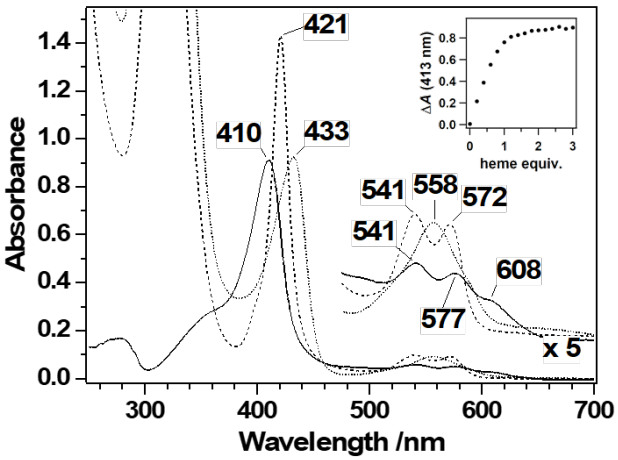

Fig. 9. **Absorption spectra of the heme-H170A mutant.** The protein concentration was ~5 μM in 50 mM Tris-HCl/150 mM NaCl, pH 8.0. Spectra shown are in the ferric (solid line), ferrous (dotted line), and CO-bound (dashed line) forms. Inset: Heme-binding curve generated from difference absorbance spectra by plotting ΔA_{413} versus the molar ratios of heme to the protein

His170/His63 Double Mutant.

The H170A mutant displayed a heme-binding affinity similar to that of WT HutZ, and the shapes of absorption spectra were also comparable to those seen in heme-WT[4]. These results indicate that a nearby His alternatively binds to heme as an axial ligand. A closer look at the

crystal structure of HugZ, a homolog of HutZ, suggests that His63 is the sole possible heme ligand (Fig. 1). To confirm the coordination of His63 to heme in the hemin-reconstituted H170A mutant, I constructed a H63L/H170G double mutant. A heme titration experiment revealed that this double mutant had almost completely lost the ability to bind heme (Fig. 10). These results clearly indicate that His63 makes a coordination bond with heme in the H170A mutant.

Fig. 10. Heme titration plot of the H63L/H170G double mutant.

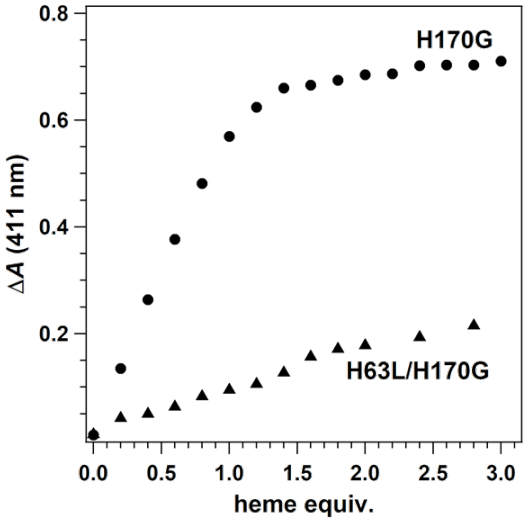

Heme Degradation Reaction of the Heme-H170A Mutant.

The heme degradation reaction of the heme-H170A mutant was first monitored using H_2O_2 (Fig. 11A). During the reaction, the intensity of the Soret band decreased, with a moderate increase in the absorbance at ~672 nm derived from verdoheme (k_{Soret} = 0.58 min^{-1}). This result indicates that the heme-H170A mutant retains heme degradation activity. Added excess imidazole replaces the internal heme ligand, His63, in the heme-H170A mutant. Therefore, the same reaction was conducted in the presence of 10 mM imidazole. Under these conditions, the Soret band decreased, with a k_{Soret} of 0.35 min^{-1}, but absorption at ~670 nm was smaller than that observed in the heme-H170A mutant in the absence of added imidazole (Fig. 11B). This behavior is similar to that of the heme-D132N mutant, indicating that exogenous imidazole does not help restore heme degradation activity. This characteristic is clearly different from that

of other heme-degrading enzymes[26–28].

The heme degradation activity of the heme-H170A mutant was also examined using ascorbic acid as an electron donor. The Soret band was only slightly diminished after addition of ascorbic acid at pH 8.0, and no clear band was observed in the 500–800 nm region (Fig 11C). This behavior is the same as that observed for heme-WT HutZ[4]. In the case of heme-WT, the enzyme is converted to an active form at lower pH[4]. However, almost no heme degradation occurred in the heme-H170A complex, even at pH 6.0, although the heme was converted to the high-spin state (Fig. 11D). Thus, replacement of His170 with Ala eliminates pH-dependent activation.

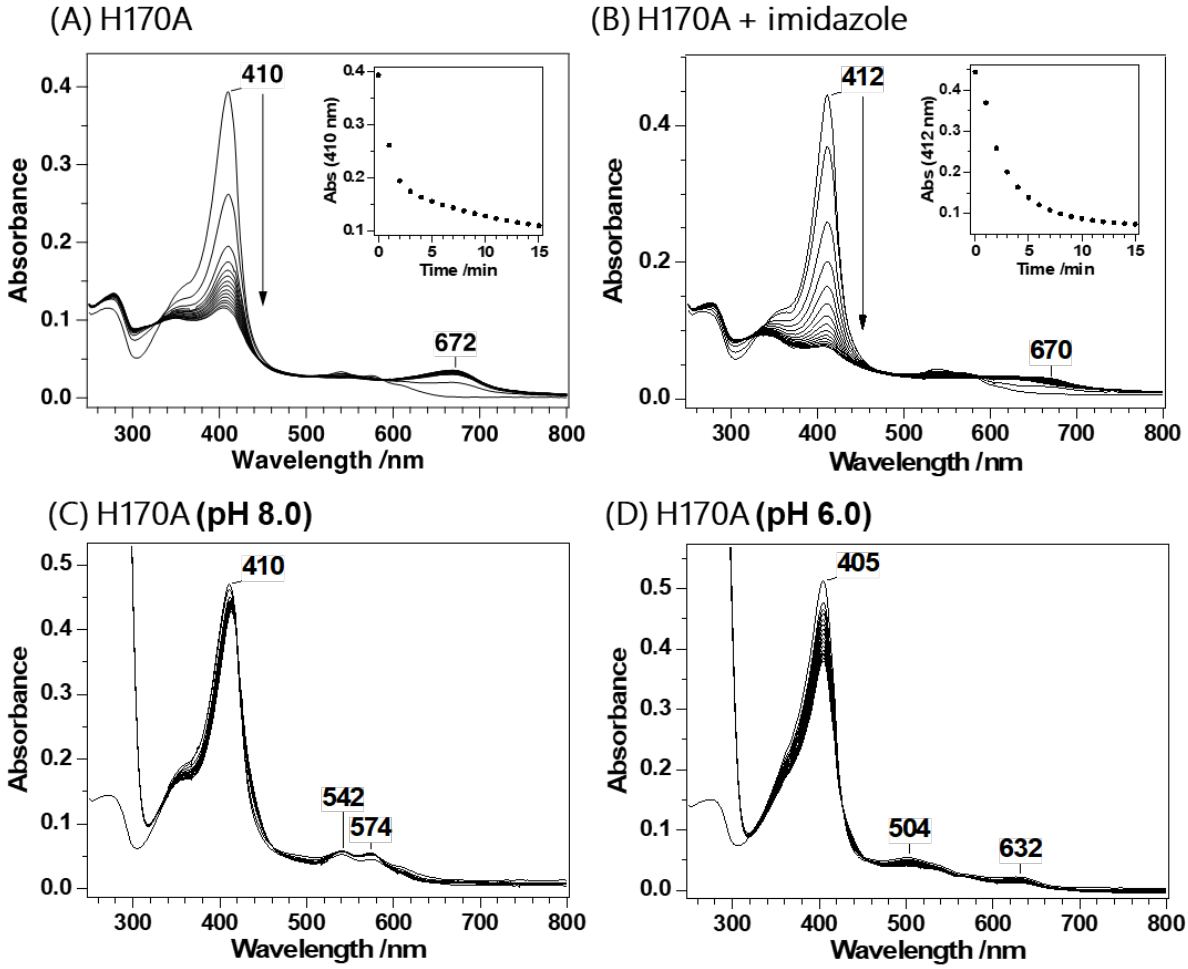

Fig. 11. **Heme degradation reaction of the H170A mutant**. Reaction with 0.2 mM H_2O_2 at pH 8.0 in the (A) absence and (B) presence of 2000 equivalents of imidazole. Reaction with mM ascorbic acid at (C) pH 8.0 and (D) pH 6.0.

Resonance Raman Spectra of the H170A Mutant.

Resonance Raman spectra of the heme-H170A HutZ mutant are illustrated in Fig. 12. The spin-state marker band, ν_3, for the ferric heme-H170A mutant contains three bands at 1474, 1490, and 1502 cm^{-1} characteristic of the six-coordinate high-spin, five-coordinate high-spin, and six-coordinate low-spin heme, respectively (Fig 12A). In the spectrum of the ferrous heme-H170A mutant, the $\nu_{Fe\text{-}His}$ band was observed at 228 cm^{-1} (Fig. 12B), supporting His coordination in the heme-H170A mutant, even though the intact axial His was replaced by Ala. The frequency of the $\nu_{Fe\text{-}His}$ of the heme-H170A mutant was close to that of heme-WT HutZ (227 cm^{-1})[4]. Addition of exogenous imidazole to the heme-H170A mutant enhanced $\nu_{Fe\text{-}His}$ and slightly upshifted it to 231 cm^{-1} (Fig. 12B), indicating that the probable heme ligand, His63, in this mutant was replaced with the exogenous imidazole.

An isotope-sensitive band appeared at 502 cm^{-1} for the CO-bound heme-H170A mutant (Fig. 12B). On the basis of the isotope shifts, this 502 cm^{-1}-band, which was almost the same as that observed in the heme-WT[4], was assigned to $\nu_{Fe\text{-}CO}$. The $\nu_{C\text{-}O}$ mode appeared at 1955 cm^{-1}; the frequencies of $\nu_{Fe\text{-}CO}$ and $\nu_{C\text{-}O}$ are plotted in Fig. 7D.

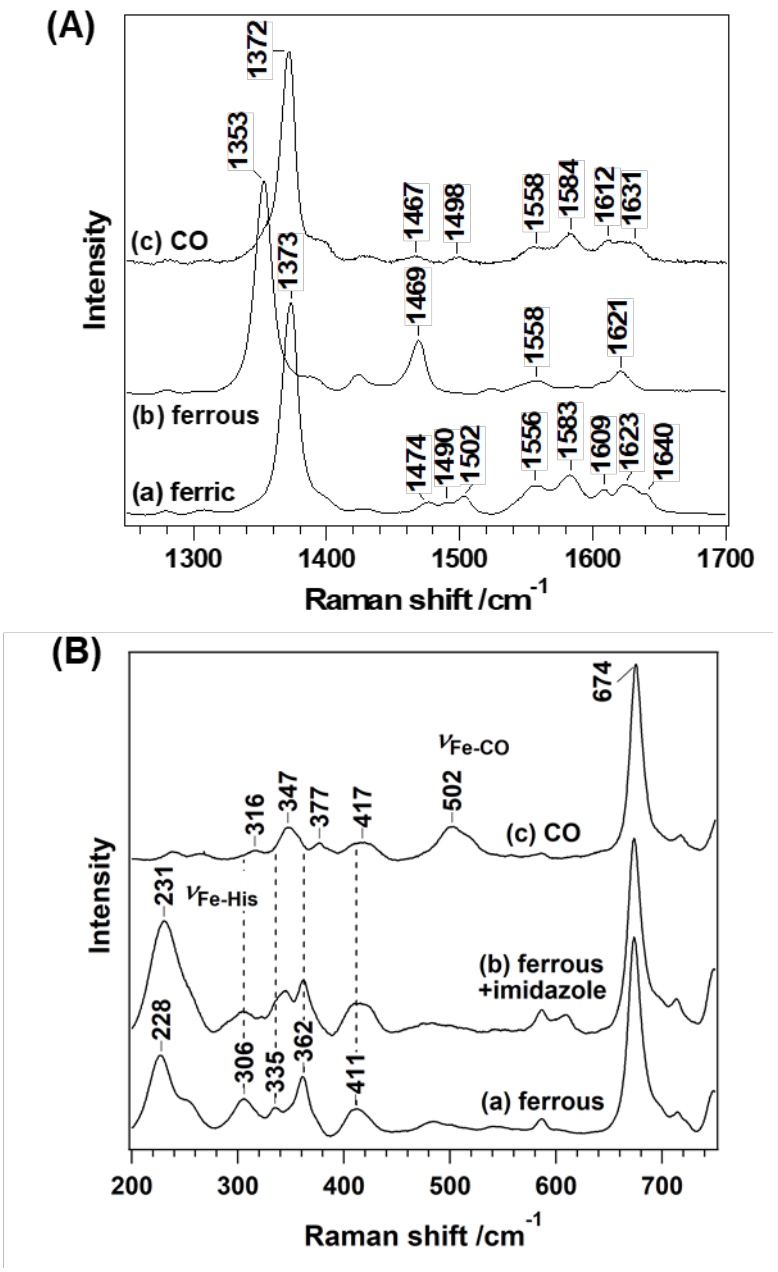

Fig. 12: **Resonance Raman spectra of the H170A mutant**. The protein concentration was 10 μM in 50 mM Tris-HC/150 mM NaCl, pH 8.0. (A) High-frequency region; (B) low-frequency region. The excitation wavelength for ferric and CO-bound forms was 413.1 nm, and that for the ferrous form was 441.6 nm.

2.2.4. Discussion

Role of Hydrogen Bonding Between Asp132 and His170 in Heme Degradation by HutZ.

The X-ray crystal structure of the homologous protein, HugZ, from *H. pylori* (Fig. 1)[29], and a sequence alignment of HugZ with HutZ from *V. cholerae* raises the possibility that Asp132 of HutZ is hydrogen bonded to the heme axial ligand His170. A correlation plot of $\nu_{Fe\text{-}CO}$ versus $\nu_{C\text{-}O}$ for heme-WT HutZ support the presence of hydrogen bonding between Asp132 and His170[4]. This hydrogen bonding causes strong electron donation from the proximal His, preventing the ferric heme from being reduced and resulting in inactivation of the heme degradation reaction. In contrast, at the lower pH, proximal hydrogen bonding is weakened; thus, the depressed electron donation from the axial His enables the ferric heme to be more easily reduced, leading to enhanced activity.

To examine the role of the proximal hydrogen bond in the heme degradation reaction, I constructed Asp132 mutants that disrupt this bond. Replacement of Asp132 with the aliphatic residue Leu (D132L) caused a drastic downshift in the frequency of $\nu_{Fe\text{-}His}$, reducing it by 17 cm^{-1} (Fig. 7B). In addition, the correlation plot of $\nu_{Fe\text{-}CO}$ versus $\nu_{C\text{-}O}$ was observed to shift from the line of proteins with neutral His as an axial ligand to that of proteins with a five-coordinate CO-heme in the heme-D132L mutant (Fig. 7D). These results suggest that electron donation from the proximal His is significantly reduced in the heme-D132L mutant owing to disruption of the proximal hydrogen bond by the mutation. Therefore, it was expected that this Asp132 mutation would lead to enhancement of heme degradation activity; instead, it resulted in a prominent decrease in activity (Fig. 3A). Considering that the ligand-binding rate of the heme-D132L complex was comparable to that of heme-WT HutZ (Fig. 4; Table 1), it is unlikely that inhibition of H_2O_2 binding to the heme-D132L mutant accounts for the inactivation. In contrast to the heme-D132L and heme-D132N mutants, a significant amount of verdoheme was formed by the D132E mutant in the reaction with H_2O_2, judging from the appearance of a band at ~652 nm (Fig. 3C). Because the frequency of $\nu_{Fe\text{-}His}$ of the heme-D132E mutant is close to

that of heme-WT (Fig. 7B), proximal hydrogen bonding is likely conserved in this mutant. These results clearly suggest that the proximal hydrogen bond between the amino acid residue at position 132 and axial His170 is essential for the heme degradation reaction of HutZ.

The CN binding rate of the heme-D132L mutant is comparable to that of heme-WT HutZ (Fig. 4), indicating that the rate of hydroperoxy (Fe^{3+}-OOH) formation is most likely not affected by the mutation of Asp132. The hydroperoxy heme is converted to the *meso*-hydroxyheme, and then decays to verdoheme in HO[15,30]. One possible explanation for the loss of heme-degradation activity in the heme-D132L mutant is that the OH group of the hydroperoxy heme less efficiently attacks the *meso*-carbon of the heme. Without this proximal hydrogen bond, the degrees of freedom of heme rotation inside the protein would be greater than that in the WT enzyme. Thus, the OH group of the hydroperoxy species does not appropriately orient for the attack, leading to reduced reactivity in the heme-D132L mutant.

Among the three Asp132 mutants, only the heme-D132E mutant was active toward H_2O_2 at levels comparable to that of heme-WT. However, it was inactive toward ascorbic acid, even when the heme was in a high-spin state (Fig. 6B). The large absorption at 373 nm observed for the heme-D132E mutant suggests partial dissociation of the heme from the protein. Furthermore, a five-coordinate heme appeared in the CO-bound form (Fig. 13). The $K_{d,heme}$ of the D132E mutant was almost identical to that of WT HutZ at pH 8.0 (Table 1), whereas the $K_{d,heme}$ of the D132E mutant at pH 6.0 was 4.1 μM (Fig. 6C), a value more than 100-fold larger than that at pH 8.0. In the case of WT HutZ, $K_{d,heme}$ at pH 6.0 was only 2-fold larger than that at pH 8.0 (data not shown). The occurrence of a five-coordinate heme in the heme-D132E mutant indicates that the proximal His is prone to dissociate from the heme. The fact that the other two Asp132 mutants also exhibit a five-coordinate heme and higher $K_{d,heme}$ values suggests that Asp132 is essential for heme to coordinate to the protein, especially in the high-spin form. Because of the weak bond between His170 and heme in the heme-Asp132 mutants, the proximal His can be released from the heme when O_2 binds to the ferrous heme. Such breakage

of the Fe-His bond would account for the lower activity of the heme-Asp132 mutants even in the high-spin state.

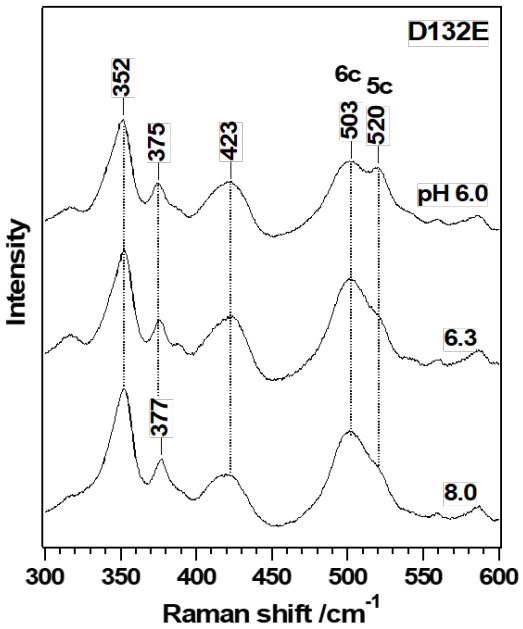

Fig. 13. Resonance Raman spectra of the heme-D132E mutant in the CO-bound form.

Role of His170 in Heme Degradation by HutZ.

To investigate the role of proximal hydrogen bonding in HutZ, I also replaced His170 with Ala. A heme titration plot showed that heme bound to the H170A mutant at 1:1 ratio, and yielded a $K_{d,heme}$ comparable to that of WT HutZ (Fig. 9). Absorption and resonance Raman spectra showed that the heme in the hemin-reconstituted H170A mutant is composed of the six-coordinate species (Fig. 12A). The appearance of the $\nu_{Fe\text{-}His}$ mode in the heme-H170A mutant (Fig. 12B) suggests that His is coordinated to the heme, despite replacement of His170 with Ala. A closer look at the structure of HugZ suggests that His63, which is within hydrogen bond distance of the heme propionate, is the sole His in the putative heme-binding site (Fig. 1)[29]. Additional replacement of His63 with Leu in the H170G mutant resulted in a significant loss of heme-binding ability (Fig. 10), implying that His63 in the H170A mutant is capable of coordinating heme. Although the $K_{d,heme}$ of the H170A mutant is similar to that of WT HutZ

(Fig. 9), exogenous imidazole replaced His63, considering that addition of imidazole to the ferrous heme-H170A mutant shifted the frequency of $\nu_{Fe\text{-}His}$ by 3 cm^{-1} and significantly enhanced it (Fig. 12B). Therefore, although His63 can bind heme, the bond strength is not sufficient to allow exogenous imidazole to replace it.

The moderate increase in absorption at 672 nm observed in the reaction of the H170A mutant with H_2O_2 suggests relatively modest heme degradation activity (~60% of WT) (Fig. 11A). The amount of verdoheme was much larger than that produced by the heme-D132L and heme-D132N mutants, and was comparable to that produced by heme-WT HutZ and the heme-D132E mutant (Fig. 3). The frequency of $\nu_{Fe\text{-}His}$ for the heme-H170A mutant was higher than that for the heme-D132L and heme-D132N mutants, but close to those for heme-WT HutZ and the heme-D132E mutant (Fig. 7 and 12). Therefore, the coordination structure of His63 to the heme is serendipitously suitable for heme degradation when H_2O_2 is used. The proximal mutant (H245A) of HugZ from *H. pylori* also bound heme and retained the heme degradation activity[29], which is in contrast to human HO[31,32]. The amino acid residue corresponding to His63 of HutZ are conserved in a HugZ family[29], indicating coordination of this histidine to heme of the H245A mutant HugZ. Thus, heme binding to the proximal heme mutant is likely to be common in this family.

Addition of imidazole to the heme-H170A complex led to a significant decrease in the amount of verdoheme formation (Fig. 11B). There is a possibility that imidazole binds to heme as the sixth heme ligand, which inhibits H_2O_2 binding to heme. Absorption and resonance Raman spectra of ferric heme-H170A in the presence of imidazole showed that heme is in six-coordinate low-spin state. Although it is difficult to distinguish between imidazole-bound low-spin heme and OH^--bound low-spin heme, the sixth heme ligand is OH^-, but not imidazole, considering that the ferric heme converted to ferrous five-coordinate heme, not six-coordinate heme, upon reduction. These results suggest that distal imidazole ligand is not a reason for the

less amount of verdoheme formation in the heme-H170A mutant in the presence of imidazole (Fig. 11B). Accordingly, the added imidazole replaced His63 and coordinated to the heme, but could not act as an axial ligand for heme degradation. Thus, the covalent bond between the imidazole ring of His and the protein is essential for the heme degradation activity of HutZ. In the case of HO-1, the helix containing the axial His in the apoprotein adopts an "open" conformation for heme binding[33,34]. When heme binds the protein, the helix moves to adopt a "closed" conformation[5]. Although the crystal structure of heme-bound HutZ has not been solved and no sequence homology was found between HutZ and HO, such structural changes would occur in WT HutZ in the presence of imidazole, but would not occur in the H170A mutant owing to loss of the covalent bond between heme and the polypeptide chain.

2.2.5. Conclusions

In summary, I investigated the role of proximal hydrogen bonding between Asp132 and His170. Breakage of the proximal hydrogen bond between His170 and Asp132 destabilizes the coordination of the proximal His to heme, leading to a drastic loss of heme degradation activity. This proximal hydrogen bonding plays a key role in retaining the heme in an appropriate position for the terminal oxygen of the hydroperoxy species to attack the *meso*-carbon of the porphyrin ring. The structural difference between HutZ and HO-1 suggests that HutZ has evolved from ancestral distinct from that of HOs, although their heme degradation mechanism is conserved.

REFERENCES

(1) Goodin, D. B.; McRee, D. E. *Biochemistry* **1993**, *32* (13), 3313.

(2) Poulos, T. L. *Curr. Opin. Biotechnol.* **1993**, *4* (4), 484.

(3) Gajhede, M.; Schuller, D. J.; Henriksen, A.; Smith, A. T.; Poulos, T. L. *Nat. Struct. Biol.* **1997**, *4* (12), 1032.

(4) Uchida, T.; Sekine, Y.; Matsui, T.; Ikeda-Saito, M.; Ishimori, K. *Chem. Commun.* **2012**, *48* (53), 6741.

(5) Schuller, D. J.; Wilks, A.; Ortiz de Montellano, P. R.; Poulos, T. L. *Nat. Struct. Biol.* **1999**, *6* (9), 860.

(6) Sugishima, M.; Omata, Y.; Kakuta, Y.; Sakamoto, H.; Noguchi, M.; Fukuyama, K. *FEBS Lett.* **2000**, *471* (1), 61.

(7) Liu, Y.; Moënne-Loccoz, P.; Hildebrand, D. P.; Wilks, a; Loehr, T. M.; Mauk, a G.; Ortiz de Montellano, P. R. *Biochemistry* **1999**, *38* (12), 3733.

(8) Harbury, H. A. *J. Biol. Chem.* **1957**, *225* (2), 1009.

(9) Takahashi, S.; Wang, J.; Rousseau, D. L.; Ishikawa, K.; Yoshida, T.; Host, J. R.; Ikeda-Saito, M. *J. Biol. Chem.* **1994**, *269* (2), 1010.

(10) Kitagawa, T.; Kyogoku, Y.; Iizuka, T.; Saito, M. I. *J. Am. Chem. Soc.* **1976**, *98* (17), 5169.

(11) Kitagawa, T.; Nagai, K.; Tsubaki, M. *FEBS Lett.* **1979**, *104* (2), 376.

(12) Nagai K; Kitagawa T; Morimoto H. *J. Mol. Biol.* **1980**, *136* (3), 271.

(13) Hashimoto, S.; Teraoka, J.; Inubushi, T.; Yonetani, T.; Kitagawa, T. *J. Biol. Chem.* **1986**, *261* (24), 11110.

(14) Smulevich, G.; Mauro, J. M.; Fishel, L. A.; English, A. M.; Kraut, J.; Spiro, T. G. *Biochemistry* **1988**, *27*, 5477.

(15) Wilks, A.; Ortiz de Montellano, P. R. *J. Biol. Chem.* **1993**, *268* (30), 22357.

(16) Unno, M.; Matsui, T.; Ikeda-Saito, M. *Nat. Prod. Rep.* **2007**, *24* (3), 553.

(17) Takahashi, S.; Wang, J. L.; Rousseau, D. L.; Ishikawa, K.; Yoshida, T.; Takeuchi, N.; Ikeda-saito, M. *Biochemistry* **1994**, *33* (18), 5531.

(18) Dawson, J. H. *Science* **1988**, *240* (4851), 433.

(19) Uchida, T.; Sasaki, M.; Tanaka, Y.; Ishimori, K. *Biochemistry* **2015**, *54* (43), 6610.

(20) Matera, K. M.; Takahashi, S.; Fujii, H.; Zhou, H.; Ishikawa, K.; Yoshimura, T.;

Rousseau, D. L.; Yoshida, T.; Ikeda-Saito, M. *J. Biol. Chem.* **1996**, *271* (12), 6618.

(21) Kitagawa, T.; Hashimoto, S.; Teraoka, J.; Nakamura, S.; Yajima, H.; Hosoya, T. *Biochemistry* **1983**, *22* (12), 2788.

(22) Spiro, T. G.; Soldatova, A. V.; Balakrishnan, G. *Coord. Chem. Rev.* **2013**, *257* (2), 511.

(23) Ray, G. B.; Li, X. Y.; Ibers, J. A.; Sessler, J. L.; Spiro, T. G. *J. Am. Chem. Soc.* **1994**, *116* (1), 162.

(24) Lou, B.-S.; Snyder, J. K.; Marshall, P.; Wang, J.-S.; Wu, G.; Kulmacz, R. J.; Tsai, A.-L.; Wang, J. *Biochemistry* **2000**, *39* (40), 12424.

(25) Spiro, T. G.; Wasbotten, I. H. *J. Inorg. Biochem.* **2005**, *99* (1), 34.

(26) Wilks, A.; Sun, J.; Loehr, T. M.; Ortiz de Montellano, P. R. *J. Am. Chem. Soc.* **1995**, *117* (10), 2925.

(27) Wilks, A.; Moenne-Loccoz, P. *J. Biol. Chem.* **2000**, *275* (16), 11686.

(28) Chu, G. C.; Couture, M.; Yoshida, T.; Rousseau, D. L.; Ikeda-Saito, M. *J. Am. Chem. Soc.* **2000**, *122* (50), 12612.

(29) Hu, Y.; Jiang, F.; Guo, Y.; Shen, X.; Zhang, Y.; Zhang, R.; Guo, G.; Mao, X.; Zou, Q.; Wang, D. C. *J. Biol. Chem.* **2011**, *286* (2), 1537.

(30) Ishikawa, K.; Takeuchi, N.; Takahashi, S.; Matera, K. M.; Sato, M.; Shibahara, S.; Rousseau, D. L.; Ikeda-Saito, M.; Yoshida, T. *J. Biol. Chem.* **1995**, *270* (11), 6345.

(31) Ito-Maki, M.; Ishikawa, K.; Matera, K. M.; Sato, M.; Ikeda-Saito, M.; Yoshida, T. *Arch. Biochem. Biophys.* **1995**, *317* (1), 253.

(32) Sun, J.; Loehr, T. M.; Wilks, A.; Ortiz de Montellano, P. R. *Biochemistry* **1994**, *33* (46), 13734.

(33) Sugishima, M.; Sakamoto, H.; Kakuta, Y.; Omata, Y.; Hayashi, S.; Noguchi, M.; Fukuyama, K. *Biochemistry* **2002**, *41* (23), 7293.

(34) Lad, L.; Schuller, D. J.; Shimizu, H.; Friedman, J.; Li, H.; Ortiz de Montellano, P. R.; Poulos, T. L. *J. Biol. Chem.* **2003**, *278* (10), 7834.

Part III: Acquisition Mechanism for Heme-Degradation Activity of HutZ-Type Enzymes through the Molecular Evolution

Abstract

HutZ from *Vibrio cholerae* (*Vc*HutZ) is a dimeric protein that catalyzes oxygen-dependent degradation of heme. The reaction mechanism is the same as that of canonical heme oxygenase (HO), but the structure of HutZ is quite different from that of HO. Thus, I postulate that HutZ has evolved via a different pathway from that of HO. Alr5027 from cyanobacteria *Nostoc* sp. PCC7120, which would have ancestral proteins utilizing O_2 in enzymatic reactions, is homologous to HutZ family proteins (67% similarity), but the heme axial ligand of HutZ is not conserved in Alr5027. To investigate whether Alr5027 can bind and degrade heme, I expressed wild-type (WT) and mutated Alr5027 proteins in an *Escherichia coli* system and purified them. Although wild-type Alr5027 did not bind heme, replacement of Lys164, corresponding to the heme axial ligand of *Vc*HutZ, with histidine conferred heme-binding capability. The K164H mutant produced verdoheme in the reaction with H_2O_2, indicating acquisition of heme-degradation ability. Among the histidine-substitution mutants created, the K164H mutant produced verdoheme most efficiently. The K164H mutant did not degrade heme through ascorbic acid, probably because of suppression of proton transfer to reduced oxyferrous heme. An analysis of Trp103 fluorescence indicated elongation of the distance between protomers in this mutant compared with *Vc*HutZ—the probable cause of the inefficiency of ascorbic acid-supported heme-degradation activity. Collectively, our findings indicate that a single lysine-to-histidine mutation converted Alr5027 to a heme-binding protein that can form verdoheme through H_2O_2, suggesting that HutZ family proteins have acquired the heme-degradation function through molecular evolution from an ancestor protein of Alr5027.

4.1. Introduction

The results and discussion in previous part clearly indicates the reaction mechanism of HutZ is the same as that of HO-1, but the structure of HutZ is quite different from that of HO-1. These observations indicate that HutZ has evolved from a different ancestor from HO-1. Thus, to search for an ancestral protein of HutZ, I focused on cyanobacteria, which evolved ~2.7 billion years ago from ancient phototrophic organisms that previously inhabited Earth [1]. These ancient organisms had evolved two photosystems, namely the high-potential water-oxidizing photosystem II and the low-potential ferredoxin-reducing photosystem I, resulting in oxygenic photosynthesis. This most decisive evolutionary step marked a turning point in evolution on Earth, opening up the era of an aerobic, oxygen-containing biosphere and atmosphere. Recent evidence suggests that as O_2 molecules became integral to biochemical pathways, many enzymatic reactions central to anoxic metabolism were effectively replaced in aerobic organisms [2]. Thus, I hypothesized that cyanobacteria, which utilize O_2 molecules in their enzymatic reactions, would have ancestral proteins. I searched for HutZ homolog proteins from cyanobacteria *Nostoc* sp. PCC7120. A BLAST (http://blast.ncbi.nlm.nih.gov/Blast.cgi) search revealed that Alr5027, a protein of unknown function [3], shared a high degree of homology with *V. cholerae* HutZ (*Vc*HutZ) (43% identity and 67% similarity) [4]. Arg92, His170, and Asp132 in *Vc*HutZ are key residues in the heme-degradation reaction [5]. Arg92, which is located in the distal site of heme, acts as a hydrogen-bond donor for iron-bound O_2 [5,6]. As shown in Part II of chapter II, His170 is a heme axial ligand, which forms a hydrogen bond with Asp132 that retains heme in an appropriate position for degradation. Although Arg92 and Asp132 of *Vc*HutZ, corresponding to Arg86 and Asp126 of Alr5027, respectively, are conserved in Alr5027, His170 of *Vc*HutZ is not conserved (the corresponding residue in Alr5027 is Lys164) (Fig. 1A). A phylogenetic tree was constructed on the basis of a multiple sequence alignment of the HugZ family by applying the maximum likelihood method using MEGA 7 [7] (https://www.megasoftware.net/) (Fig. 1B). This analysis indicated that Alr5027 is situated at a

branch that is separate from other members of the HugZ family. These findings led us to predict that members of the HutZ family share a common ancestor protein with Alr5027. However, whether Alr5027 is capable of binding and degrading heme was unknown.

In this part, I expressed Alr5027 in *Escherichia coli* and examined its heme-binding and heme-degradation properties. Alr5027 did not bind to heme, reflecting the absence of a conserved, putative heme ligand. Replacement of leucine at position 164 with histidine rendered the protein capable of binding to heme. When H_2O_2 was used as an electron source, verdoheme, an intermediate involved in heme degradation by HO, was produced. Among mutants created with histidine substitutions at different positions, the K164H mutant produced verdoheme most efficiently. However, heme was not degraded by the K164H mutant when ascorbic acid was used as an electron source. An analysis of tryptophan fluorescence spectra of Trp103 indicated that the inefficiency of ascorbic acid-assisted heme degradation was attributable to elongation of the distance between protomers, as observed in the HutZ mutant, in which Ala31 is replaced with valine. Consequently, our results show that the single replacement of Lys164 with histidine converted Alr5027 to a heme-binding protein with the ability to form verdoheme. These findings suggest that members of the HutZ family have acquired their heme-degradation function through molecular evolution from a common ancestor of *Vc*HutZ and Alr5027.

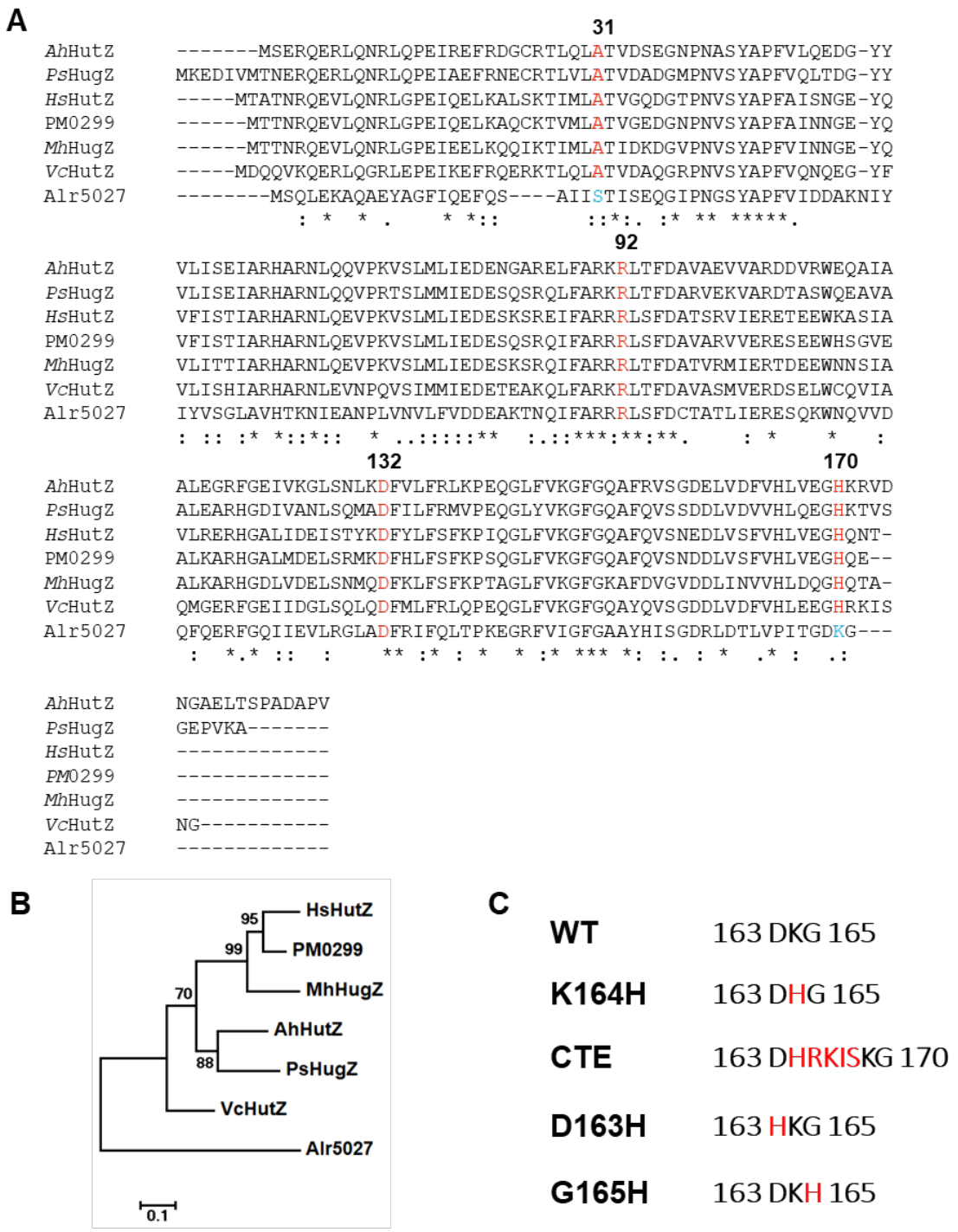

Fig. 1. **Sequence alignment of Alr5027.** (A) Sequence alignment of the HutZ family and Alr5027. The alignment was performed using ClustalW2 (http://www.ebi.ac.uk/Tools/msa/clustalw2/). The active site arginine, aspartate, and histidine are shown in red bold type. Proteins used in the alignment are (from top to bottom) *Aeromonas hydrophila* subsp. *hydrophila* ATCC 7966 HutZ, *Plesiomonas shigelloides* HugZ, *Histophilus somni* HutZ, *multocida* str. Pm70 PM0299, *Mannheimia haemolytica* PHL213 HugZ, *Vibrio cholerae* HutZ, and *Nostoc* sp. PCC 7120 Alr5027. (B) Phylogenetic tree of Alr5027 with the HutZ family. The tree was obtained from the sequence alignment in Fig. 1A. The maximum likelihood method was used for tree construction and bootstrap analysis (parameter set at 1000 resampling), performed using MEGA 7 software. (C) Alignment of Alr5027 WT and mutants in the C-terminal region (163–165).

4.2. Experimental procedures

Materials

The chemicals used in this study were purchased from Wako Pure Chemical Industries (Osaka, Japan), Nacalai Tesque (Kyoto, Japan) or Sigma-Aldrich (St. Louis, MO), and were used without further purification.

Expression and purification of Alr5027

The *alr5027* gene, with codons optimized for *E. coli* expression (Eurofins Genomics, Tokyo, Japan), was amplified by polymerase chain reaction (PCR) and cloned into a modified pET-28b vector [8]. The expression plasmid was transformed into the *E. coli* BL21(DE3) strain (Nippon Gene, Japan) and cultured at 37 °C in LB broth supplemented with 50 μg/mL kanamycin. After the optical density at 600 nm (OD_{600}) reached 0.8, expression of the His_6-tagged protein was induced with 0.4 mM isopropyl β-D-thiogalactopyranoside. The cells were further grown at 20 °C overnight and harvested by centrifugation. The cell pellet was suspended in lysis buffer containing 50 mM Tris-HCl, 500 mM NaCl (pH 8.0), 1.0% Nonidet P-40, 1 mg/mL lysozyme and DNase, and incubated on ice for 60 min. The sample was centrifuged at 18,000 rpm for 30 min, and the supernatant was mixed with 5.0 mL of Ni-NTA agarose (Nacalai Tesque, Japan) with gentle agitation for 1 h at 4 °C. The slurry was poured into a column and washed with lysis buffer supplemented with 20 mM imidazole (25 mL), after which the protein was eluted with elution buffer (50 mM Tris-HCl, 500 mM NaCl, 250 mM imidazole, pH 8.0). Eluted Alr5027 was incubated with Turbo 3C protease (Accelagen, San Diego, CA, USA) for ~16 h at 4 °C to cleave the His_6-tag. After cleavage, the reaction mixture was re-applied to the Ni-NTA resin, and the flow-through fraction was collected. Tag-cleaved Alr5027 was then applied to a HiLoad 16/600 Superdex 200 gel-filtration column (GE Healthcare, Uppsala, Sweden) pre-equilibrated with 50 mM Tris-HCl and 150 mM NaCl (pH 8.0). Protein purity, assessed by sodium dodecyl sulfate-polyacrylamide gel electrophoresis (SDS-PAGE) on 12.5% polyacrylamide gels, was determined to be ~95%.

Mutations were introduced using a PrimeSTAR mutagenesis basal kit from Takara Bio (Otsu, Japan). Primers used for construction of the clone and mutagenesis are shown in Supplementary Table 1.

Table 1 Primer used for construction of expression vectors for mutants.

Constructs	Sequence (up sense; bottom, anti-sense)
K164H_F	GGTGACCATGGCTGAAAGCTTGCGGCC
K164H_R	TCAGCCATGGTCACCGGTAATCGGAAC
D163H_F	ACCGGTCATAAAGGCTGAAAGCTTGCG
D163H_R	GCCTTTATGACCGGTAATCGGAACCAG
G165H_F	GACAAACATTGAAAGCTTGCGGCCGCA
G165H_R	CTTTCAATGTTTGTCACCGGTAATCGG
G165HG_F	GACAAACATGGCTGAAAGCTTGCGCC
G165HG_R	TCAGCCATGTTTGTCACCGGTAATCGG
CTE_F	CATCGTAAGATTTCTAAAGGCTGAAAGCTTGCG
CTE_R	AGAAATCTTACGATGGTCACCGGTAATCGGAAC
ERKT_F	CAGAACGGAAAACCGCGATCATTTCGACGATT
ERKT_R	CGGTTTTCCGTTCTGACTGAAACTCCTGAATGA
S24A/ERKT_F	ATCATTGCGACGATTAGCGAACAAGGG
S24A/ERKT_R	AATCGTCGCAATGATCGCCCTTTTCCG

F indicates the forward direction primer, and R indicates the reverse direction primer. The underlined based signify the introduced mutations.

Measurement of heme binding to Alr5027

Heme binding was tracked by difference spectroscopy in the Soret region of the UV-visible spectrum. Successive aliquots of 0.5 mM hemin in 0.1 M NaOH were added to both the sample cuvette containing 10 μM Alr5027 and reference cuvette containing buffer only. Spectra were recorded 3 min after the addition of each heme aliquot. The absorbance difference at 414 nm was plotted as a function of heme concentration, and the dissociation constant ($K_{d,heme}$) was calculated using the quadratic binding equation (equation 1):

$$\Delta A = \Delta A_{max} \frac{[P]+[H]+K_{d,heme} - \sqrt{([P]+[H]+K_{d,heme})^2 - 4[P][H]}}{2[P]}, \quad (1)$$

where [P] and [H] represent the total protein and hemin concentrations, respectively; ΔA is the change in absorption difference between the sample and reference cell upon addition of hemin; and ΔA_{max} is the maximum of the absorption difference upon addition of hemin. The millimolar extinction coefficient was determined using the pyridine hemochrome method [9].

Spectroscopy

Optical spectra of purified proteins were recorded with a UV-visible spectrophotometer (V-660; Jasco, Tokyo, Japan) at 25 °C. Fluorescence spectra were recorded using a FP-8500 spectrometer (Jasco). Protein samples were excited at 295 nm to avoid contribution from tyrosine resides. The Alr5027 concentration was 5 μM in 50 mM Tris-HCl and 150 mM NaCl (pH 8.0). The distance (r) between tryptophan and heme was estimated from the efficiency (E) of Förster energy transfer from tryptophan to heme, defined as:

$$E = \frac{R_0^6}{R_0^6 + r^6} \quad (2)$$

where R_0 represents the Förster distance and is 29 Å for heme and tryptophan [10]. The energy transfer efficiency, E, was calculated using the fluorescence intensity of apo-Alr5027 (F_{apo}) and heme-Alr5027 (F_{heme}):

$$E = \frac{F_{apo} - F_{heme}}{F_{apo}} \quad (3)$$

Heme-degradation activity

The heme-degradation reaction of Alr5027 was monitored by spectrophotometry. Briefly, 1.9 mL of a hemin-reconstituted protein solution (final concentration, 3.0 μM) in 50 mM Tris-HCl and 150 mM NaCl (pH 8.0) was placed in a cuvette, and the reaction was started by adding 100

μL of 2 mM H_2O_2 or 20 mM ascorbic acid in the same buffer at 25 °C. Spectra were recorded at 1-min intervals for 10 min for H_2O_2 (final concentration, 0.1 mM), and at 2-min intervals for 30 min for ascorbic acid (final concentration, 1 mM). In the case of reactions with ascorbic acid, 1 mg/mL of bovine liver catalase was added to cause H_2O_2 dismutation. Iron liberated from products by heme Alr5027 was obtained by adding a saturated solution of HCl (~8 M) to the heme-degradation reaction mixture, resulting in efficient extraction of pigments from the proteins. Solid-phase extraction of the reaction products was performed using a Supelclean LC-18 column (Supelco, Bellefonte, PA, USA). The column-bound sample was washed with 20% (v/v) methanol and 80% (v/v) water, and eluted with methanol. The effluents were analyzed on an LC-2000 HPLC system (Jasco) equipped with a ZORBAX Extend-C18 column (3.0 × 150 mm, 3.5 μm silica; Agilent Technologies, Palo Alto, CA, USA) using a linear gradient from 50% (v/v) methanol and 50% (v/v) 0.1 M ammonium acetate to 80% (v/v) methanol over 60 min at a flow rate of 0.5 mL/min. The eluent was monitored at 380 nm. Biliverdin dimethyl esters standards were prepared as previously described [11].

Heme reduction rate

The heme reduction rate, k_{red}, was determined by monitoring changes in absorbance at 418 nm. The ferric heme-Alr5027 complex (10 μM) was reduced with 1 mM ascorbic acid. In addition to an oxygen-scavenging system composed of glucose and glucose oxidase, catalase was added to the solution to maintain anaerobic conditions [12]. The reaction was conducted under a CO atmosphere to prevent heme degradation and/or auto-oxidation by trace levels of contaminating O_2. The k_{red} was obtained by fitting the time course of changes in absorbance at 418 nm to a single-exponential expression.

4.3. Results and Discussion

Expression and purification of Alr5027

The *alr5027* gene was expressed in *E. coli* and purified using a His_6-tag affinity column. After cleavage of the His_6-tag and size-exclusion chromatography, only a single band with an apparent molecular mass of approximately 16 kDa was observed on SDS-PAGE gels (Fig. 2A), in agreement with the calculated molecular mass of Alr5027 (18 kDa). An analysis of purified Alr5027 by size-exclusion chromatography indicated that the protein existed as a dimer (40 kDa) (Fig. 2B), as observed for *Vc*HutZ [5] .

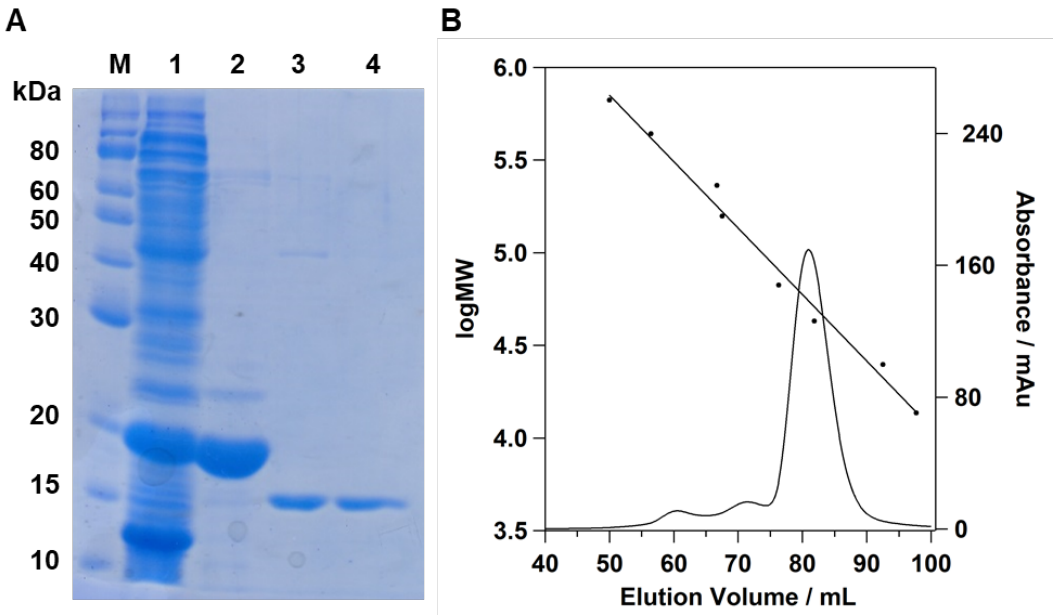

Fig. 2. **Purification of Alr5027.** (A) SDS-PAGE gel of purified Alr5027 stained with Coomassie Brilliant Blue, including molecular mass marker (lane M), whole-cell protein extracts (lane 1), purified His-tagged Alr5027 (lane 2), purified His-tag–cleaved Alr5027 (lane 3), and purified Alr5027 after gel-filtration chromatography (lane 4). (B) Profile of Alr5027 on a gel-filtration column pre-equilibrated with 50 mM Tris-HCl and 150 mM NaCl (pH 8.0). The retention volumes of standard proteins were as follows: thyroglobulin, 50.0 mL; ferritin, 56.4 mL; catalase, 66.7 mL; aldose, 67.5 mL; albumin, 76.3 mL; ovalbumin, 81.8 mL; chymotrypsinogen A, 92.5 mL; and RNase A, 97.6 mL.

Heme-binding properties of Alr5027

The purified protein showed no absorption in the visible region, indicating that it was purified in a pigment-free form (i.e., without heme) (Fig. 3, red line). Addition of an aliquot of hemin solution to Alr5027 resulted in the appearance of a broad Soret band at ~389 nm (Fig. 3, blue line), which was almost identical to that of free hemin (Fig. 3, black line). To determine whether Alr5027 is capable of binding to heme, I performed a heme-titration experiment. The absorbance difference at 414 nm (ΔAbs_{414}), obtained by subtracting the spectrum of free hemin at various concentrations, increased only slightly with increasing concentrations of heme (Fig. 3, inset), indicating that wild-type (WT) Alr5027 did not bind heme.

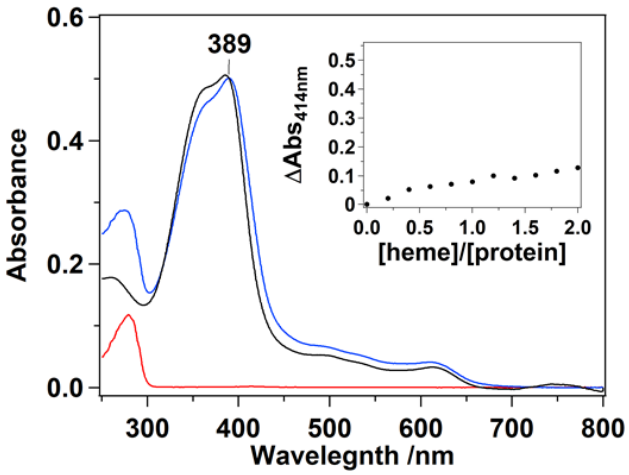

Fig. 3. Absorption spectra of the heme-WT Alr5027 complex. Spectra are for purified apo-Alr5027 (red line), free heme (black line), and heme-Alr5027 (blue line). The inset shows differences at 414 nm following incremental addition of heme (2–30 μM) to Alr5027 (10 μM) in 50 mM Tris-HCl and 150 mM NaCl (pH 8.0), measured against a blank cell containing buffer alone.

Heme-binding properties of the K164H mutant

A sequence alignment of the HugZ family is shown in Fig. 1A. His170, the heme axial ligand in *Vc*HutZ, is conserved among members of the family except Alr5027. Thus, I predicted that Alr5027 would attain heme-binding ability if histidine were introduced at the corresponding position. To this end, I replaced Lys164 with histidine (Fig. 1C) and purified the resulting K164H mutant using the same procedure as used for WT Alr5027. Following addition of hemin

to the mutant, the resultant solution exhibited a Soret band at 413 nm (Fig. 4A), which was almost identical to that of heme-HutZ [5]. The spectrum was clearly distinguishable from that of WT Alr5027 with hemin (Fig. 3), suggesting that heme specifically bound to the mutant. The apparent dissociation constant ($K_{d,heme}$), calculated by fitting the data to equation 1, was determined to be 0.24 ± 0.03 μM, which is approximately 5-fold larger than that reported for *Vc*HutZ (0.052 ± 0.020 μM) [5]. These results show that the replacement of Lys164 with histidine converts Alr5027 into a heme-binding protein.

Heme-degradation activity of the K164H mutant

Because I found that the K164H mutant binds heme, I next examined whether it also degrades heme. I first used H_2O_2 as an electron source because verdoheme, a key intermediate in the heme-degradation reaction, is formed when heme-bound *Vc*HutZ reacts with H_2O_2 [5]. In the reaction of the heme-K164H mutant with H_2O_2, the absorbance at 652 nm increased (Fig. 4B), reaching a value approximately 72% of that for *Vc*HutZ[22]. This band did not appear following treatment of heme-bound WT Alr5027 with H_2O_2 (Fig. 4C). The peak position at 652 nm corresponded to that of the verdoheme of *Vc*HutZ [5,13], indicating that verdoheme was produced in the reaction of the mutant with H_2O_2.

A decrease in the Soret band does not always indicate heme degradation, because compound I and compound II, which are produced by the reaction of hemoproteins with H_2O_2, are known to have features of a relatively weak Soret band [14,15]. The reaction of myoglobin with H_2O_2 resulted in a decrease in the intensity of the Soret band (Fig. 5A), but absorption was restored by the addition of *o*-methoxyphenol (guaiacol) (Fig. 5B). To investigate whether the decrease in Soret absorbance in the K164H mutant (Fig. 4B) was reversible, I added guaiacol. The intensity of the Soret band did not change after the addition of guaiacol (Fig. 5C). Collectively, these results indicate that the heme-K164H mutant produced verdoheme, but not compound I or compound II.

Heme can be cleaved at any one of four structurally nonidentical *meso* positions, producing

four isomers of verdoheme, whose absorption spectra are different from each other [16]. To identify the oxidation site of verdoheme of the K164H mutant, I added pyridine to the reaction solution, which resulted in a visible band at 660 nm typical of pyridine-verdohemochrome [11] (Fig. 6A). The absorption maximum of verdohemochrome of the K164H mutant (660 nm) was close to that of β-verdoheme (663 nm) and δ-verdoheme 660 nm), but not to that of α-verdoheme (680 nm) or γ-verdoheme (648 nm) [11], suggesting that the β- or δ-*meso* position was cleaved in the reaction of the K164H mutant with H_2O_2, as observed for *Vc*HutZ [5].

Once verdoheme is produced, further oxidation would lead to the production of biliverdin. To confirm the formation of biliverdin by the K164H mutant, I treated the verdoheme of the K164H mutant with ascorbic acid. The maximum of the visible band shifted from 652 to 672 nm within 5 min (Fig. 4D), indicating the conversion of ferric verdoheme to ferrous verdoheme [13]. Thereafter, the intensity of the 672-nm band gradually decreased. Addition of ferrozine, which forms a stable complex with ferrous iron, to the product caused the appearance of a new band at 562 nm, typical of the Fe^{2+}-ferrozine complex, indicating that ferrous iron was released (Fig. 4D). To determine the regioselectivity of the heme breakage, I analyzed the products by high-performance liquid chromatography (HPLC). Biliverdin IXα, IXβ, IXδ and IXγ isomers, produced from the reaction of free heme with ascorbic acid, corresponded to peaks at 15.5, 21.1, 23.3, and 32.7 min, respectively, in the HPLC chromatogram (Fig. 4E). Peaks were assigned on the basis of a previous report [11]. In the chromatogram of the K164H mutant, two large peaks appeared at 21.3 and 23.4 min, which corresponded to biliverdin IXβ and biliverdin IXδ, respectively (Fig. 4E). Thus, the cleavage site of biliverdin produced by the K164H mutant was the β- or δ-*meso* position, which is the same as that of *Vc*HutZ [5]. Accordingly, verdoheme is formed during heme degradation by the K164H mutant.

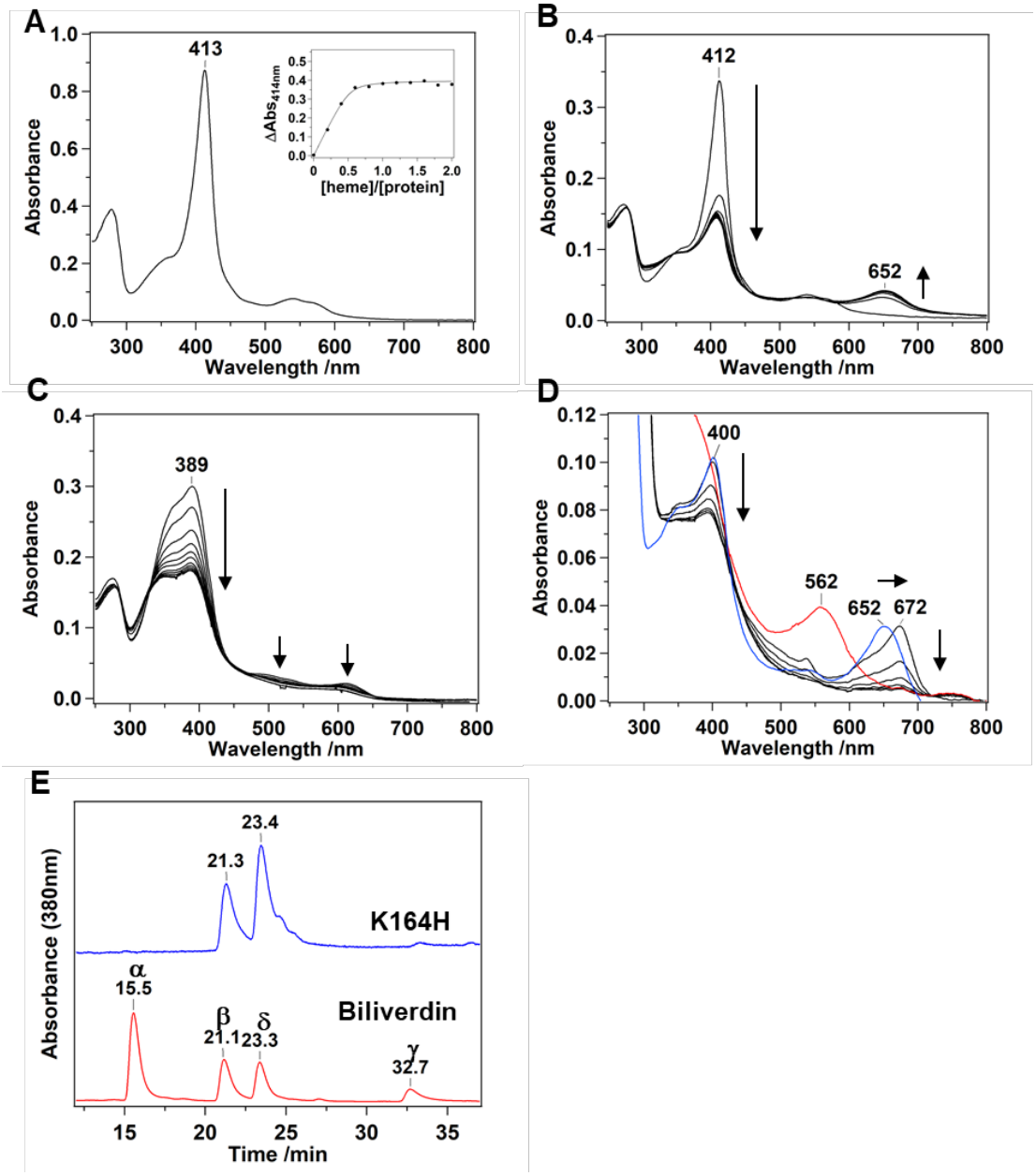

Fig. 4. **Absorption spectra and chromatogram of the heme-K164H mutant**. (A) Absorption spectra of the heme-K164H mutant at pH 8.0. The inset shows differences at 414 nm following incremental addition of heme (2–30 μM) to the mutant (10 μM) in 50 mM Tris-HCl and 150 mM NaCl (pH 8.0), measured against a blank cell containing buffer alone. (B, C) Heme-degradation reaction of the heme-K164H mutant (B) and heme-WT Alr5027 (C) reacted with 0.1 mM H_2O_2 at pH 8.0. Spectra were obtained before and after the addition of H_2O at 1-min intervals over 10 min. (D) Reaction of the verdoheme-K164H mutant with 1 mM ascorbic acid at pH 8.0. Absorption spectra in the reaction with ascorbic acid after the formation of verdoheme (blue line) by addition of 0.1 mM H_2O_2. Spectra were recorded before and after the addition of ascorbic acid at 4, 8, 16, 24, and 32 min (black line). Ferrozine (0.10 mM) was added 32 min after the reaction (green line). (E) HPLC chromatograms of biliverdin standard (red line) and final products of the heme-K164H mutant (blue line) monitored at 380 nm.

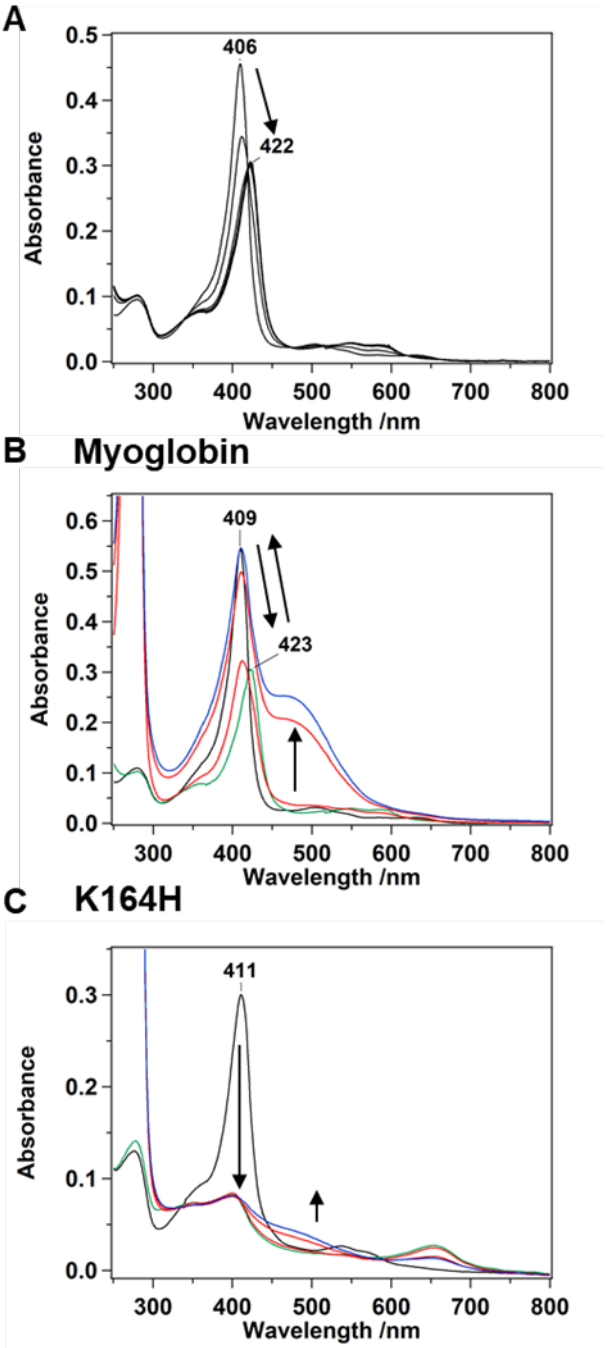

Fig. 5. (A) Absorption spectra of myoglobin in a reaction containing 0.1 mM H_2O_2 at pH 8.0. Spectra were measured before the addition of H_2O_2, and at 1-min intervals for 10 min after the addition of H_2O_2. (B, C) Reaction of myoglobin (B) and heme-K164H mutant (C) with H_2O_2 (90 μM) in the presence of 0.45 mM guaiacol at pH 8.0. The absorption spectrum before the reaction is shown as a black line. The reaction with guaiacol was monitored before mixing (green line), and 1, 20 (red lines), and 30 min (blue line) after mixing.

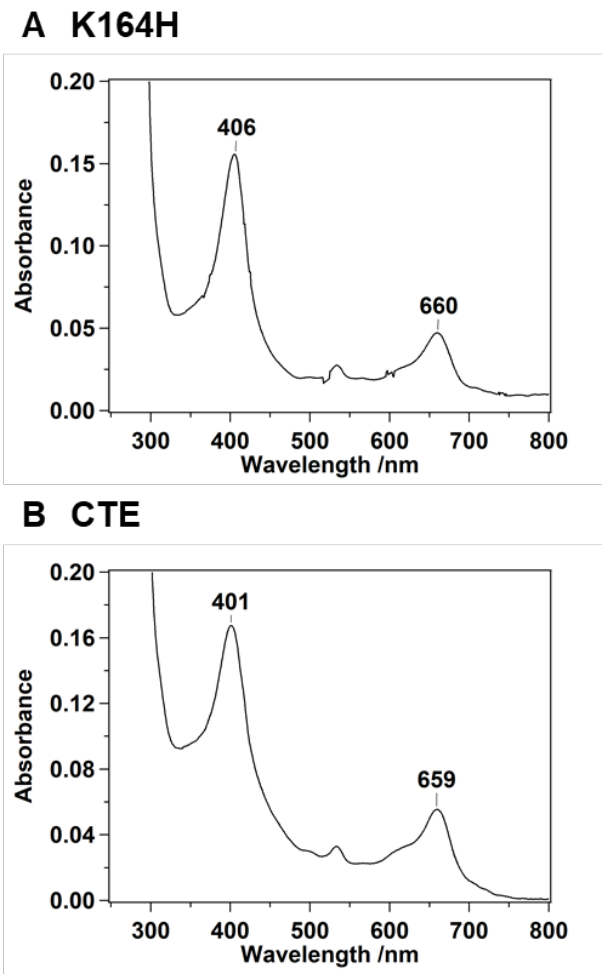

Fig. 6. Absorption spectra of verdoheme in aqueous pyridine. (A) K164H and (B) CTE heme-bound mutants were reacted with H_2O_2 under the same conditions at those in Fig. 5. Pyridine (final concentration, 33%) was added to the reaction mixture 10 min after the reaction to liberate the product from the protein.

To demonstrate the catalytic activity of the K164H mutant, I also examined the heme-degradation reaction of the heme-K164H mutant using ascorbic acid as an electron source. The reaction was conducted in the presence of the H_2O_2-scavenger catalase. Spectral changes following addition of ascorbic acid at pH 8.0 are shown in Fig. 5A. The Soret band showed very little decrease, and no clear band appeared in the 500–800 nm region, suggesting that no heme-degradation occurred under these conditions [17]. As reported previously [5], the heme-degradation reaction of heme-*Vc*HutZ with ascorbic acid is significantly accelerated at pH 6.0. However, lowering the pH from 8.0 to 6.0 did not promote a decrease in the Soret band,

indicating that heme in the K164H mutant was not degraded in the reaction with ascorbic acid

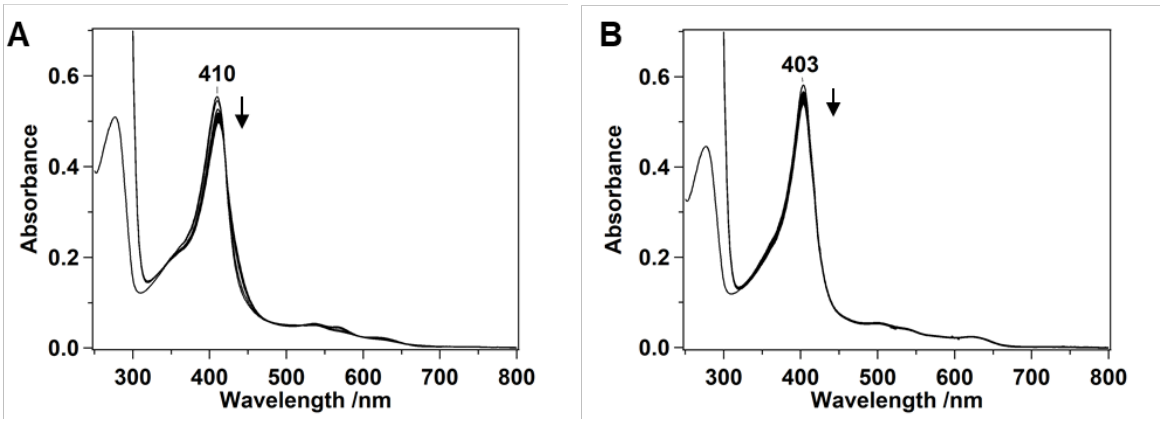

(Fig. 7B).

Fig. 7. **Heme-degradation reaction of the K164H mutant with ascorbic acid.** (A) pH 8.0 and (B) pH 6.0. Spectra were recorded before the addition of ascorbic acid, and at 2-min intervals for 30 min after the addition of ascorbic acid. The concentrations of the protein and ascorbic acid were 5 μM and 1.0 mM, respectively.

Heme-binding properties and degradation ability of D163H and G165H mutants

As described above, the K164H mutant bound to heme and converted it to verdoheme using H_2O_2, whereas it did not degrade heme in the reaction with ascorbic acid, despite possessing a proximal histidine at position 164. I postulated that the position of the proximal histidine is not appropriate for heme degradation. Thus, to shift the position of histidine, I replaced Asp163 or Gly165 with histidine. The sequence of mutants in the C-terminal region (163–165) is shown in Fig. 1C. The absorption spectrum of the D163H mutant in the presence of heme was similar to that of WT Alr5027 (Fig. 8A), suggesting that heme did not bind to the histidine at position 163. In contrast, addition of heme to the G165H mutant resulted in the appearance of a Soret band at 414 nm (Fig. 8B), indicating that this mutant specifically bound to heme. The $K_{d,heme}$ value was 0.44 ± 0.06 μM, which is similar to that of the K164H mutant (0.24 ± 0.03 μM). Thus, the introduced histidine at position 165 also coordinates with heme.

Next, I conducted the heme-degradation reaction for the heme-G165H mutant using H_2O_2 as an electron donor. A small band from verdoheme appeared at 653 nm following addition of

H_2O_2 to the heme-G165H mutant (Fig. 8C). This behavior of the heme-G165H mutant was quite similar to that of the heme-K164H mutant, but the amount of verdoheme was smaller—approximately 34% that of *Vc*HutZ (Fig. 4B).

In addition, I prepared the G165HG mutant, in which histidine was inserted between Lys164 and Gly165, and examined its heme-binding ability and heme-degradation activity. The absorption spectrum of the heme-reconstituted G165HG mutant was indistinguishable from that of the heme-G165H mutant (Fig. 8D). Verdoheme was formed following reaction of the heme-G165HG mutant with H_2O_2, but the amount (52% of *Vc*HutZ) was less than that of the K164H mutant (Fig. 8E), suggesting that the enzymatic activity was not improved by the mutation. These results imply that histidine at position 164 is the most favorable location for heme binding and verdoheme formation.

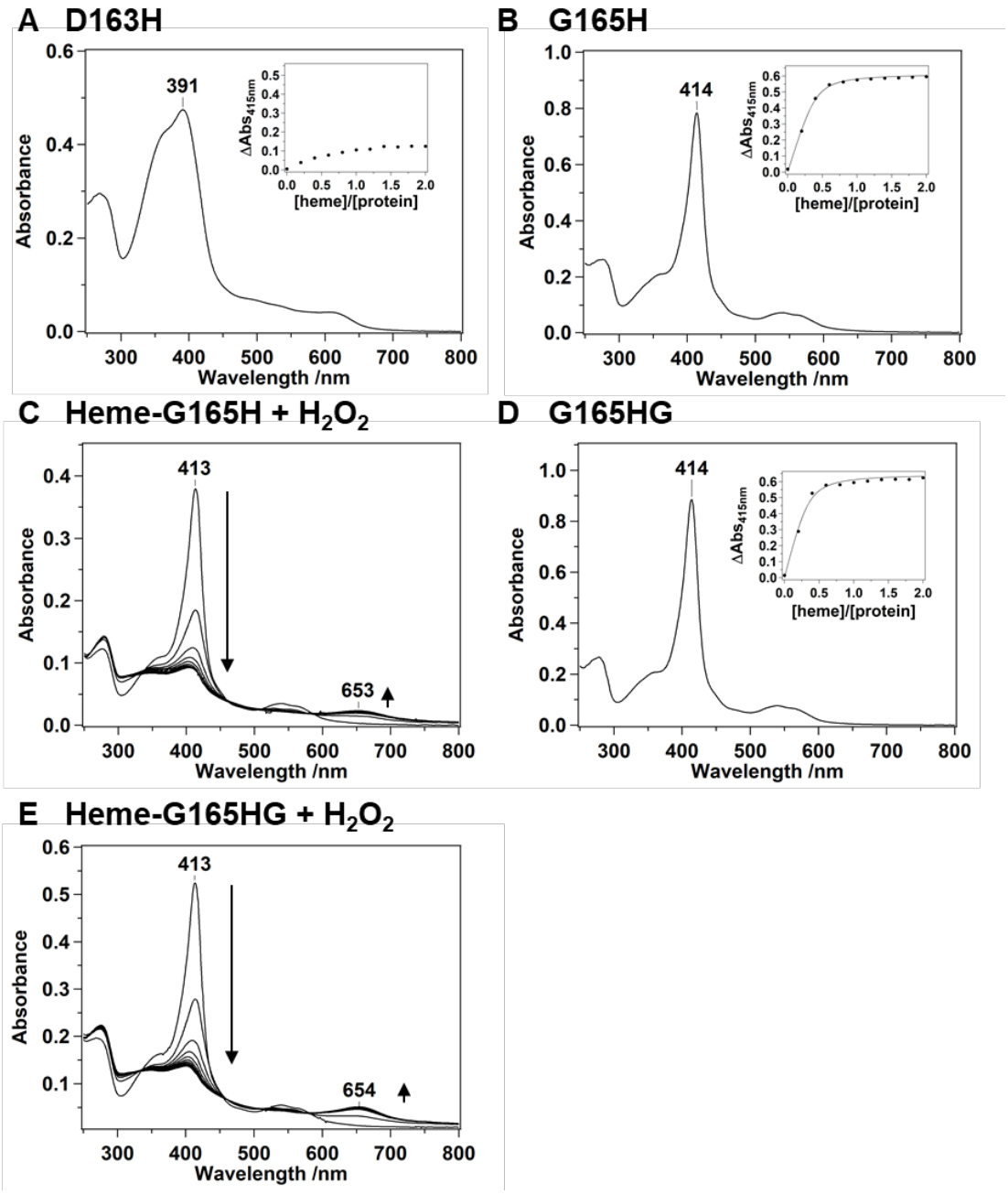

Fig. 8. **Absorption spectra of the D163H, G165H, and G165HG mutants.** (A, B) Absorption spectra of heme-D163H (A) and heme-G165H (B) mutants at pH 8.0. The inset shows differences at 414 nm following incremental addition of heme (2–30 μM) to Alr5027 (10 μM) in 50 mM Tris-HCl and 150 mM NaCl (pH 8.0), measured against a blank cell containing buffer alone. (C) Heme-degradation reaction of the heme-G165H mutant with H_2O_2 (0.1 mM) at pH 8.0. Spectra were measured before and after the addition of H_2O_2 at 1-min intervals for 10 min. (D) Absorption spectrum of the heme-G165HG mutant at pH 8.0. (E) Heme-degradation reaction of the G165HG mutant with H_2O_2. The reaction conditions were same as those in (C).

Heme-binding properties and degradation ability of a CTE mutant

To further improve heme-degradation activity, I next focused our attention on the C-terminal sequence of Alr5027. The crystal structure of HugZ from *H. pylori* shows that the C-terminal loop functions as a flexible portion of the active site that serves to keep the substrate heme in a proper conformation for HO activity [6]. Thus, I considered that the C-terminal region of Alr5027 is also important in improving enzymatic activity. A sequence alignment of Alr5027 with HutZ revealed that the sequence of Alr5027 lacks amino acid residues that correspond to the C-terminal region in *Vc*HutZ. Accordingly, I prepared an Alr5027 mutant containing a C-terminal extension (CTE) that mimics the C-terminal region of *Vc*HutZ (Fig. 1A) by inserting the sequence His-Arg-Lys-Ile-Ser between Asp163 and Lys164 (Fig. 1C). Addition of hemin to the CTE mutant yielded a Soret band at 412 nm in the resultant solution that was indistinguishable from that of the heme-K164H mutant (Fig. 9A). A titration curve clearly indicated that the CTE mutant was capable of binding to heme. The calculated $K_{d,heme}$ for the CTE mutant was 0.31 ± 0.07 μM (Fig. 7A, inset), a value comparable to that of the K164H mutant (0.24 ± 0.03 μM).

After the addition of H_2O_2 to the heme-CTE mutant, the absorbance at 652 nm increased (Fig. 9B), indicating that verdoheme accumulated in the reaction with H_2O_2. Addition of pyridine to the reaction solution caused the visible band to shift to 659 nm, suggesting that the β- or δ-*meso* position was cleaved (Fig. 6B), a behavior similar to that of the heme-K164H mutant (Fig. 6A). The heme-degradation reaction of the heme-CTE mutant was also examined using ascorbic acid as an electron source. Under these conditions, the Soret band remained after the addition of ascorbic acid at pH 8.0 and pH 6.0 (Fig. 9C, D), indicating that heme was not degraded in the reaction with ascorbic acid, as observed in the heme-K164H mutant (Fig. 7).

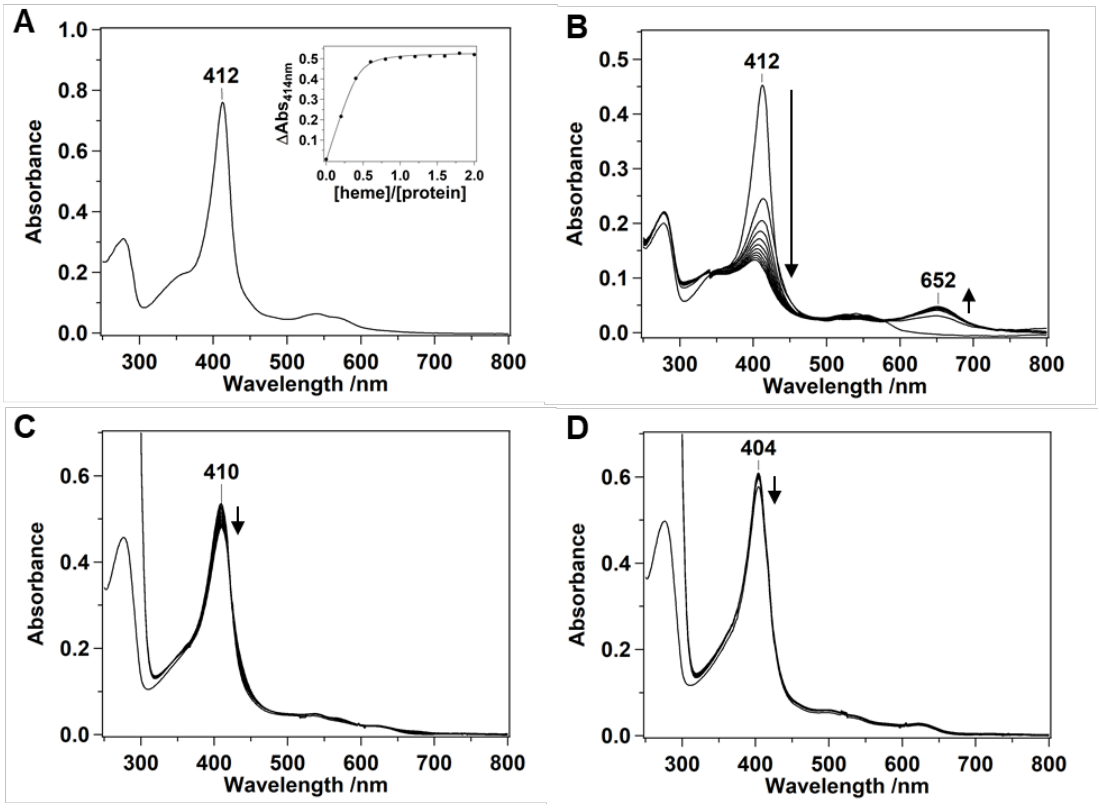

Fig. 9. **Absorption spectrum of the heme-CTE mutant.** (A) Absorption spectrum of the heme-CTE mutant. The inset shows differences at 414 nm. (B) Heme-degradation reaction of the CTE mutant with H_2O_2 (0.1 mM) at pH 8.0. The reaction conditions in (A) and (B) were same as those in Fig. 6A and C, respectively. (C, D) Heme-degradation reaction of the CTE mutant with 1.0 mM ascorbic acid at pH 8.0 (C) and pH 6.0 (D). Spectra were recorded before addition of ascorbic acid, and at 2-min intervals for 30 min after addition of ascorbic acid.

Reduction mechanism of heme-Alr5027

To investigate why the heme-K164H mutant was inactive toward ascorbic acid, I took into account the reaction mechanism of *Vc*HutZ. The heme-degradation reaction of *Vc*HutZ is mainly regulated by three key factors: (i) heme reduction [5], (ii) proton transfer from water molecules to reduced oxyferrous heme, and (iii) protomer-protomer interaction (unpublished observation). I first focused on heme reduction [factor (i)]. The reaction of heme-HutZ with ascorbic acid proceeds at pH 6.0, but not at pH 8.0. This is partially because the reduction rate of heme (k_{red}), the first step in the heme-degradation reaction, is ~3-fold faster at pH 6.0 than at pH 8.0. Thus, I measured the k_{red} of the heme-K164H mutant at pH 6.0 and 8.0. Fig. 10 shows

the time course of absorption changes at pH 8.0 after the addition of ascorbic acid to the ferric heme-K164H mutant in the presence of CO to prevent oxidation to ferric heme. Upon reduction, the Soret maximum at 410 nm underwent a red shift to 418 nm, the same position of the Soret band in the CO-bound heme. The time course of the absorption changes at 418 nm was fit to a single exponential, yielding a k_{red} of 2.8 ± 0.2 h^{-1} at pH 8.0. This value was larger than that of *Vc*HutZ at pH 8.0 (1.1 ± 0.5 h^{-1}) and similar to that of *Vc*HutZ at pH 6.0 (3.2 ± 0.3 h^{-1}). When measured at pH 6.0, the k_{red} was 4.0 ± 0.6 h^{-1}, showing that the k_{red} of Alr5027 at pH 6.0 and 8.0 were almost the same as that of heme-*Vc*HutZ at pH 6.0. Thus, based on k_{red} values, the reduction rate of heme does not account for the quite small amount of ascorbic acid-assisted heme-degradation by the heme-K164H mutant.

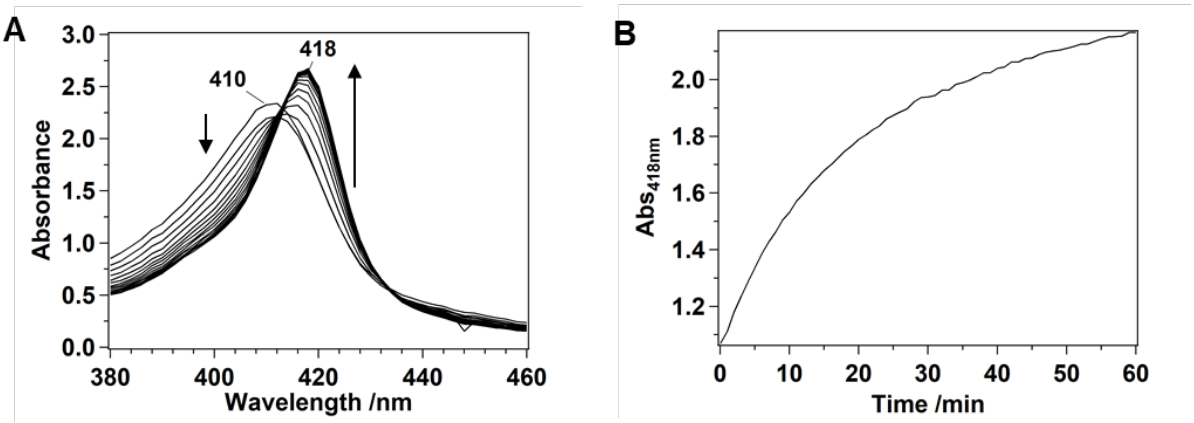

Fig. 10. Determination of the reduction rate of heme. (A) Absorption spectra of heme-K164H after the addition of 1 mM ascorbic acid at pH 8.0 under a CO atmosphere. (B) Time course of absorbance changes at 418 nm.

Heme-degradation activity through perturbation of the proton transfer pathway

To improve the heme-degradation activity of the K164H mutant, I next considered proton transfer from water molecules to reduced oxyferrous heme [factor (ii)]. Because replacement of Thr27 with valine substantially suppressed proton transfer to the reduced oxyferrous [Fe(III)-OO^{-}] species, I hypothesized that water molecules in the active site of *Vc*HutZ, which are potentially fixed by Thr27, act as proton sources. A sequence alignment of Alr5027 with HutZ

revealed that the sequence of Alr5027 lacks four corresponding amino acid residues, including Thr27 (Fig. 1A). Accordingly, I inserted a Glu-Arg-Lys-Thr (ERKT) sequence between Ser20 and Ala21 in the K164H mutant. At pH 6.0, the Soret maximum of the ferric heme of the resulting heme-ERKT mutant was 405 nm (Fig. 11A), which was almost the same as that of the heme-K164H mutant (Fig. 7B). The intensity of the Soret band was very little diminished after the addition of ascorbic acid at pH 6.0, and no clear band was observed in the 500–800 nm region (Fig. 11A). These spectral changes suggest that the heme-ERKT mutant caused no heme-degradation under these conditions, as observed for the heme-K164H mutant. A similar lack of ascorbic acid-assisted heme degradation was observed at pH 8.0 (Fig. 11B).

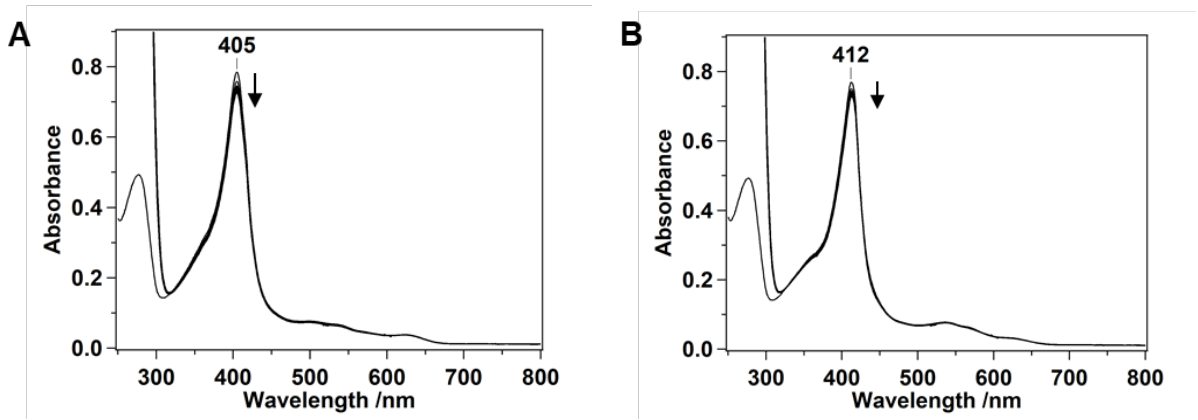

Fig. 11. **Absorption spectrum of the heme-ERKT mutant.** Heme-degradation reaction of the heme-Alr5027 ERKT mutant with ascorbic acid at pH 6.0 (A) and pH 8.0 (B). Spectra were monitored before the addition of ascorbic acid, and at 2-min intervals for 30 min after the addition of ascorbic acid.

Structural characterization of heme-K164H and heme-ERKT mutants

Finally, I focused on protomer-protomer interaction [factor (iii)]. Our group have found that replacement of Ala31 of *Vc*HutZ with valine at the subunit-subunit interface results in the loss of the ascorbic acid-assisted heme-degradation activity (unpublished observation). Thus, I considered the possibility that the heme in K164H and ERKT mutants was not degraded by ascorbic acid because the distance between the subunits was elongated compared with that in *Vc*HutZ. The distance between subunits can be inferred from the distance between heme and

Trp103 (Fig.. 12). To estimate the distance between heme and Trp103 of the heme-K164H mutant, I measured the fluorescence spectra of tryptophan. Following excitation at 295 nm, the fluorescence of Trp103, which is the sole tryptophan in Alr5027, was observed at ~334 nm. The fluorescence for the heme-bound K164H mutant was much smaller than that of the heme-unbound K164H mutant (Fig. 13A), suggesting that the fluorescence of Trp103 was quenched by heme. Using the intensity of the fluorescence at 334 nm for the K164H and heme-K164H mutant, I calculated the energy transfer efficiency, *E*, and estimated the distance between heme and Trp103 on the basis of Equations 2 and 3, respectively. For the K164H mutant, the distance at pH 6.0 was estimated to be 23 Å, which is much larger than that of heme-WT *Vc*HutZ (18 Å) (unpublished observation). The intensity at 333 nm for the heme-K164H mutant at pH 8.0 was almost the same as that at pH 6.0 (Fig. 13A). Thus, the decrease in the quenching of tryptophan fluorescence by energy transfer to heme indicated that the distance between heme and Trp103 at pH 6.0 was the same as that at pH 8.0 within 1 Å (Fig. 13B). The fluorescence of the ERKT mutant was significantly decreased upon heme binding, and the estimated distance of 17–22 Å (Fig. 13B, C) was much larger than that of heme-WT *Vc*HutZ (16–18 Å) (unpublished obsevation). These results suggest that the diminished heme-degradation activity of the ERKT mutant when ascorbic acid is used as an electron source is related to elongation of the distance between heme and Trp103, as observed in the heme-A31V mutant *Vc*HutZ.

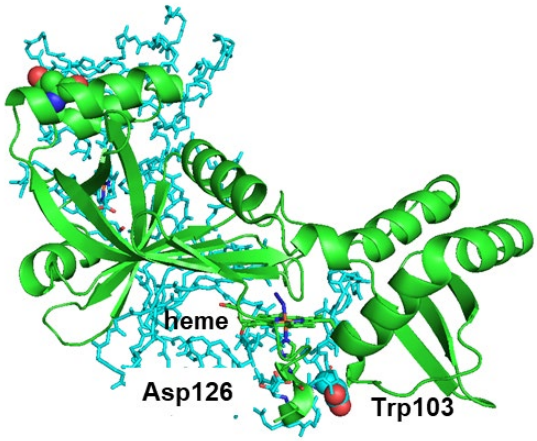

Fig. 12. **Location of Trp103 and heme on the HugZ crystal structure (PBD 3GAS).** Residues are numbered according to the amino acid sequence of Alr5027 from cyanobacteria *Nostoc sp*. PCC7120. Green and cyan show each protomer. Trp103 is present in a different protomer (green) from that (cyan) containing the nearby Asp126.

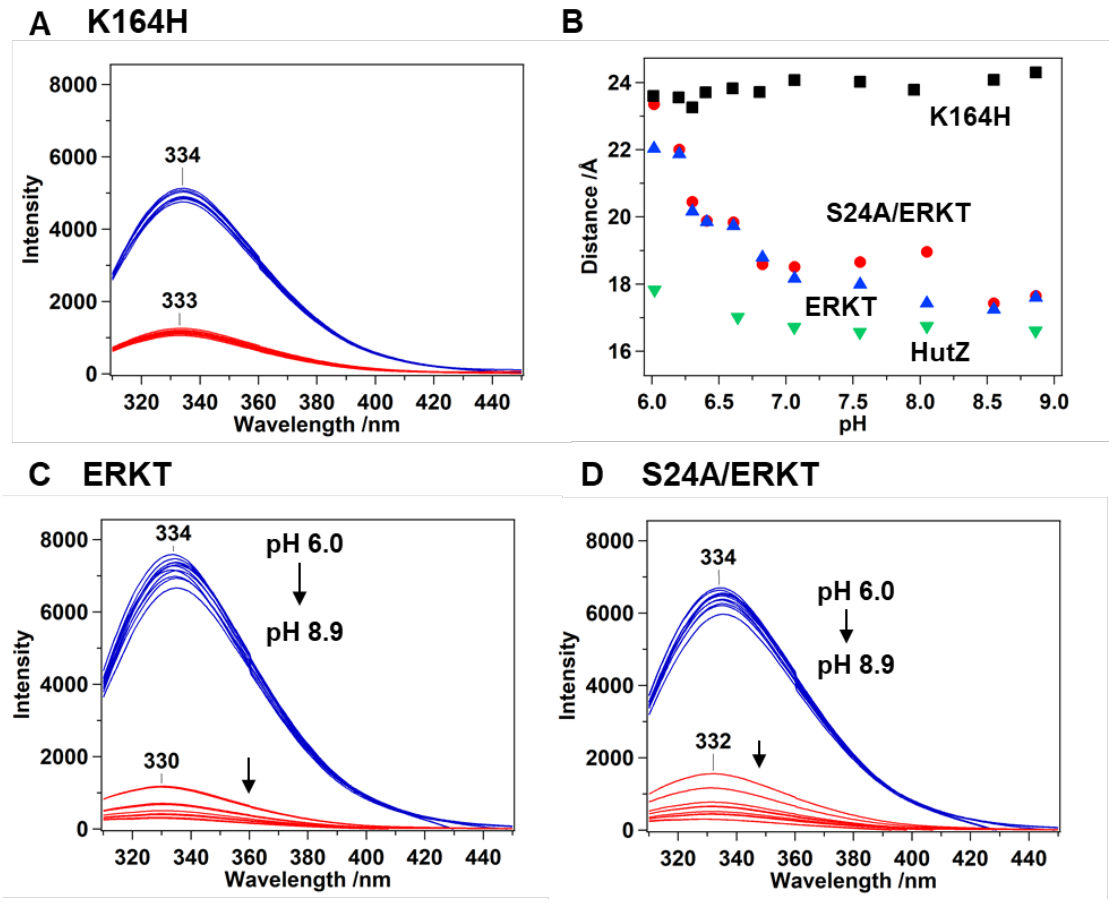

Fig. 13. **Fluorescence spectra.** Fluorescence spectra of heme-K164H, heme-ERKT, and heme-S24A/ERKT Alr5027 mutants. (A–C) Fluorescence spectra of K164H (A), ERKT (B) and S24A/ERKT (C) mutants in the absence (red lines) and presence (blue lines) of heme. Spectra were recorded at pH 6.0, 6.2, 6.3, 6.4, 6.6, 6.8, 7.0, 7.5, 8.0, 8.5 and 8.8, with excitation at 295 nm. The sample concentration was 5 □M. (D) pH dependence of the distance between heme and Trp103 in K164H, ERKT, and S24A/ERKT mutants.

Heme-degradation activity following introduction of alanine at the subunit-subunit interface

Because a sequence alignment revealed that Ser24 of Alr5027 corresponds to Ala31 in *Vc*HutZ (Fig. 1A), I predicted that replacement of Ser24 with alanine in the ERKT mutant would reduce the distance between protomers at pH 6.0 and lead to enhanced heme degradation by ascorbic acid. Accordingly, I replaced Ser24 with alanine in the ERKT mutant and measured the fluorescence spectra of tryptophan (Fig. 13D). I also calculated the energy transfer efficiency, *E*, and the distance, using the fluorescence intensity at 334 nm of heme-bound and unbound S24A/ERKT mutant. The estimated distance was 17–23 Å (Fig. 13B, D), which is similar to that of the ERKT mutant. The heme-degradation reaction of the S24A/ERKT mutant was also examined using ascorbic acid. The Soret band remained even after the addition of ascorbic acid at both pH 6.0 and pH 8.0 (Fig. 14), indicating that heme was not degraded in the reaction with ascorbic acid. This is because the distance between protomers at pH 6 was still greater than optimal.

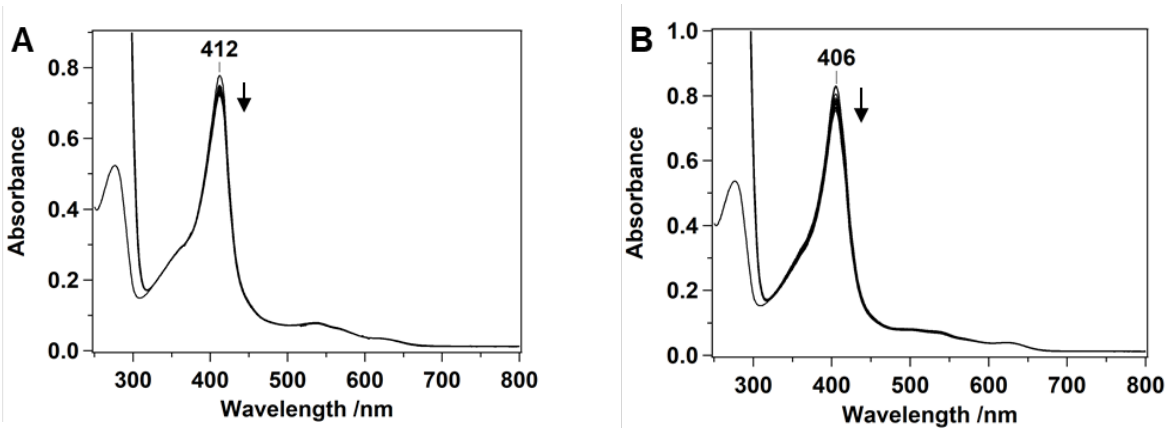

Fig. 14. **Heme-degradation reaction of the heme-Alr5027 S24A/ERKT mutant with ascorbic acid at pH 8.0 (A) and pH 6.0 (B).** Spectra were monitored before the addition of ascorbic acid, and at 2-min intervals for 30 min after the addition of ascorbic acid.

4.4. Conclusions

Previous study shows that HutZ from *V. cholerae* has heme-degrading ability and produces the same reaction products as HOs [5,13,18]. The structure of heme-bound HugZ from *H. pylori* suggests that members of the HugZ family are structurally distinct from HOs. Thus, I predicted that the ancestor protein of HutZ is different from that of canonical HOs. In the current study, I found that Alr5027 from *Nostoc* sp. PCC 7120 is homologous to HutZ (Fig. 1A) and belongs in a phylogenetic group apart from other HutZ family members (Fig. 1B). Characterization of the heme-binding ability and heme-degradation activity of Alr5027 showed that Alr5027 did not bind to heme (Fig. 3), because the heme axial histidine ligand was not conserved in Alr5027 (Fig. 1A). However, introduction of histidine at position at 164 conferred heme-binding ability on Alr5027. Although none of the mutants degraded heme with ascorbic acid because of elongation of the distance between the subunit and subunit interface (Fig. 13), the K164H and G165H mutants formed verdoheme with H_2O_2. Our results indicate that a lysine-to-histidine substitution at residue 164 was the mutation that most effectively enabled Alr5027 to bind heme and produce verdoheme (Fig. 4). These findings suggest that pathogenic bacteria that possess HutZ family members may have acquired heme-degradation ability from a common ancestor of Alr5027 through molecular evolution.

References

(1) Rasmussen, B.; Fletcher, I. R.; Brocks, J. J.; Kilburn, M. R. *Nature* **2008**, *455* (7216), 1101.

(2) Raymond, J.; Blankenship, R. R. E. *Geobiology* **2004**, *2* (4), 199.

(3) Domitrovic, T.; Raymundo, D. P.; da Silva, T. F.; Palhano, F. L. *PLoS One* **2015**, *10* (9), e0136761.

(4) Kaneko, T.; Nakamura, Y.; Wolk, C. P.; Kuritz, T.; Sasamoto, S.; Watanabe, A.; Iriguchi, M.; Ishikawa, A.; Kawashima, K.; Kimura, T.; Kishida, Y.; Kohara, M.; Matsumoto, M.; Matsuno, A.; Muraki, A.; Nakazaki, N.; Shimpo, S.; Sugimoto, M.; Takazawa, M.; Yamada, M.; Yasuda, M.; Tabata, S. *DNA Res* **2001**, *8* (5), 205.

(5) Uchida, T.; Sekine, Y.; Matsui, T.; Ikeda-Saito, M.; Ishimori, K. *Chem. Commun.* **2012**, *48* (53), 6741.

(6) Hu, Y.; Jiang, F.; Guo, Y.; Shen, X.; Zhang, Y.; Zhang, R.; Guo, G.; Mao, X.; Zou, Q.; Wang, D. C. *J. Biol. Chem.* **2011**, *286* (2), 1537.

(7) Kumar, S.; Stecher, G.; Tamura, K. *Mol. Biol. Evol.* **2016**, *33* (7), 1870.

(8) Uchida, T.; Sasaki, M.; Tanaka, Y.; Ishimori, K. *Biochemistry* **2015**, *54* (43), 6610.

(9) Berry, E. A.; Trumpower, B. L. *Anal. Biochem.* **1987**, *161* (1), 1.

(10) Wu, P. G.; Brand, L. *Anal. Biochem*. **1994**, *218*(1), 1.

(11) Sakamoto, H.; Omata, Y.; Adachi, Y.; Palmer, G.; Noguchi, M. *J. Inorg. Biochem.* **2000**, *82* (1–4), 113.

(12) Englander, S. W.; Calhoun, D. B.; Englander, J. J. *Anal. Biochem.* **1987**, *161* (2), 300.

(13) Uchida, T.; Sekine, Y.; Dojun, N.; Lewis-Ballester, A.; Ishigami, I.; Matsui, T.; Yeh, S.-R.; Ishimori, K. *Dalton Trans.* **2017**, *46* (25), 8104.

(14) King, N. K.; Wingield, M. E. *J. Biol. Chem.* **1963**, *238* (4), 1520.

(15) Wilks, A.; Ortiz de Montellano, P. R. *J. Biol. Chem.* **1992**, *267* (13), 8827.

(16) Zhang, X.; Fujii, H.; Mansfield Matera, K.; Migita, C. T.; Sun, D.; Sato, M.; Ikeda-Saito, M.; Yoshida, T. *Biochemistry* **2003**, *42* (24), 7418.

(17) Liu, Y.; Lightning, L. K.; Huang, H.; Moënne-Loccoz, P.; Schuller, D. J.; Poulos, T. L.; Loehr, T. M.; Ortiz de Montellano, P. R. *J. Biol. Chem.* **2000**, *275* (44), 34501.

(18) Uchida, T.; Dojun, N.; Sekine, Y.; Ishimori, K. *Biochemistry* **2017**, *56* (21), 2723.

PART IV: Iron Chelators Inhibit Heme-Degradation Activity of HutZ

Abstract

I try to observe the heme-degradation reaction in the presence of the iron chelator, ferrozine, which reduced the ratio of iron liberated from heme to the starting heme concentration by ~50%. The chelating agents, deferoxamine and citric acid, also inhibited the reaction. To investigate the inhibition mechanism, I measured the rate of each heme-degradation step in the presence of iron chelators. This analysis revealed that chelators did not affect rate constants for heme reduction, ligand binding, or verdoheme formation. Therefore, we postulated that iron chelators inhibited the remaining step: protonation of Fe(III)-OO–. The candidate for this protonation is a water molecule stabilized by the heme-binding site-proximate residue, Thr27. Mutation of Thr27 to valine also inhibited the reaction, but mutation to serine did not. These results suggest that water molecules hydrogen bonded to Thr27 are involved in proton transfer to Fe(III)-OO–, and that this step is inhibited by iron chelators. Tetracycline, which is the effective antibiotics for cholera, has iron chelating ability. Thus, I suspected that tetracycline affects the heme degradation activity of HutZ in term of the own iron chelating ability. The ratio of released iron from heme is reduced by ~50% in the presence of tetracycline, suggesting that this inhibition is derived from iron chelating ability. This finding indicates that iron chelators are good candidates as antibiotics against *V. cholerae*.

3.1. **Introduction**

The results and discussion in previous part clearly elucidates the heme degradation reaction mechanism of HutZ. The heme-degradation enzymes cannot report a turnover number because the heme-degradation is a single-turnover reaction. The heme-degradation enzymes can release biliverdin and ferrous iron from themselves in the presence of biliverdin reductase and/or iron chelator. To estimate the enzymatic activity of heme-degradation enzymes, the detection of the amount of biliverdin or ferrous iron is needed. In HO-1, the amount of biliverdin per unit time is increase in the presence of iron chelators[1]. However, the heme-degradation activity of HutZ remains unknown.

In this part, I observed the heme degradation activity of HutZ in the presence of ferrozine, and serendipitously found the inhibition of heme degradation activity of HutZ. When iron chelators were added to a reaction solution containing heme-HutZ and ascorbic acid, I found that the reaction proceeded very slowly in the presence of iron chelators. To determine the inhibition steps of heme-degradation reaction, I observed the rate of heme-degradation reaction by HutZ in the presence of iron chelator, suggesting that iron chelators inhibit the protonation of oxyheme to hydroperoxyheme. The heme-degradation activity of Thr27Val mutant also was repressed as well as HutZ with iron chelators. This result indicates that iron chelators can inhibit the heme-degradation reaction of HutZ. Thus, in the current study, I investigated the mechanism by which iron chelators inhibit heme degradation.

3.2. Experimental Produres

Materials.

The chemicals used in this study were purchased from Wako Pure Chemical Industries (Osaka, Japan), Nacalai Tesque (Kyoto, Japan), or Sigma-Aldrich (St. Louis, MO), and used without further purification.

Expression and Purification of HutZ.

Mutant HutZ proteins were expressed in *Escherichia coli* and purified as described previously. Mutagenesis was conducted utilizing a PrimeSTAR mutagenesis basal kit from Takara Bio (Otsu, Japan). DNA oligonucleotides were purchased from Eurofins Genomics Inc. (Tokyo, Japan). The mutated genes were sequenced by Eurofins Genomics to ensure that only the desired mutations were introduced.

Spectroscopy.

Optical spectra of the purified protein were recorded with UV-visible spectrophotometer (V-660, Jasco, Tokyo, Japan) at room temperature. Resonance Raman spectra were obtained with a single monochromator (SPEX500M; Jobin Yvon, Edison, NJ, USA) equipped with a liquid nitrogen-cooled CCD detector (Spec-10:400B/LN; Roper Scientific, Princeton, NJ). The excitation wavelengths employed were 413.1 and 441.6 nm from a krypton ion laser (BeamLok 2060; Spectra Physics, MO, USA) and helium-cadmium laser (IK5651R; Kimmon Koha, Tokyo, Japan), respectively. The laser power at the sample point was adjusted to 0.1 mW for the CO-bound form to prevent photodissociation. Raman shifts were calibrated with indene, CCl_4, acetone, and an aqueous solution of ferrocyanide. The accuracy of the peak positions of well-defined Raman bands was ±1 cm^{-1}. Sample concentrations for resonance Raman experiments were about 10 μM in 50 mM MES-OH 150 mM NaCl, pH 6.0. Circular dichroism (CD) spectra were observed by a JASCO J-1500 CD spectropolarimeter operating. The sample concentration was 5.0 μM in 50 mM sodium phosphate, 100 mM NaCl at pH 6.0

Isothermal Titration Calorimetry.

Calorimetry measurements were performed with a NANO-ITC titration calorimeter instrument from TA Instruments (Delaware, USA). The sample cell was filled with 30 μM of heme-HutZ complex. The injection syringe contained 3 mM DFO, and this experiment was performed in triplicate at 25 ℃. Experiments were performed using 25 injections, a stirring speed of 250 rpm, and a 180 seconds delay between injections. The injection volumes for the heme-HutZ complex consisted of 2 μL each. The heat values recorded were integrated, and the data were fit to a one-to-one binding mode.

Reduction Rate of Heme.

The reduction rate of heme, k_1 (Figure S4), was determined by following changes in absorbance at 418 nm. 10 μM of ferric heme-HutZ complex was reduced by 1 mM ascorbic acid in the presence or absence of 0.1 mM DFO. Although an oxygen scavenging system composed of glucose, glucose oxidase, and catalase was added to the solution to anaerobic, the reaction was conducted under carbon monoxide (CO) atmosphere to prevent from oxidation of heme and/or re-oxidation by contaminated O_2. The k_1 was obtained by fitting the time course of the absorbance change to a single exponential expression.

Cyanide Binding Rate Constants.

Cyanide binding (CN) was measured by s stopped-flow apparatus (Unisoku, Osaka, Japan) by following the decrease of absorbance at 403 nm. In a typical cyanide binding experiment, one syringe contained 3 μM HutZ in 50 mM MES 150 mM NaCl (pH 6.0), and another syringe contained at least a 100-fold excess of CN. Three determinations were performed for each ligand concentration. The mean of the pseudo-first-order rate constants, k_{obs}, was used in the calculation of the second-order rate constants obtained from the slope of a plot of k_{obs} versus ligand concentration ($k_{obs} = k_{on}[CN] + k_{off}$).

3.3. Results and Discussion

Heme Degradation Reaction in the Presence of Iron Chelators

To investigate the heme-degradation activity of HutZ, I observed the heme degradation reaction in the presence of iron chelators for the detection of amount of ferrous iron. As shown in Fig.1, which presents spectral changes following addition of ascorbic acid to ferric heme-HutZ, ascorbic acid caused a decrease in the Soret band at 406 nm, attributable to heme breakdown (Fig. 1A), as previously reported[2]. By contrast, addition of ferrozine prior to the reaction caused little decrease in the Soret band (Fig. 1B), and the heme-degradation ratio was 32 ± 7 %, suggesting that the heme-degradation reaction is repressed by ferrozine. This change was not caused by pH change upon addition on ferrozine to the solution and irreversible.

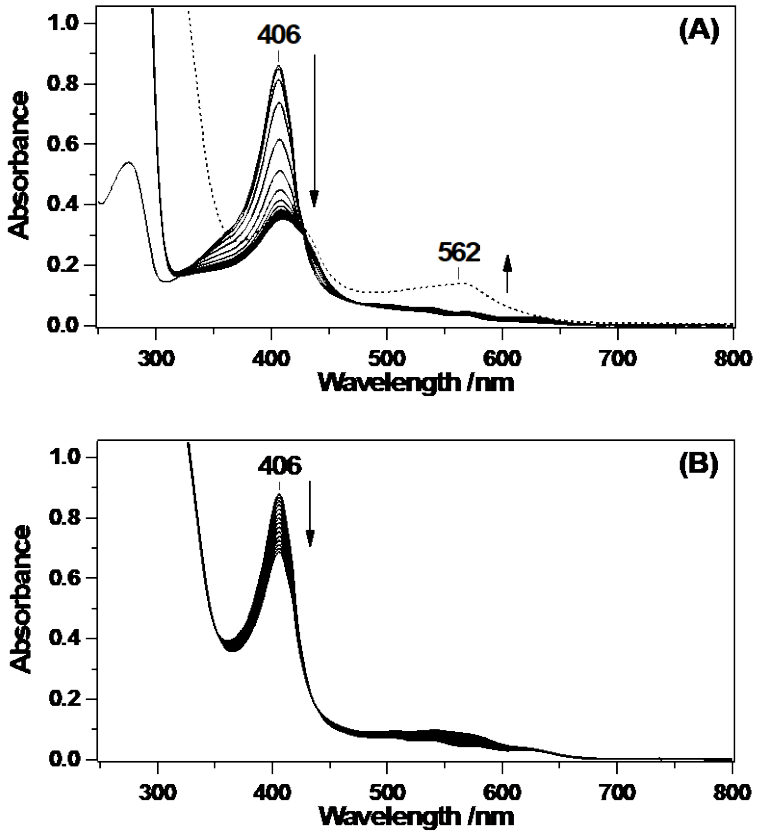

Fig. 1 Heme-degradation reaction of the heme-HutZ complex with ascorbic acid (1.0 mM) in 50 mM MES-OH/150 mM NaCl (pH 6.0) at 25 °C. To prevent nonenzymatic coupled oxidation, approximately 1 μM catalase was included (ε_{405} = 420 mM^{-1} cm^{-1} for the tetramer[3]). Spectra were measured before addition of ascorbic acid and at 8-min intervals for 56 min after the addition of ascorbic acid. Ferrozine (0.10 mM)

was added (A) 30 min after the reaction or (B) before the reaction. Dotted line in (A) is the spectrum obtained following addition of ferrozine 60 min after initiation of the reaction.

To determine whether inhibition of heme degradation by ferrozine requires the iron-chelating property of ferrozine or a specific interaction of ferrozine with HutZ, we monitored the same reaction in the presence of the typical iron chelators, EDTA, citric acid, and deferoxamine (DFO). Although EDTA did not affect the heme-degradation reaction, DFO and citric acid, in addition to ferrozine, significantly slowed the reaction (Fig. 2). The dependence of this inhibition on the concentration of citric acid, ferrozine, and DFO was investigated. Fig. 3 shows the relative intensity ratio of the absorbance at 406 nm at 30 min after the reaction to the initial absorbance, where larger values indicate greater inhibition. The addition of chelators increased this ratio, indicating that the amount of heme degradation was decreased with increasing chelator concentration. The inhibition constant (K_i) for DFO was 5.7 μM, which is smaller than that for ferrozine (52 μM) and citric acid (6.0×10^2 μM) (Fig. 3). The stability constant (K_M) of ferrous iron for DFO (~10^{10} M)[4] is higher than that of citric acid ($10^{4.6}$ M)[5], but smaller than that of ferrozine ($10^{15.6}$ M)[6]. These results indicate that the inhibition mechanism of iron chelators does not necessarily involve metal chelation.

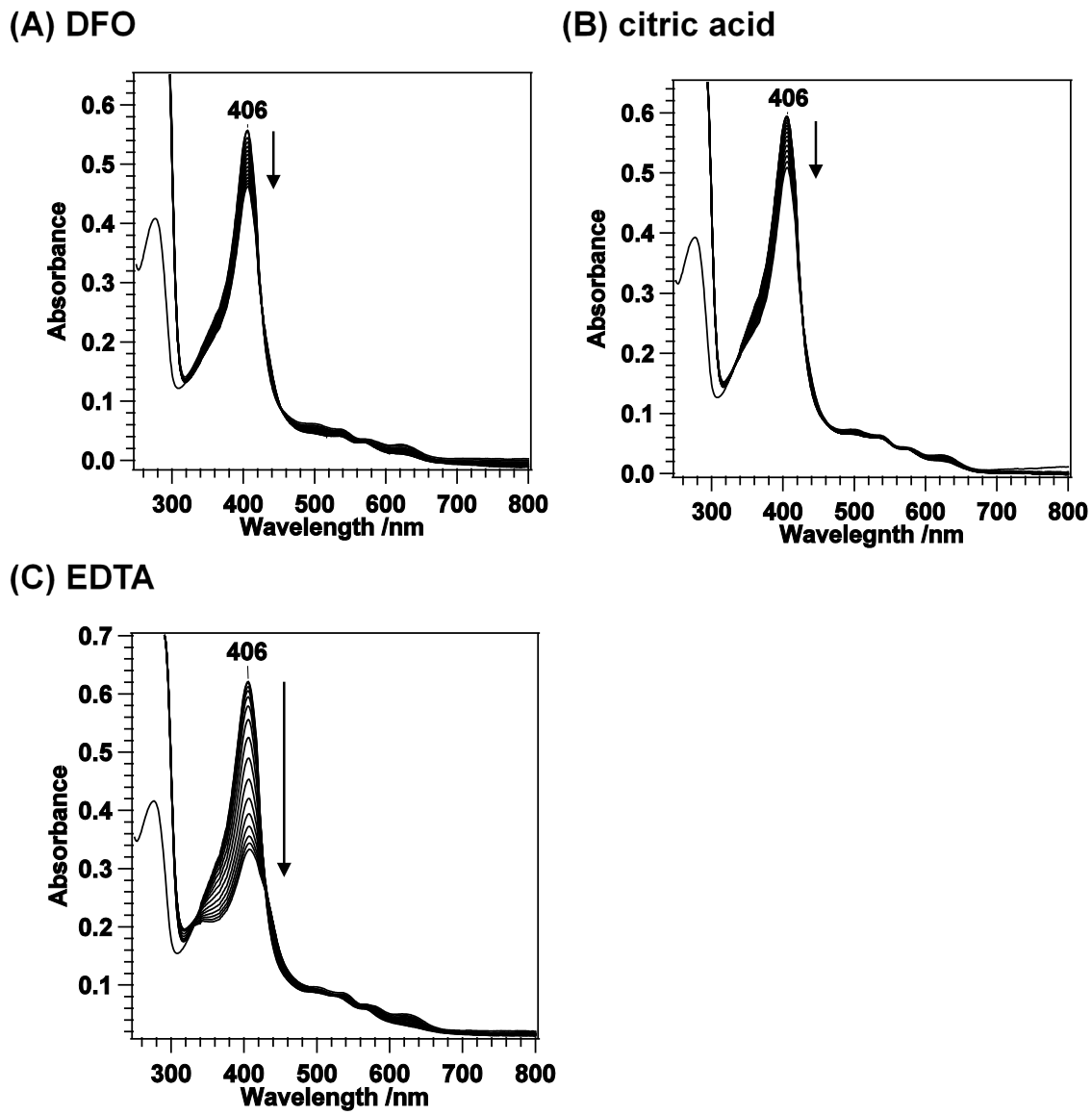

Fig. 2 Heme-degradation reaction of the heme-HutZ complex with ascorbic acid (1.0 mM) at pH 6.0. Spectra were measured before addition of ascorbic acid, and at 2-min intervals for 30 min after addition of ascorbic acid in the presence of (A) 0.10 mM DFO, (B) 1.0 mM citric acid, and (C) 0.10 mM EDTA.

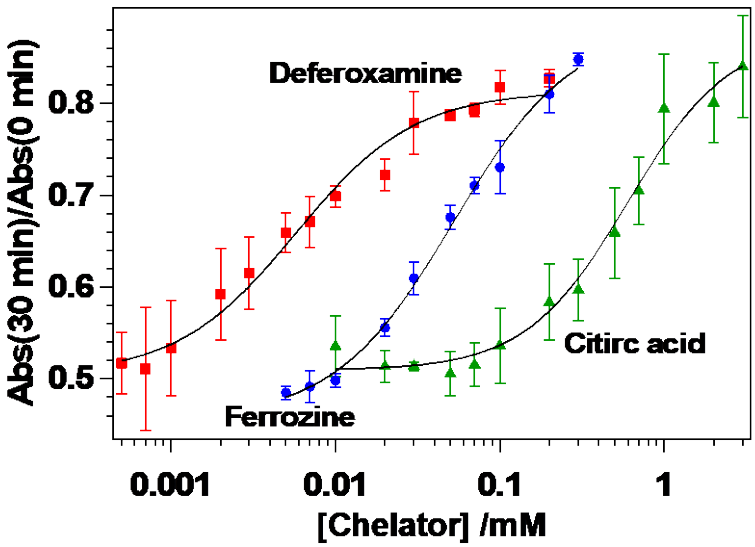

Fig. 3 Changes in absorbance at 406 nm during heme degradation by HutZ in the presence of DFO, citric acid, or ferrozine. The data points in UV-vis spectra were obtained before addition of ascorbic acid (1 mM) and 30 min after addition. Abs(30 min)/Abs(0 min) values are plotted against iron chelator concentration, and the data were fit to the Hill equation.

Affection on the Active Site of HutZ in the Presence of Iron Chelators

The deceleration of the enzymatic reaction of HutZ by iron chelators raised the possibility that the chelators affect the structure of the active site of heme-HutZ. To test this, we measured UV-vis absorption and resonance Raman spectra of heme-HutZ. The Soret maximum of ferric heme-HutZ at 406 nm remained after the addition of DFO (Fig. 4A). Moreover, resonance Raman spectra of the CO-heme complex of HutZ revealed that the addition of DFO did not shift Fe-CO ($\nu_{Fe\text{-}CO}$) or C-O ($\nu_{C\text{-}O}$) stretching modes from their original values of 506 cm^{-1} and 1933 cm^{-1}, respectively, measured in the absence of chelators (Fig. 4B). We also measured circular dichroism spectra of heme-HutZ to determine whether the addition of DFO caused any secondary structural changes. The ellipticity at 222 nm, which represents the α-helical structure, was virtually insensitive to DFO (Fig. 4C), although that below 215 nm was slightly decreased in the presence of DFO. This latter change likely reflects the absorption of DFO itself, which exhibits a broad band between 200 and 240 nm (Fig. 4D). These results suggest that DFO does not induce a detectable change in secondary structure. Thus, we postulated that the chelators do not bind to heme-HutZ and disturb its active site. To confirm this, we applied isothermal titration calorimetry to study the energetics of chelator binding to heme-HutZ. Indeed, no binding heat was detected for a solution of DFO and heme-HutZ (Fig. 5), indicating that DFO does not likely bind HutZ directly.

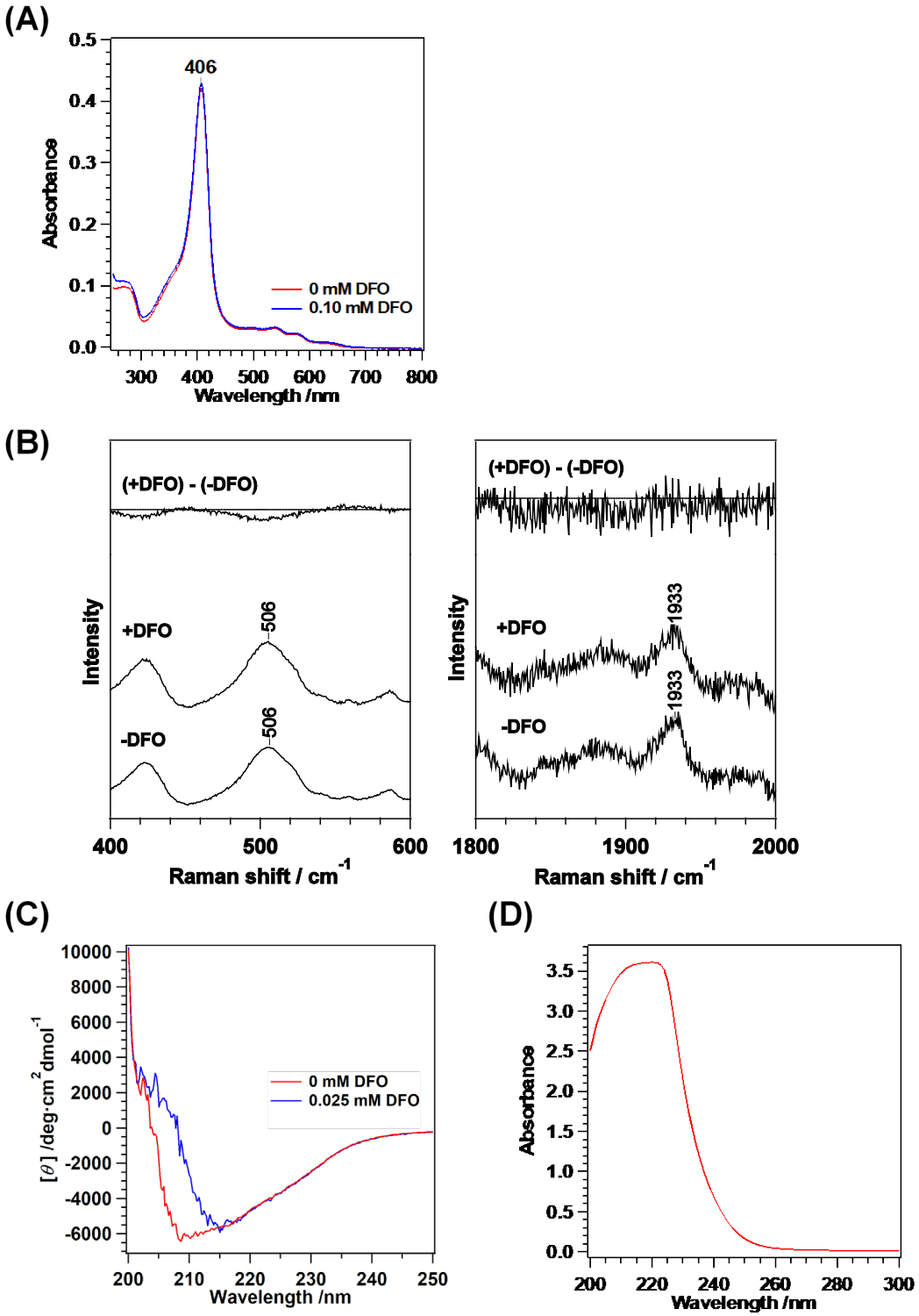

Fig. 4 (A) Absorption spectra of the heme-HutZ in the absence (red) and presence of 0.1 mM DFO (blue). (B) Resonance Raman spectra of the heme-HutZ in the CO-bound form. The protein concentration is 10 mM in 50 mM Tris-HCl/150 mM NaCl (pH 6.0). (C) CD spectra of heme-HutZ in the absence (red) and presence of DFO (blue). Protein concentration was 5.0 μM in 50 mM sodium phosphate/100 mM NaCl. (D) Absorption spectra of 1.0 mM DFO in 50 mM sodium phosphate/100 mM NaCl.

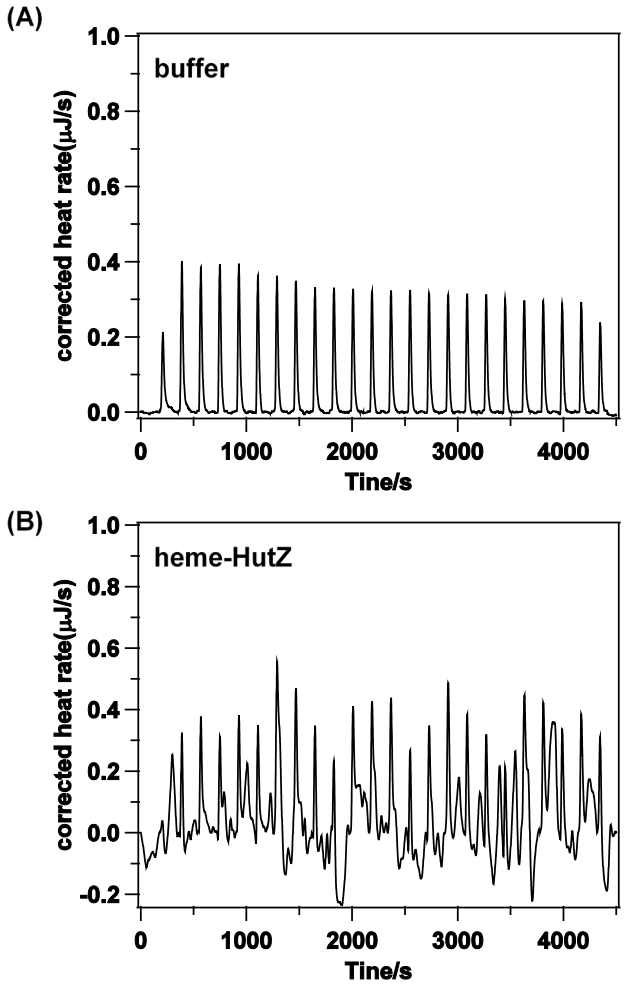

Fig. 5 ITC data for titration of 3 μM DFO into (A) buffer, and (B) 35 μM heme-HutZ. Injections (25 × 2 μL) were made at 180 sec intervals in 50 mM Tris-HCl/150 mM NaCl (pH 8.0) at 25 °C.

Inhibition Steps of Heme Degradation Reaction by Iron Chelators

To clarify how chelators cause inhibition, we focused on the heme-degradation mechanism of HutZ, which is a multistep reaction, as shown in Fig. 6[2,7,8]. Accordingly, we next sought to determine which step is inhibited by the chelators. First, we measured the reduction rate of heme, k_1, the first step of heme degradation (Fig. 6). Fig. 7 shows the time course of absorption changes after the addition of ascorbic acid to ferric heme-HutZ, in the presence of CO to prevent oxidation to ferric heme. Upon reduction, the Soret maximum at 406 nm underwent a red shift to 418 nm—the same position of the Soret band in CO-bound heme[2]. The time course of absorbance changes at 418 nm in the absence of DFO was fit to a single exponential, which yielded a k_1 of 0.052 ± 0.005 min^{-1}. In the presence of DFO, the k_1 was 0.045 ± 0.008 min^{-1},

showing that DFO does not affect this step.

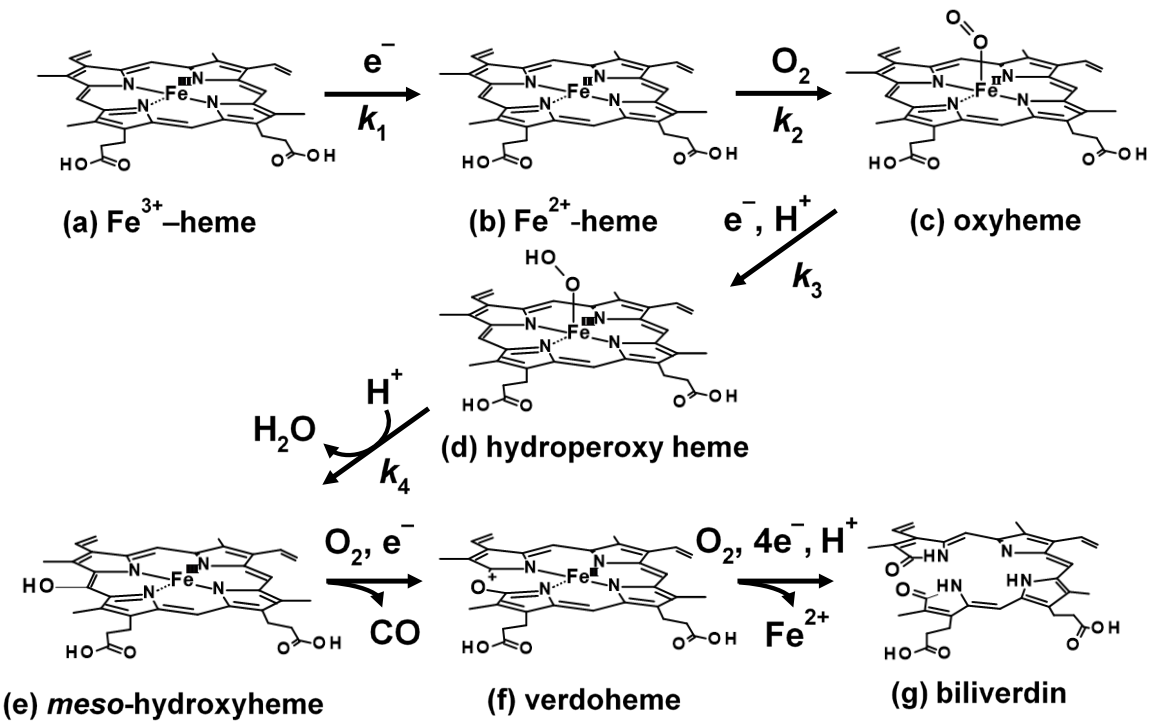

Fig. 6 Heme degradation mechanism in HutZ

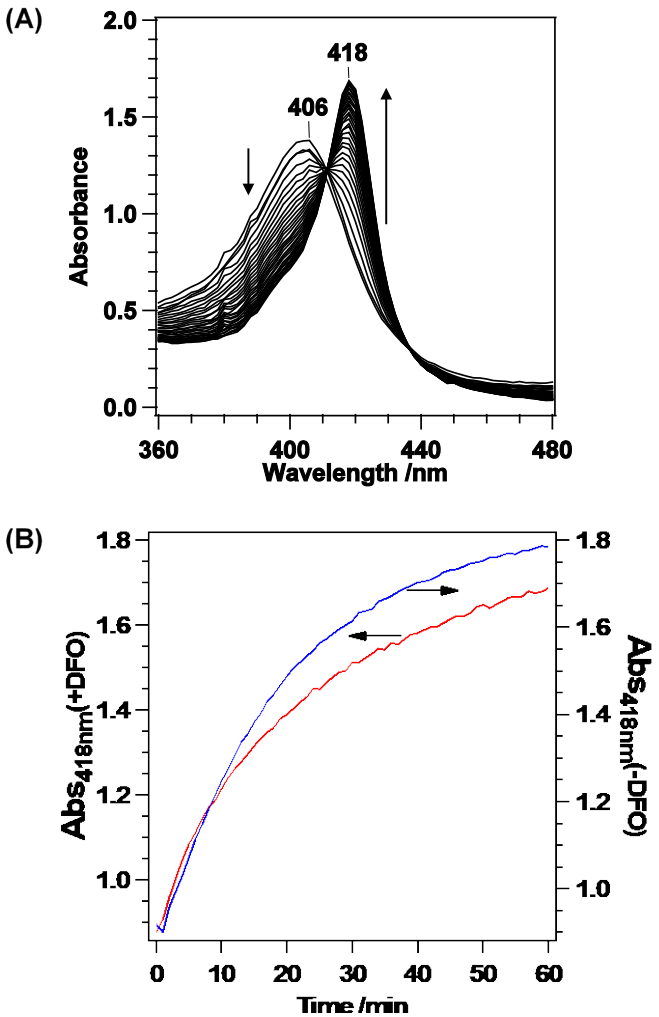

Fig. 7 Determination of reduction rate of heme. (A) UV-vis spectra of heme-HutZ after addition of ascorbic acid (1 mM) in the presence of DFO at pH 6.0 under CO atmosphere. (B) Time course of absorbance change at 418 nm in the presence (red, left axis) and absence (blue, right axis) of DFO.

The second step in heme degradation is O_2 binding to ferrous heme (Fig. 6). It is difficult to obtain the rate constant for this step (k_2), because O_2-bound heme-HutZ is rapidly autoxidized to ferric heme[2], or converted to hydroperoxy heme, leading to degradation of heme. Therefore, we measured the cyanide (CN) ion-binding rate (k_2') instead of k_2. A typical time course for the reaction of heme-HutZ with CN using a stopped-flow apparatus is shown in Fig. 8A. Under conditions of excess of CN, a pseudo-first rate constant (k_{obs}) was obtained from the single-exponential fit. The obtained k_{obs} values increased linearly with increasing concentrations of CN (Fig. 8). The second-order rate constant, k_2', obtained from the slope of this relation, was 0.88 ± 0.01 $mM^{-1}s^{-1}$ in the absence of DFO and only slightly smaller (0.76 ± 0.01 $mM^{-1}s^{-1}$) in

the presence of DFO. Therefore, the step involving ligand binding to heme is unlikely to be inhibited by DFO. Finally, the rate constant for the formation of verdoheme, k_4 (Fig. 9), was compared. In the reaction with H_2O_2, the Soret band disappeared with a concomitant increase in a band at 644 nm[2] (Fig. 9). The value of k_4 obtained by fitting the data at 644 nm to a single exponential curve, was 0.38 s^{-1}, which is approximately equal to that in the presence of DFO (0.39 s^{-1}).

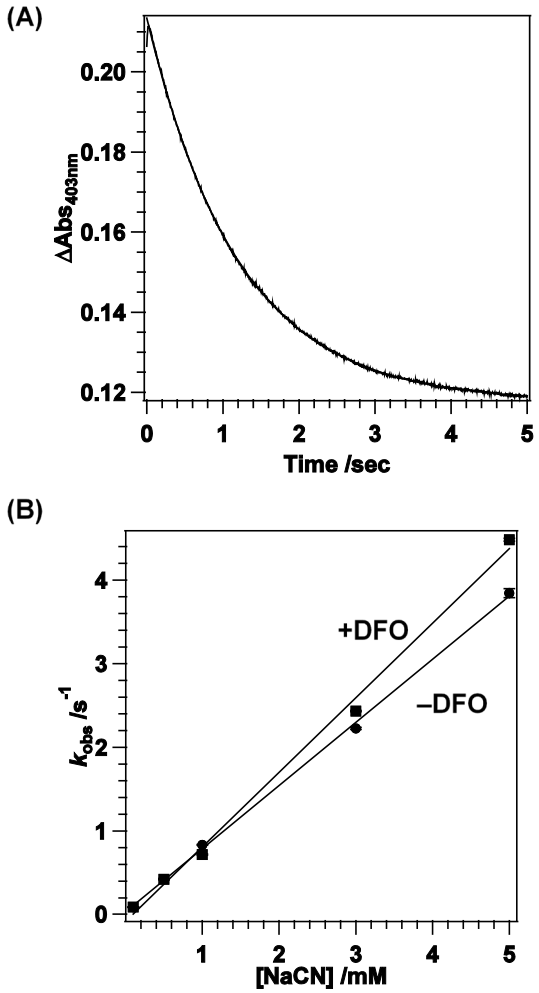

Fig. 8 Cyanide binding to heme-HutZ. (A) typical time trace of the absorbance change at 403 nm upon mixing 3.0 μM of heme-HutZ with 1.0 mM CN^- in 50 mM MES-NaOH/150 mM NaCl (pH 6.0). (B) Plots of k_{obs} versus CN^- concentrations.

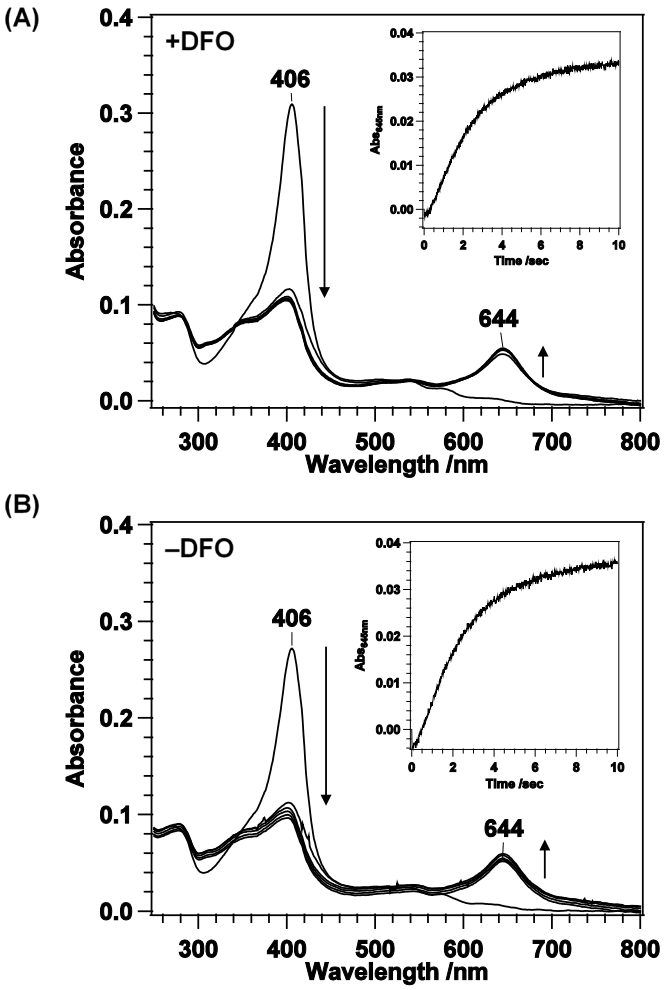

Fig. 9 Heme-degradation reaction of heme-HutZ with H_2O_2 (0.10 mM) at pH 6.0 in the presence (A), and absence of DFO (B). Spectra were measured before addition of H_2O_2, and at 1-min intervals for 5 min after addition of H_2O_2. Inset: Time course of absorbance at 644 nm.

As described above, the rates for heme reduction (k_1), ligand binding (k_2), and verdoheme formation (k_4) were unaffected by the addition of iron chelators. The remaining step is conversion of oxyheme to hydroperoxy heme, with a rate constant of k_3 (Fig. 6). However, it is difficult to directly measure k_3 owing to the extremely short lifetime of hydroperoxy heme. This step is divided into two steps: the one-electron reduction of oxyheme to Fe(III)-OO^-, and protonation of Fe(III)-OO^- to hydroperoxy heme. Considering that the addition of DFO does not change k_1, it would also not alter the redox potential of heme-HutZ, indicating that the rate of one-electron reduction of oxyheme would not be affected. Thus, we postulated that DFO inhibits the second step: protonation of Fe(III)-OO^-.

Reaction Step on the Protonation of Fe(III)-OO^- Species by HutZ

In mammalian heme oxygenase (HO), X-ray crystal structure and other biochemical and biophysical studies suggest that protonation of oxyheme is mediated by distal water molecules, which serve as proton sources (Fig. 10)[8–10]. However, it is not clear whether HutZ also contains such water molecules in the active site. To investigate whether water molecules are needed for hydroxylation of oxyheme, we monitored the heme-degradation reaction in D_2O buffer. The time courses of absorbance changes at 406 nm in reactions with ascorbic acid in H_2O and D_2O buffer are illustrated in Fig. 11. The relative absorption at 406 nm for D_2O 30 min after initiation of the reaction was higher than that of H_2O, implying that heme degradation in D_2O is slower than that in H_2O, suggesting that water molecules are involved in the process of proton transfer to Fe(III)-OO^-, as observed in HO[11–13].

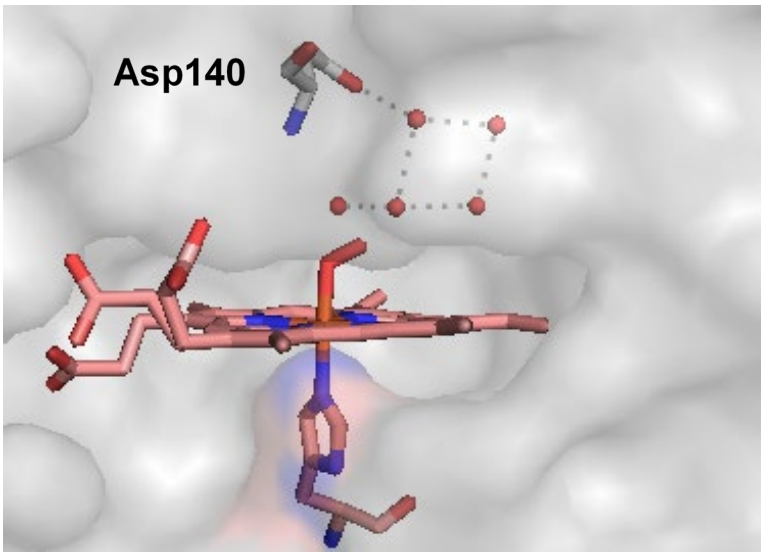

Fig. 10 Crystal structure of HO-1 form rat in the O_2-bound form (PDB ID code 4G7L).

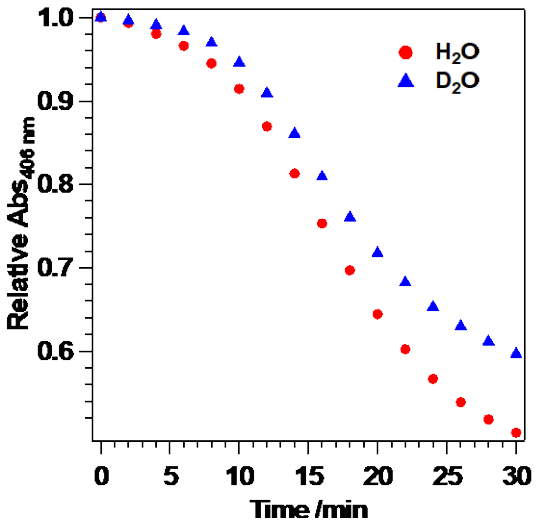

Fig. 11 Isotope effect of the heme-degradation reaction by HutZ. Time course of absorbance change at 406 nm in the reaction with ascorbic acid in H_2O/D_2O buffer at pH 6.0.

This isotope effect on heme-degradation by HutZ suggests that a proton source is required for protonation of the Fe(III)-OO^- species. In HO-1, the terminal oxygen atom of the heme-bound O_2 interacts with a water molecule, which is stabilized by Asp140 (Fig. 10)[14,15]. Replacement of Asp140 with alanine substantially suppresses proton transfer to Fe(III)-OO^- in HO-1 because of displacement and/or fluctuations of the water molecules[16–18]. The distal Asp140 allows water molecules in the distal pocket to interact with heme-bound O_2[17,19]. Although the heme complex of HutZ has not been crystallized, the crystal structure of a homologous protein, HugZ, from *Helicobacter pylori* suggests that Thr27 of HutZ is present in the active site (Fig. 12)[20]. Thus, we predicted that Thr27 plays a role in protonation of Fe(III)-OO^- analogous to that of Asp140 in HO-1. To investigate whether the hydroxyl group at position 27 is essential for protonation of the iron-bound O_2, we replaced Thr27 with valine or serine, and examined the heme-degradation activity of the resulting mutants. The time course of the decrease in the Soret band revealed that the heme-degradation rate was significantly slower for the heme-HutZ T27V mutant than for heme-HutZ wild-type (WT) (Fig. 13). In addition, mutation of Thr27 to valine caused a 2-fold decrease in the amount of liberated ferrous iron (Table 1). To investigate the step inhibited in the T27V mutant, we measured the rate

constants for heme-degradation (Fig. 6). The values for k_1, k_2, and k_4 for the heme-HutZ T27V mutant were almost the same as those for heme-HutZ WT (Table 2). In contrast, for the T27S mutant, in which the hydroxyl group at position 27 is retained, the heme-degradation rate and amount of iron released from heme were almost identical to those of heme-HutZ WT (Fig. 13, Table 1). These results suggest that the OH group of Thr27 is involved in protonation of Fe(III)-OO^-.

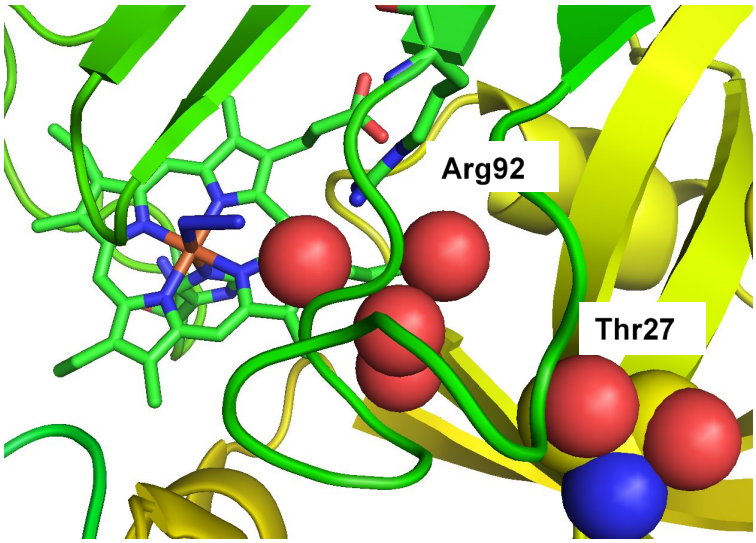

Fig. 12 Crystal structure of HugZ from *Helicobacter pylori* (PDB ID code 3GAS).

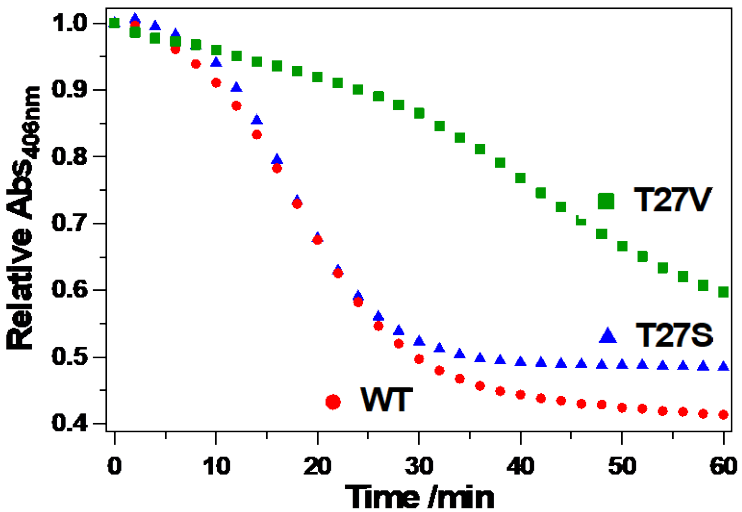

Fig. 13 Changes in absorbance intensity at 406 nm in reactions of heme-HutZ WT, and heme-HutZ T27V and T27S mutants with ascorbic acid (1 mM).

Table 1 Heme-degradation ratio determined from the amount of ferrous iron in heme-HutZ wild-type (WT) and heme-HutZ T27V and T27S mutants.

Protein	Iron yield (%)
WT	86 ± 7
WT + ferrozine	32 ± 7
T27V	61 ± 5
T27S	83 ± 3
WT + tetracycline	49 ± 4
WT + chloramphenicol	83 ± 3

Table 2 Rate constants of heme reduction (k_1), CN binding (k_2'), and H_2O_2 reaction (k_4) for heme-HutZ

Protein	k_1 (min^{-1})	k_2' ($mM^{-1}s^{-1}$)	k_4 (sec^{-1})
WT +DFO	0.045 ± 0.008	0.76 ± 0.01	0.392 ± 0.002
WT – DFO	0.052 ± 0.005	0.88 ± 0.01	0.389 ± 0.001
T27V	0.045 ± 0.000	1.09 ± 0.01	0.396 ± 0.001
T27S	0.048 ± 0.000	0.93 ± 0.00	0.401 ± 0.001

Proposed Inhibition Mechanism by Iron Chelators

These observations indicate that iron chelation perturbs proton transfer from water molecules to Fe(III)-OO^-, and Thr27 contributes to the presence of water molecules in the active site. A proposed mechanism for inhibition by iron chelators is illustrated in Fig. 14. According to this model, iron chelators inhibit the heme-degradation reaction by perturbing localization of the proton source—water molecules—making it difficult for HutZ to form the Fe(III)-OOH species. The exothermic heat of interaction of DFO with distal water molecules would be canceled by the endothermic heat of disruption of the interaction with bulk water molecules (Fig. 5).

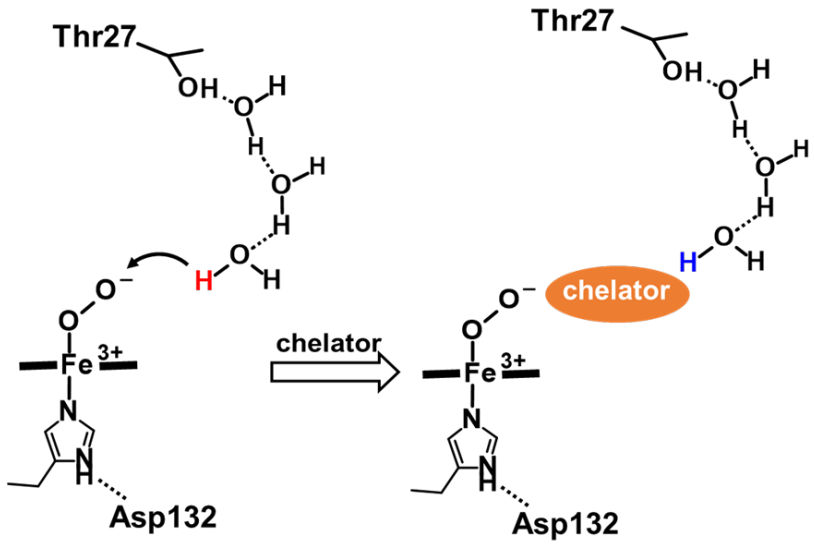

Fig. 14 Proposed mechanism for inhibition of heme-degradation reaction by iron chelators.

Heme Degradation Reaction in the Presence of Antibiotics

The inhibition of HutZ by iron chelators prompted me to investigate the possibility of using antibiotics as inhibitors of HutZ, because tetracycline, which is the most effective current treatment for cholera, is an inhibitor of protein synthesis as well as an iron chelator[21]. The spectral changes that follow addition of ascorbic acid in the presence of antibiotics are shown in Fig. 15. In the presence of chloramphenicol, a representative antibiotic, ascorbic acid caused a decrease in the Soret band at 405 nm, attributable to heme breakdown (Fig. 15A). Addition

of ferrozine 60 min after the reaction resulted in the appearance of a new band at 562 nm that reflected the formation of a ferrozine-iron complex[22]. The heme-degradation ration, defined as the ration of iron concentration captured by ferrozine, to the initial heme concentration, was 83 ± 3 %, which is similat to that of heme-HutZ (86 ± 7 %) (Fig. 2A). In contrast, the Soret band diminished very little in the presence of tetracycline (Fig. 15B). The heme-degradation ratio was 49 ± 4 %, indicating that the heme-degradation reaction was repressed in the presence of tetracycline. These observations support the conclusion that substrates possessing an iron-chelating ability could be possible treatments for cholera.

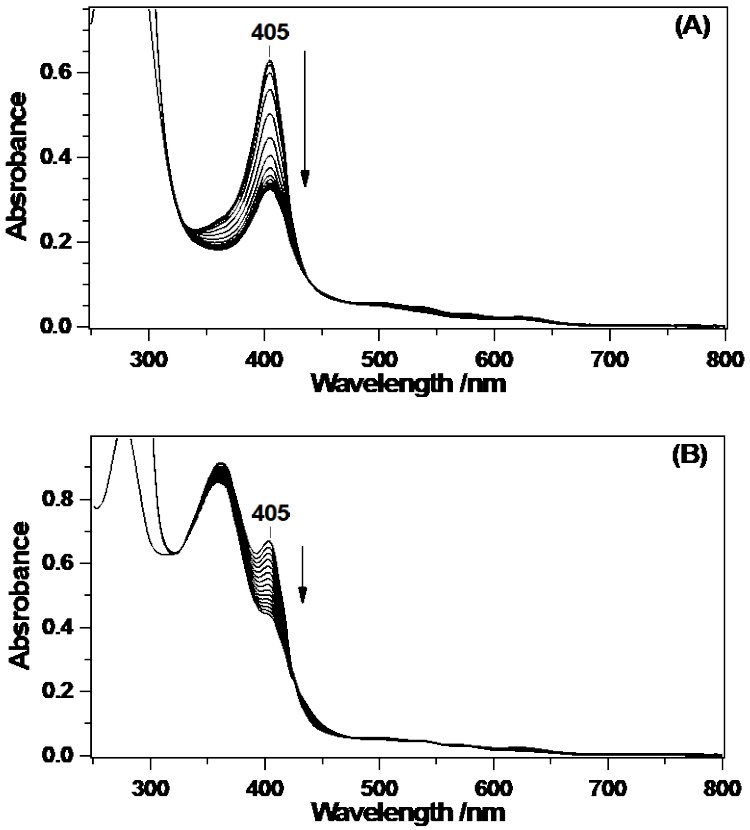

Fig. 15 Heme-degradation reaction of the heme-HutZ complex with ascorbic acid (1.0 mM) at pH 6.0 (A) in the presence of 50 μM chloramphenicol and (B) 50 μM tetracycline. Spectra were measured before addition of ascorbic acid and at 8-min intervals for 56 min after addition of ascorbic acid. Tetracycline caused a large absorption below 400 nm.

3.4. Conclusions

HutZ is needed for the efficient use of heme as an iron source. Most effective treatment for cholera is the utilization of antibiotics. Tetracycline is an inhibitor of protein synthesis as well as an iron chelator. Thus, I predicted that tetracycline affects the heme degradation activity of HutZ. The spectroscopy experiment showed that iron chelators inhibit the heme degradation activity of HutZ (Fig. 1). Based on the kinetic analysis (Table 2), I found that iron chelators are able to inhibit the heme-degradation reaction of HutZ by perturbing proton transfer to Fe(III)-OO^- from water molecules in the distal cavity (Fig. 14). This mechanism suggests that iron chelators are good candidate antibiotics for use against *V. cholerae*.

References

(1) Muramoto, T. *Plant Physiol.* **2002**, *130* (4), 1958.

(2) Uchida, T.; Sekine, Y.; Matsui, T.; Ikeda-Saito, M.; Ishimori, K. *Chem. Commun.* **2012**, *48* (53), 6741.

(3) Reid III, T. J.; Murthy, M. R. N.; Sicignano, A.; Tanaka, N.; Musick, W. D. L.; Rossmann, M. G. *Proc. Natl. Acad. Sci.* **1981**, *78* (8), 4767.

(4) Keberle, H. *Ann. N. Y. Acad. Sci.* **1964**, *119* (2), 758.

(5) Rauen, U.; Springer, A.; Weisheit, D.; Petrat, F.; Korth, H. G.; De Groot, H.; Sustmann, R. *ChemBioChem* **2007**, *8* (3), 341.

(6) Gibbs, C. *Anal. Chem.* **1976**, *48* (8), 1197.

(7) Ortiz de Montellano, P. R. *Curr. Opin. Chem. Biol.* **2000**, *4* (2), 221.

(8) Unno, M.; Matsui, T.; Ikeda-Saito, M. *Nat. Prod. Rep.* **2007**, *24* (3), 553.

(9) Sugishima, M.; Moffat, K.; Noguchi, M. *Biochemistry* **2012**, *51* (43), 8554.

(10) Chen, H.; Moreau, Y.; Derat, E.; Shaik, S. *J. Am. Chem. Soc.* **2008**, *130* (6), 1953.

(11) Hallén, S.; Nilsson, T. *Biochemistry* **1992**, *31* (47), 11853.

(12) Aikens, J.; Sligar, S. G. *J. Am. Chem. Soc.* **1994**, *116* (3), 1143.

(13) Davydov, R.; Matsui, T.; Fujii, H.; Ikeda-Saito, M.; Hoffman, B. M. *J. Am. Chem. Soc.* **2003**, *125* (52), 16208.

(14) Schuller, D. J.; Wilks, A.; Ortiz de Montellano, P. R.; Poulos, T. L. *Nat. Struct. Biol.* **1999**, *6* (9), 860.

(15) Sugishima, M.; Omata, Y.; Kakuta, Y.; Sakamoto, H.; Noguchi, M.; Fukuyama, K. *FEBS Lett.* **2000**, *471* (1), 61.

(16) Davydov, R.; Kofman, V.; Fujii, H.; Yoshida, T.; Ikeda-Saito, M.; Hoffman, B. M. *J. Am. Chem. Soc.* **2002**, *124* (8), 1798.

(17) Fujii, H.; Zhang, X.; Tomita, T.; Ikeda-Saito, M.; Yoshida, T. *J. Am. Chem. Soc.* **2001**, *123* (27), 6475.

(18) Lightning, L. K.; Huang, H. W.; Moënne-Loccoz, P.; Loehr, T. M.; Schuller, D. J.; Poulos, T. L.; Ortiz de Montellano, P. R. *J. Biol. Chem.* **2001**, *276* (14), 10612.

(19) Lad, L.; Wang, J.; Li, H.; Friedman, J.; Bhaskar, B.; Ortiz de Montellano, P. R.; Poulos, T. L. *J. Mol. Biol.* **2003**, *330* (3), 527.

(20) Hu, Y.; Jiang, F.; Guo, Y.; Shen, X.; Zhang, Y.; Zhang, R.; Guo, G.; Mao, X.; Zou, Q.; Wang, D. C. *J. Biol. Chem.* **2011**, *286* (2), 1537.

(21) Albert, A.; Rees, C. W. *Nature* **1956**, *177*, 433.

(22) Stookey, L. L. *Anal. Chem.* **1970**, *42* (7), 779.

PART V: Conclusions

One of the ways through which *V. cholerae* acquires iron is by deploying the *hut* (heme utilization) system which constitutes cell surface receptors, HutA and HutR, a periplasmic heme binding protein HutB, ATP-dependent permease proteins, HutC/HutD, and cytoplasmic proteins, HutZ/HutX[1,2]. Once in the cytosol, the heme is degrade by heme degrading enzyme to release iron that is then available to the bacteria as an essential nutrient. Although the structure of HutZ is different from that of HO-1, both heme degradation enzymes can produce bliverdin from heme[3], suggesting that HutZ has evolved from ancestral distinct from that of HO-1. However, the heme-degradation mechanism of HutZ-type enzymes have not been fully understood. In this study I investigated the heme degradation mechanism and a common ancestral protein of HutZ-type enzymes by using the structural and kinetic analyses, the various spectroscopic techniques. The results and conclusions drawn on the basis experimental data are summarized below.

HutZ can converts heme to biliverdin *via* the same steps as HO-1. (Part II of chapter I)

In this part, I focused on the heme degradation mechanism of HutZ-type enzymes because the structure of HutZ is different from that of HO-1. To characterize reaction intermediates of HutZ, I observed UV-vis spectra for *meso*-hydroxyheme and verdoheme. The heme degradation intermediates of HutZ are the same as that of HO-1, although the valence of verdoheme of HutZ is different from that of HO-1 because the structure of HutZ is unique in the presence of proximal hydrogen bond.

Role of heme proximal side hydrogen bonding is appropriate position for heme to attack the *meso*-carbon of porphyrin. (Part II of Chapter II)

As revealed in previous chapter, the proximal hydrogen bond between Asp132 and His170 is unique in the heme degradation enzymes because this hydrogen bond is disadvantage to convert hydoxyheme to *meso*-hydoroxyheme. To determine the role of hydrogen bond between Asp132 and His170, the heme degradation activity of mutants of mutating Asp132 to leucine, asparagine, glutaminate acid, or His170 to alanine was measured. The hydrogen bond between

Asp132 and His170 destabilizes the coordination of the proximal histidine to heme, leading to a drastic loss of heme degradation activity. The role of proximal hydrogen bond is necessary for HutZ to bind heme and form verdoheme, likely because heme is held in an appropriate position for heme degradation.

HutZ is a different ancestral protein from that of HO-1. (Part III)

HutZ, which can convert heme to biliverdin *via* the same steps as HO-1, is the different structure from that of HO-1 (Part II). I predicted that the ancestral protein of HutZ-type enzymes is distinct from that of HO-1. To investigate the ancestral protein of HutZ-type enzymes, I focus on Alr5027 from cyanobacteria *Nostoc sp.* PCC7120, which is acquired for the heme binding and degradation ability by mutating of Lys164 to histidine. Introduction of His at position 164 rendered the mutant with high affinity for heme. Although heme was not degraded by the K164H mutant when ascorbic acid was used as an electron source, it was degraded by H_2O_2 to produce verdoheme. Fluorescence spectra suggested that the inefficient heme-degradation activity of the K164H mutant by ascorbic acid is due to an elongation of distance between each protomers containing Asp132 and His170 (Part II of chapter II). Therefore, a single replacement of Lys164 with His in Alr5027 converts non-heme binding protein to a heme-degradation protein, suggesting that the HutZ-type enzymes acquire for the function of the heme-degradation from a common ancestor of Alr5027 through molecular evolution.

Iron chelators can act as inhibitor for HutZ. (Part IV)

To detect the amount of ferrous iron by the heme-degradation reaction, I tried to observe the heme-degradation reaction in the presence of iron chelators, and I found that iron chelators inhibit the heme degradation ability of HutZ. Based on kinetic analysis of the heme degradation reaction pathway of HutZ, iron chelator is likely to inhibit the proton transfer from water molecules fixed by Thr27 in the active site to reduced oxyferrous heme by the interaction with the water molecules. Thus, the results of various spectroscopic measurements in this part suggested that iron chelators are the candidate for antibiotics of *V. cholerae.*

As summarized above, spectroscopic and kinetic analyses in Part II, III and IV, I found that HutZ-type enzymes are a unique structural heme-degrading enzyme, which is distinct from other HOs family, and the pathogen bacteria would acquire HutZ-type enzymes through molecular evolution from a common ancestor of Alr5027. The mammalian organisms express HO-1, whose structure is different from that of HutZ. Thus, HutZ-type enzymes have become the drug target for cholera by inhibiting only pathogen bacteria. Recently, to inhibit the some pathogen bacterial heme-degradation enzymes, heme analogues such as metal-substituted protoporphyrins showed antibacterial activity[4,5]. However, there is a risk to replace the cofactor of mammalian heme enzymes with these metal-substituted protoporphyrins. On the other hand, small iron chelators does not inhibit the heme-degrading enzymes except for HutZ. In this thesis, I believe that study on HutZ-type enzymes paves the way for the development of more effective medicines.

References

(1) Payne, S.; Whiteley, M.; Davies, B.; Molineux, I.; Que, E. **2016**.

(2) Wyckoff, E. E.; Schmitt, M.; Wilks, A.; Payne, S. M. *J. Bacteriol.* **2004**, *186* (13), 4142.

(3) Uchida, T.; Sekine, Y.; Matsui, T.; Ikeda-Saito, M.; Ishimori, K. *Chem. Commun.* **2012**, *48* (53), 6741.

(4) Cupello, M. P.; Souza, C. F. de; Buchensky, C.; Soares, J. B. R. C.; Laranja, G. A. T.; Coelho, M. G. P.; Cricco, J. A.; Paes, M. C. *Acta Trop.* **2011**, *120* (3), 211.

(5) Hijazi, S.; Visca, P.; Frangipani, E. *Front. Cell. Infect. Microbiol.* **2017**, *7* (January), 1.